AD-A134 465 URBAN MILLIMETER WAVE PROPAGATION STUDIES(U) ARMY COMMUNICATIONS-ELECTRONICS COMMAND FORT MONMOUTH NJ E J VIOLETTE ET AL. APR 83 CECOM/DRSEL-83-3 1/2

UNCLASSIFIED F/G 20/14 NL

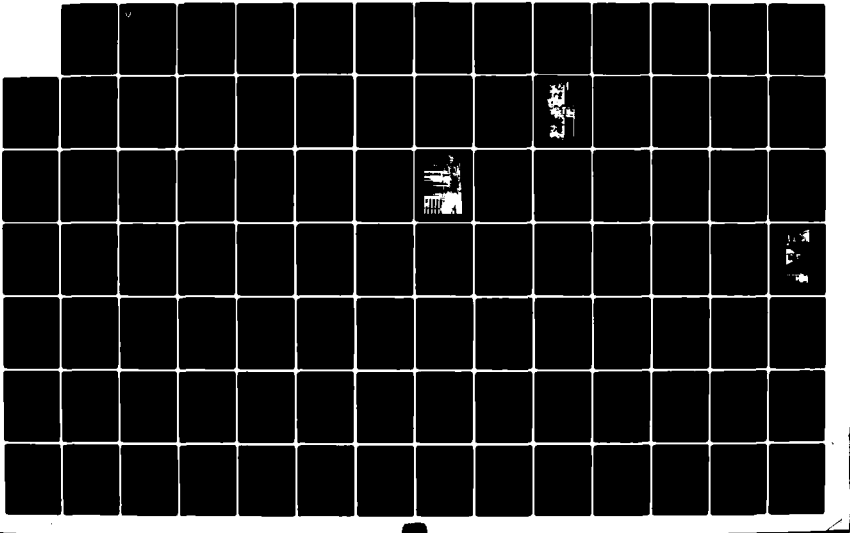

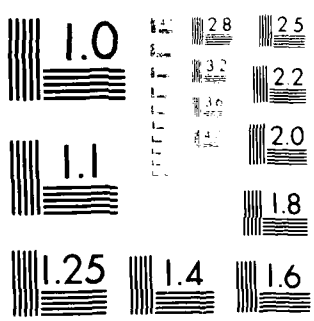

RESEARCH AND DEVELOPMENT TECHNICAL REPORT

CECOM-83-3

URBAN MILLIMETER WAVE PROPAGATION STUDIES

E. J. VIOLETTE, R. H. ESPELAND, AND K. C. ALLEN
U.S. DEPARTMENT OF COMMERCE
NTIA/ITS
BOULDER, CO 80303

F. SCHWERING
CENTER FOR COMMUNICATIONS SYSTEMS

APRIL 1983

CECOM
U S ARMY COMMUNICATIONS-ELECTRONICS COMMAND
FORT MONMOUTH, NEW JERSEY 07703

NOTICES

Disclaimers

The citation of trade names and names of manufacturers in this report is not to be construed as official Government indorsement or approval of commercial products or services referenced herein.

Disposition

Destroy this report when it is no longer needed. Do not return it to the originator.

UNCLASSIFIED

SECURITY CLASSIFICATION OF THIS PAGE (When Data Entered)

REPORT DOCUMENTATION PAGE		READ INSTRUCTIONS BEFORE COMPLETING FORM
1. REPORT NUMBER CECOM-83-3	2. GOVT ACCESSION NO.	3. RECIPIENT'S CATALOG NUMBER
4. TITLE (and Subtitle) Urban Millimeter Wave Propagation Studies		5. TYPE OF REPORT & PERIOD COVERED Final Report 1 Oct 1981 - 31 Dec 1982 6. PERFORMING ORG. REPORT NUMBER
7. AUTHOR(s) E. J. Violette, R. H. Espeland, K. C. Allen and F. Schwering		8. CONTRACT OR GRANT NUMBER(s)
9. PERFORMING ORGANIZATION NAME AND ADDRESS U S Department of Commerce, National Telecommunication and Information Administration, Inst. for Telecommunication Sciences, Boulder, CO 80303		10. PROGRAM ELEMENT, PROJECT, TASK AREA & WORK UNIT NUMBERS 1L1 611102.H48.PM.11.01
11. CONTROLLING OFFICE NAME AND ADDRESS U S Army Communications-Electronics Command Center for Communications Systems ATTN: DRSEL-COM-RM-4		12. REPORT DATE April 1983 13. NUMBER OF PAGES 97
14. MONITORING AGENCY NAME & ADDRESS(if different from Controlling Office)		15. SECURITY CLASS. (of this report) Unclassified 15a. DECLASSIFICATION/DOWNGRADING SCHEDULE

16. DISTRIBUTION STATEMENT (of this Report)

Approved for Public Release; Distribution Unlimited

17. DISTRIBUTION STATEMENT (of the abstract entered in Block 20, if different from Report)

18. SUPPLEMENTARY NOTES

19. KEY WORDS (Continue on reverse side if necessary and identify by block number)

Urban propagation measurements; millimeter wave; multipath; diffraction

20. ABSTRACT (Continue on reverse side if necessary and identify by block number)

Measurements of millimeter wave propagation in urban areas at 9.6, 28.8 and 57.6 GHz, and a determination of signal levels reflected from several building surfaces, were made to study wave propagation characteristics in a city environment. Principal emphasis was on the evaluation of communications link reliability, detectability and usable bandwidth as a function of position of terminals. Reflected signal level measurements were performed on building surfaces of concrete aggregate, painted smooth concrete with protruding ribs, brick, and metal

DD FORM 1 JAN 73 1473 EDITION OF 1 NOV 65 IS OBSOLETE

UNCLASSIFIED

SECURITY CLASSIFICATION OF THIS PAGE (When Data Entered)

20. (contd)

siding. Multipath measurements were recorded as a function of distance for several runs over paths of about 1 kilometer in the center of the Denver metro area. Non-line-of-sight observations showed a large number of substantial signals arriving from a wide range of angles. This report contains the results and analysis from single-path and multipath reflections recorded for the study. Included are an evaluation of multipath effects for both urban and non-urban line-of-sight path and measurements of signals received on non-line-of-sight paths, using edge diffraction effects.

SUMMARY

Reflection properties of a variety of building surfaces were measured at frequencies of 9.6, 28.8 and 57.6 GHz. Buildings with metal facing provided a nearly perfect reflecting surface at normal incidence; however, considerable spatial dependence and less than expected aspect sensitivity were observed in the reflected signals. All metal surfaces measured had the typical vertical rib pattern at either 12 or 24 inch (30.5 and 61.0 cm) separation which produces a surface perturbation that accounts for some of the signal phase interference pattern observed with small changes in terminal position. Brick, concrete, and concrete aggregate types of building surfaces were found to have a lower reflection coefficient at normal incidence, but they displayed similar spatial properties and somewhat greater angular scattering components compared to metal surfaces. At the two highest frequencies, surface roughness clearly distorted the phase front of the reflected wave. Also phase front changes were induced when the transmitter or receiver terminal was moved parallel to an apparently flat wall. Large scale irregularities (several rf wavelengths) over the illuminated surface produced large signal interference patterns at the receiving antenna. A reference reflector, a 90 cm square-metal plate, was measured as an instrumentation verification exercise and produced the predicted sharp angular response (high aspect sensitivity) and unity reflection coefficients.

A line-of-sight path of about 1 km was selected in downtown Denver to measure signal characteristics as a function of range. For these measurements the transmitter terminal was moved at a uniform rate toward the receiver terminal. Antennas used for the transmitter had beamwidths of 10 degrees to eliminate problems in antenna tracking. The stationary receiver antenna beamwidths were 4 degrees at 9.6 GHz and 1.2 degrees at 28.8 GHz and 57.6 GHz. Fades on this LOS path were as deep as 30 dB, the result of reflection from the asphalt street and buildings. Similar measurements were recorded with the receiving antennas beamed to illuminate building surfaces on one side of the street. Numerous signal fades of about 30 dB occurred, indicating the likelihood of two discrete ray paths of nearly equal amplitudes.

On the same street, the transmitter terminal was located 485 meters from the receiver and its antenna was stepped in azimuth by 10 degree increments to cover all portions of one side of the street. At each antenna step, the receiving antenna was scanned in azimuth to record the direction and amplitude of signals reflected from the buildings. Single reflected and multi-reflected modes, up to

4 hops, were recorded and traced onto a scaled drawing in order to locate the reflection points, type of reflecting surfaces, and time delay compared to the direct signal. The amplitude of these reflections was also compared according to antenna polarizations. For these cases, the angles of incidence to the reflecting surfaces were quite shallow, 1 to 10 degrees. Only for the case of the 28.8 GHz pattern was there a clear antenna polarization dependence. Surface roughness at shallow angles can be quite large relative to an rf wavelength without producing a distorted wave front. There were many protrusions along the street such as trees, light poles, and traffic signs as well as large uneven structures. Even so, reflected signals reached levels of 8 dB below the direct signal. Estimates of bit error rates resulting from the multipath signal amplitude and delay times observed on the 485 meter street path were included for selected digital data rates.

To separate the fade components of building reflections from fade components produced by reflections from the street, measurements were recorded in a rural area where only an asphalt road and a gravel road could produce a reflection. The results of these measurements showed that the street or roadway provided the dominant surface for reflections and was responsible for all deep fades. Antenna heights of 1 to 3.5 meters were compared over the roadway for path lengths up to 2 km. The lower heights did not create large fades, even though the road was in the main beam. A low reflection angle and greater than first Fresnel reflection area appeared to cause a lower fade level.

Diffraction characteristics from vertical edges of buildings were recorded. A polarization dependence amounting to as much as a 10 dB higher signal in the shadow region was observed with the electric field vector perpendicular to the edge compared to the level with the electric field vector parallel to the edge. The signal level in the shadow region decreased with increased frequency but was independent of terminal distance from the edge for the paths measured. A calculation of the predicted values resulted in good agreement with antenna polarization differences. The predicted levels were higher than the measured data in the shadow region. It is believed that agreement in predicted levels of the shadow region is not as much a function of knife edge versus rounded edge, but more a function of the electrical properties of the material.

TABLE OF CONTENTS

LIST OF FIGURES

LIST OF TABLES

I. INTRODUCTION

Measurements of millimeter wave propagation in urban areas and a determination of signal levels reflected from several building surfaces have been made for the Army Communications-Electronics Command. The objective of the project has been to study millimeter wave propagation characteristics in a city environment with principal emphasis on the evaluation of communication link reliability, detectability, and usable bandwidth as a function of position of terminals.

Reflected signal level measurements were performed on building surfaces of concrete aggregate, painted smooth concrete with protruding ribs, brick, and metal siding. Data were recorded to determine aspect sensitive of the reflected signal in a backscatter mode. Special tests were conducted, using a 3-foot square, flat reflector. The reflector was rotated in a plane perpendicular to the transmitter-reflector path to establish a reference for aspect sensitivity under controlled conditions. Two oblique angle reflection measurements, from brick and concrete surfaces, were performed including aspect sensitivity recordings. Multipath measurements were recorded as a function of distance for several runs over paths of about 1 kilometer in the center of the Denver metro area. Additional runs were recorded over paths in open (nonurban) areas for comparison to the multipath runs made in the Denver metro area.

Non-line-of-sight observations were made in the Denver area which showed a surprisingly large number of substantial signals arriving from a wide range of angles. Many signals showed multiple reflections, most pronounced at 9.6 GHz and decreasing with increasing frequency. A pair of 60 GHz handheld communicators were also used in this exercise. Voice quality was always good when lock-up was achieved, but a slow search rate requiring a long lock-up time caused difficulty in establishing a contact in the urban environment. Several line-of-sight contacts were made and a single reflection, non-line-of-sight link was established over a 400 meter path, all with good voice reception.

An initial calibration and gain stability check was performed on a far-field path with good ground clearance to provide a free space reference for all further measurements. Because the transmitter and receiver are co-located for folded path measurements and are in near field for many oblique measurements, leakage signal levels were recorded. The leakage levels were obtained by directing both transmitting and receiving antennas into an essentially nonreflecting atmosphere at the edge of an abrupt 600 foot drop in terrain. Worst case values of -30 dB, -50 dB,

and -52 dB, in the order of ascending frequency and relative to a 106 meter path were recorded with the transmitting antenna located directly below the receiving antennas (1 meter separation) and for transmitter positions on a line perpendicular to receiver antenna pointing. These values of leakage level provide a measure of the resolution limit for reflected signal determination.

This report contains the results and analysis from single-path and multipath reflection conditions recorded for the study. Included are an evaluation of multipath effects for both urban and nonurban line-of-sight paths, measurements of signals received on non-line-of-sight paths, and diffraction effects.

II. EQUIPMENT AND CALIBRATION

The instrumentation for these measurements was developed from a system used earlier for a study of millimeter wave propagation through vegetation[1]. For the urban studies, the principal modifications were made on the primary power sources and for terminal portability. The receiver terminal has been changed to be totally contained within a van including power generator and storage of hardware and accessories. The rf hardware and antennas are mounted on an elevator adjustable for heights above ground from 1 to 3 meters. The receiving antennas and the rf hardware are mounted on a remote-controlled positioner permitting both azimuthal and elevation scans at all elevator heights. All the antennas are linearly polarized and can be readily changed from vertical, to horizontal, to cross polarization.

The transmitter terminal is attached to a manual positioner, powered by rechargeable batteries and mounted on a four-wheel dolly.

The link operates at three coherent frequencies: 9.6, 28.8, and 57.6 GHz. Beamwidths of the transmitting antennas are 10 degrees at all frequencies. Receiver beamwidths are 4.8 degrees at the 9.6 GHz frequency and 1.2 degrees at 28.8 and 57.6 GHz. A 60 dB dynamic range limited by the last IF amplifier stage and a sensitivity of at least -110 dBm is available with all three receivers.

A. Instrumentation Description

A functional diagram of the transmitting terminal is shown in Figure 2.1. All three rf frequencies are derived from a 100 MHz temperature compensated crystal oscillator. A phased-locked, cavity-tuned (X96) multiplier is used to generate 30 mW at 9.6 GHz. An identical (X96) multiplier drives a varactor tripler which injection locks an 85 mW Gunn source at 28.8 GHz through a high isolation ferrite circulator. The Gunn power is fed to a directional coupler providing 20 mW to a 25 dB gain horn antenna, and the remaining power drives a varactor doubler. A directional coupler is used to inject a locking signal from the doubler into the 57.6 GHz IMPATT source. With a bias current of 260 ma, the IMPATT provides 120 mW to a 25 dB gain horn antenna. The entire transmitter is mounted in a temperature controlled enclosure which is held at 45°C ± 1°C to reduce power variation, in the worst case, to less than ± 0.5 dB at 57.6 GHz.

A functional diagram of the receiving terminal is given in Figure 2.2. All of the receiving rf components and the low noise IF preamplifiers are contained in a 45° + 1°C temperature controlled enclosure. Three parabolic reflectors (18, 24, and 12-inch, in the order of ascending frequency) are mounted on the enclosure with

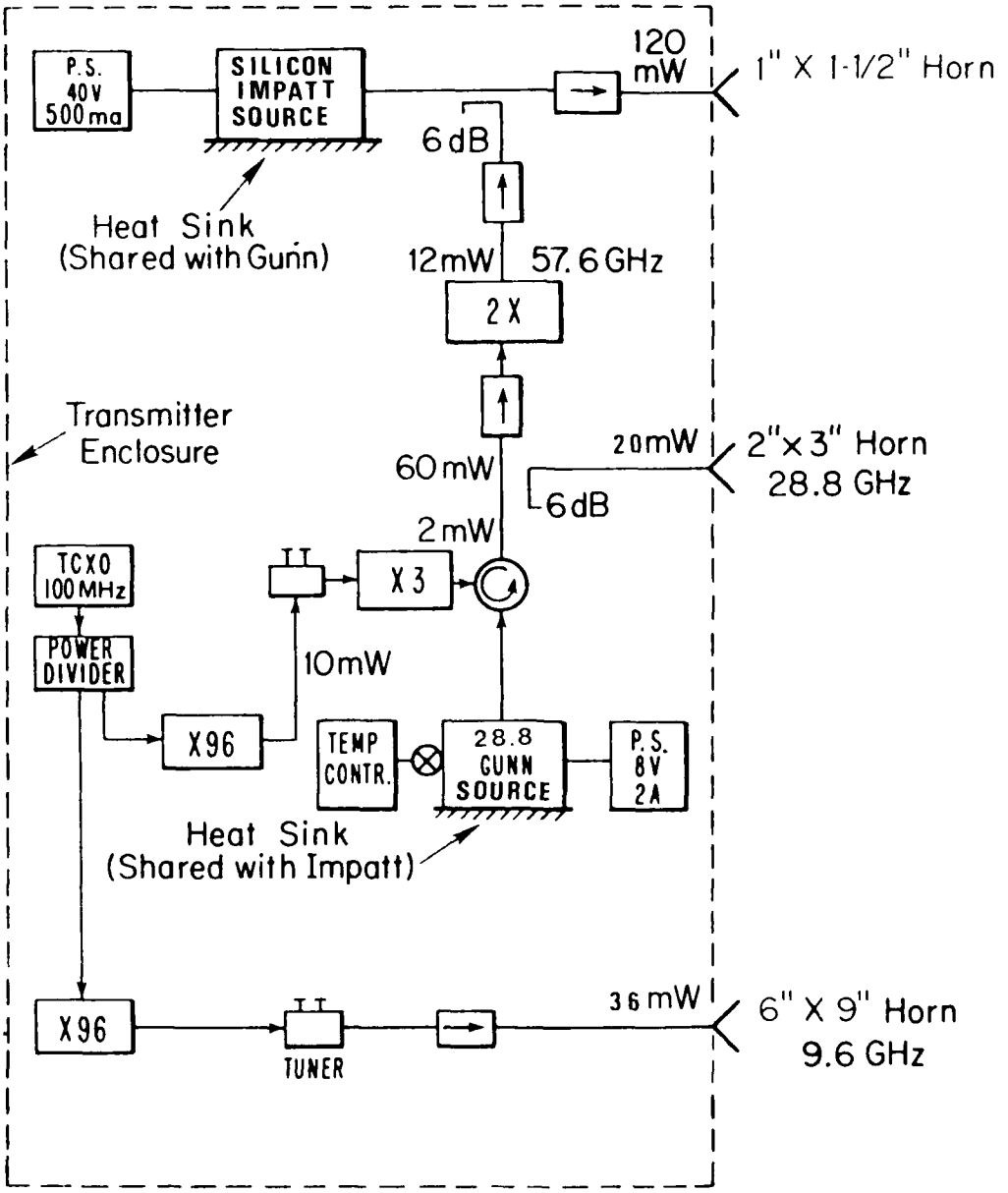

Fig. 2.1 A functional diagram of the transmitting terminal.

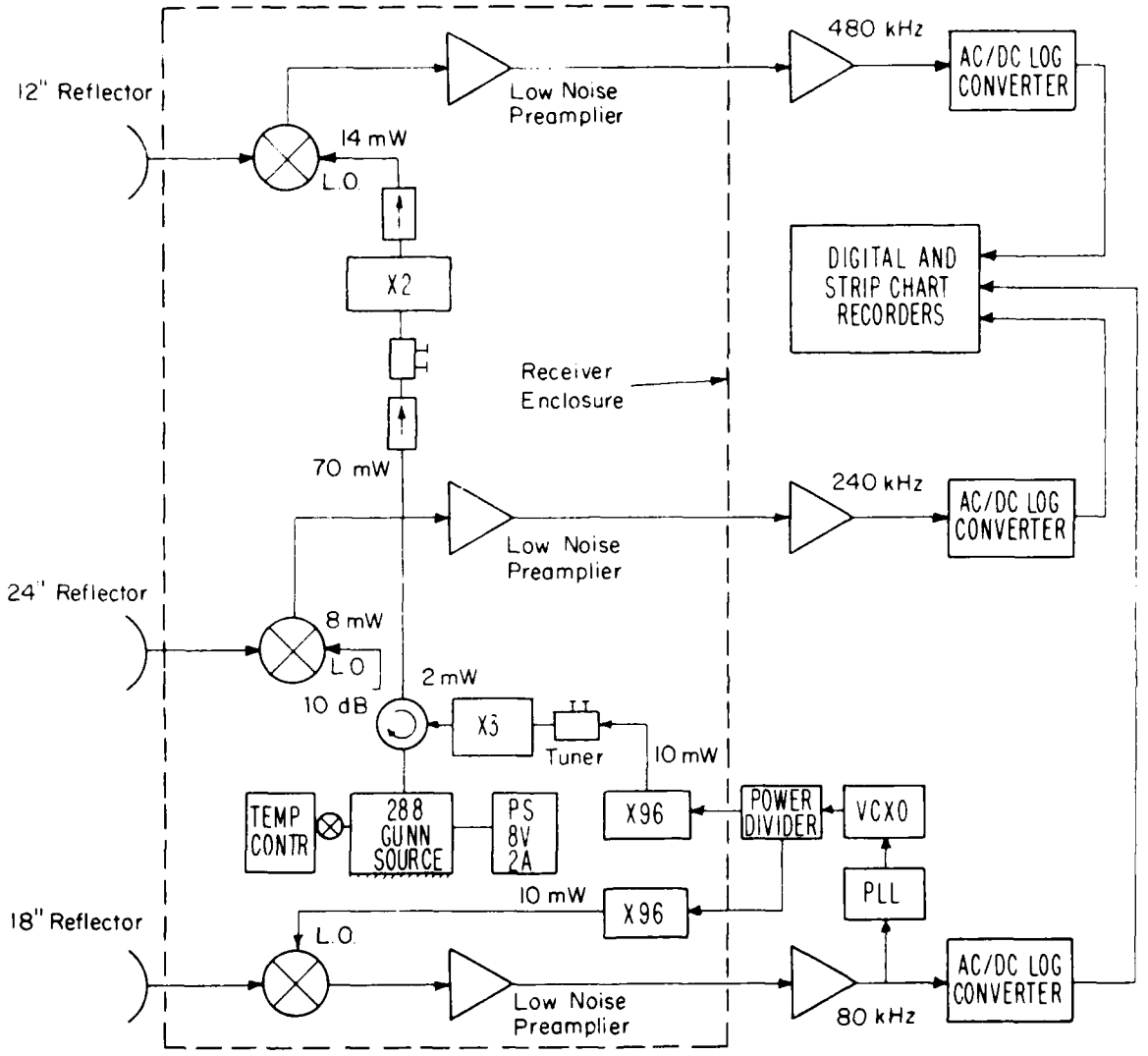

Fig. 2.2 A functional diagram of the receiving terminal.

low-noise down converters coupled directly to the antenna feeds. This total assembly is mounted on the remote controlled positioner. The receiver noise figure is determined by the input down converter, which is a double-balanced mixer at 9.6 GHz with a 7.5 dB double sideband noise figure. The 28.8 and 57.6 GHz input mixers are of the stripline-waveguide-junction balanced type with double sideband noise figures of 5.5 and 6.0 dB, respectively. All local oscillator (LO) signals are generated from a voltage controlled crystal oscillator which is phase locked to the 9.6 GHz received signal with an 80 kHz reference offset frequency. The multipliers for the voltage controlled 100 MHz reference (+ IF/multiplying factor) to derive the LO injection signals are identical to the scheme used for the transmitter sources, except, at 57.6 GHz, the doubler alone provides sufficient LO level. Long term (weeks) gain stability for each receiver is less than + 0.1 dB.

A block diagram of the data acquisition system is shown in Figure 2.3. The three IF frequencies of 80, 240, and 480 kHz are brought to the receiving van via coaxial cables, filtered, and amplified before entering an ac to dc log converter. The received IF signals are converted to a dc level that is logarithmically related to the rf signal amplitude. These dc levels drive a multi-channel strip chart recorder for monitoring, and they also appear at the input of a digital scanner that is capable of switching between each receiver level at rates of up to 100 times per second determined by the data-logging desk computer. The desk computer is also interfaced with a 5-1/2 digit voltmeter and is programmed to perform data collecting, data processing, tape storage, and data plotting functions.

B. Calibration and Path Characterization

The initial instrumentation calibration was performed on a far-field path of 106 meters. A definition of a minimum far-field distance is $d_{min} = 2D^2/\lambda$, where D is the receiving antenna aperture, and λ is the rf wavelength. The calibration path was chosen to be free of any significant reflecting components from either ground or above ground obstacles so that the on-path signal amplitude is not altered. For path lengths of less than 2 km and consistent with the system measurement accuracies, only the molecular oxygen absorption losses at 57.6 GHz need to be included. In the Denver, CO, area where the elevation is 1600 meters above sea level, the attenuation at 57.6 GHz is 10.5 dB/km for an ambient temperature of 20°C and 50% relative humidity; that value is used for all path calculations. By comparison, losses at 9.6 GHz are 0.006 dB/km and at 28.8 GHz are 0.017 dB/km for the same temperature and relative humidity. The signal amplitude values presented in the later sections are relative to free space with molecular oxygen absorption loss corrections applied to the 57.6 GHz data only.

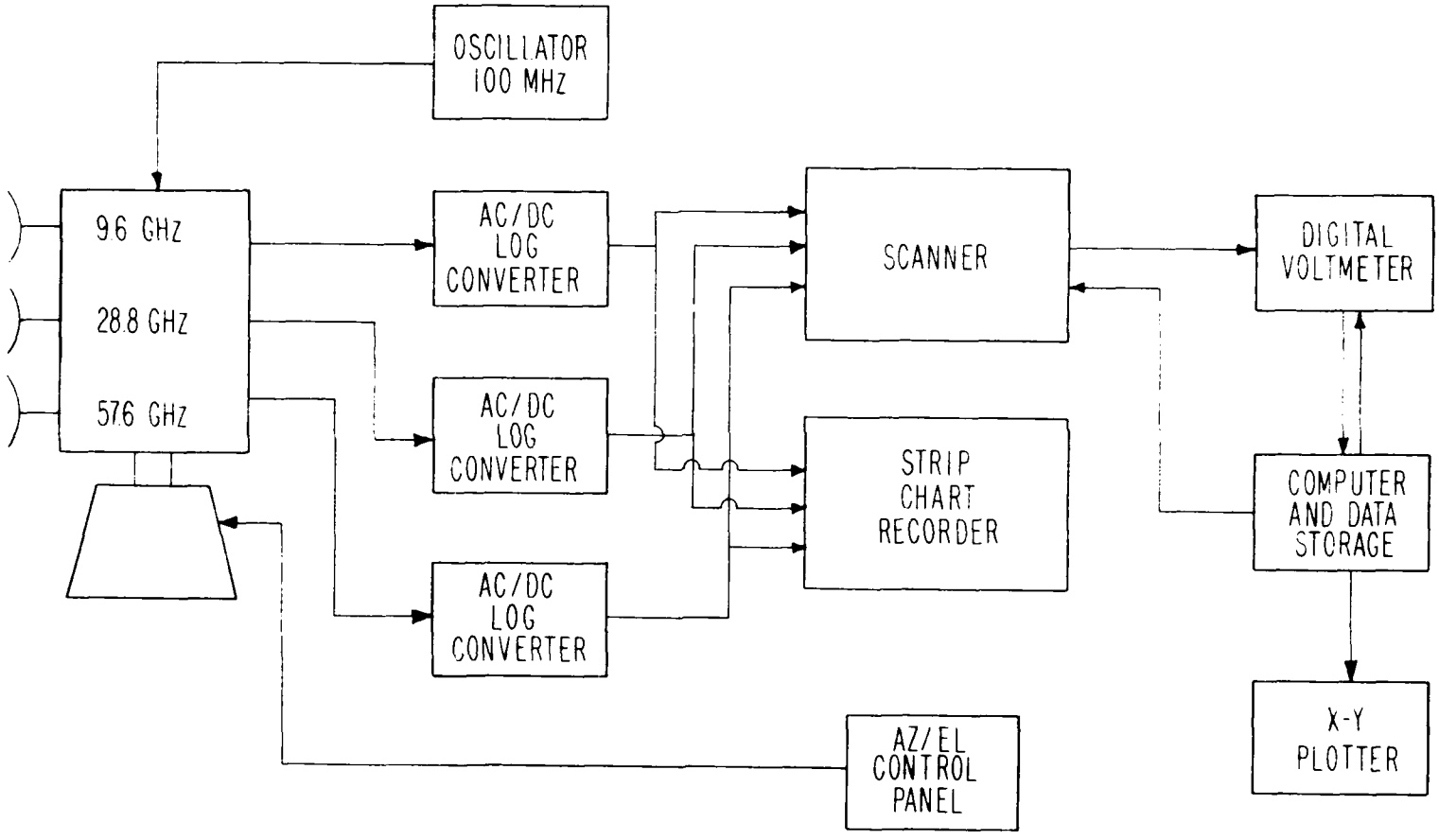

Fig. 2.3 A block diagram of the data acquisition system.

C. Measurement Types

The transmitter-receiver pairs operating at 9.6, 28.8, and 57.6 GHz, formed the test links for the measurements recorded in this study. Various link configurations were used to optimize each of the several propagation factors investigated. The diagrams in Figure 2.4 show four operating configurations, and the accompanying signal amplitude patterns illustrate the results obtained. A description of each configuration and a comment on the data obtained follows:

1. Azimuthal and Elevation Scans

In this configuration, the transmitter and receiver are set at a fixed separation distance and the receiver is scanned either in azimuth or elevation. The far-field calibration runs were performed in this mode.

2. Horizontal Scan

The receiver is set on a line perpendicular to the reflection surface and the transmitter is moved on a line parallel to the reflecting surface. This mode of operation was used to determine aspect sensitivity of the reflected signal in a folded path mode.

3. Range Scan

The receiver is stationary and the transmitter is moved along a line toward the receiver. The recorded signal represents a measure of signal amplitude as a function of distance and multipath effects.

4. Diffraction

The receiver is set at a point with the antenna pointing at a building corner (knife-edge). The transmitter is moved along a constant radius arc from line-of-sight to several degrees beyond the line-of-sight. The diffraction effects are measured as the transmitter is moved from the exposed to shadow area of the building corner.

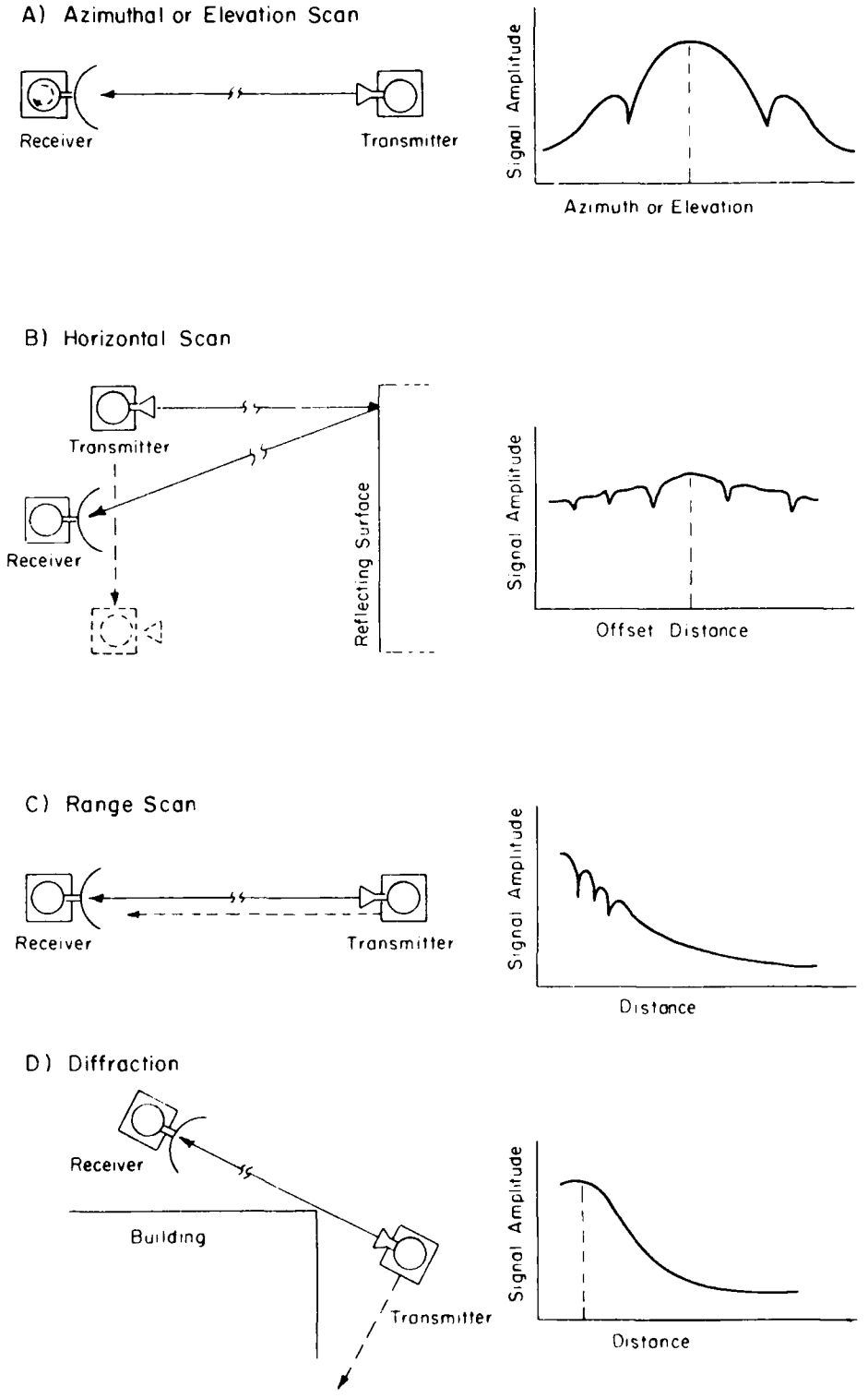

Fig. 2.4 Test link operating configurations.

III. MEASUREMENTS AT 9.6, 28.8, AND 57.6 GHz

Special sites were chosen for each of the several types of measurements made at 9.6, 28.8, and 57.6 GHz. The details of the experimental measurements for each type are discussed under the sub-headings reflection, multi-path (line-of-sight), multipath (non-line-of-sight), and edge diffraction.

A. Reflection From Building Surfaces

Measurements of reflected and/or scattered signals were made for the purpose of obtaining reflection characteristics for a variety of surfaces at selected angles of incidence for terminal to reflector path lengths of 41 meters to 135 meters. Exterior building surfaces used as reflectors were of metal, brick, concrete, and concrete aggregate. The photograph in Figure 3.1 is of the receiver terminal van and transmitter terminal as used for these measurements. In Figure 3.1 the receiving antennas (dish antennas) are positioned near the roof-top level of the van and the transmitting antennas (small horn antennas) are located on a positioner near the top of the four-wheel dolly. Both sets of antennas are pointing at a building and are positioned on a line perpendicular to the building. Measurements are made by recording the amplitude of the received signal during an azimuthal scan (+ 15) and an elevation scan (+ 10°) of the receiving antennas.

The results for zero angle of incidence measurements are presented in Table 3.1. Test numbers, building surface, signal amplitude, path length, and location are given in the table. Reradiated or reflected signal levels were significantly higher for metal than for brick and concrete walls. Values were averaged as shown in the table to indicate an order of magnitude for the reflectivity of the respective surfaces. Note an apparent reduction in signal level with increasing frequency. Most of the variability in the results is believed due to variations in surface roughness and because of the wide beamwidth, some ground multipath may appear in the 9.6 GHz data. The data shown in Table 3.2 are the results of three tests with oblique angle of incidence. Both surfaces used in these tests were irregular. The concrete building had vertical protruding ribs 5 inches (12.7 cm) wide and 12 inches (30.5 cm) deep at 48 inch intervals along the wall, and the brick building had windows and other irregularities in the area included within the common antenna beams.

A test to determine if a surface is considered smooth is the Rayleigh criterion[2]

$$H = \frac{\lambda}{8 \cos i}$$

where i is the angle of incidence, λ is the rf wavelength, and H is the height of

TABLE 3.1

RECORDED AMPLITUDES FROM SEVERAL SURFACES

ZERO ANGLE OF INCIDENCE

Test	Surface	SIGNAL AMPLITUDE (dB relative to free space) 9.6 GHz	28.8 GHz	57.6 GHz	[one-way] Path Length	
2-0-18	Metal	0	-1	-1	50 Meters	(Paint Shop)
2-1-28	"	+2	-5	-7	41 "	(North American)
2-1-0	"	-2	-3	-1	50 "	(Paint Shop)
3-0-14	"	+1	-8	-7	80 "	(Gen. Cable)
3-0-22	"	-6	+1	-9	109 "	(Gen. Cable)
		-1	-3	-5	(Average)	
3-0-44	Brick (Solid)	-2	-7	-7	95 Meters	Joslins
3-1-0	"	-6	-14	-8	47 "	"
2-0-22	Concrete (ribbed)	-6	-11	-19	64 "	Neodata
2-1-42	"	-5	-7	-18	65 "	"
2-0-42	Brick (Windows, doorway)	-9	-14	-18	93 "	RB3
2-1-22	"	-12	-15	-15	135 "	"
2-0-10	Concrete Aggregate	-6	-12	-17	75 "	Cryogenics
3-0-10	"	-12	-10	-20	75 "	"
		-8.5	-11.25	-15.25	(Average)	

TABLE 3.2

RECORDED AMPLITUDES FOR

OBLIQUE ANGLE OF INCIDENCE

Test	Surface	SIGNAL AMPLITUDE (dB relative to free space) 9.6	28.8	57.6	Path length	Angle	
2-1-50	Concrete (ribbed)	-8	-7	-13	114 m	40°	Neodata
2-1-54	"	-13	-13	-8	116 m	44°	"
2-0-48	Brick (Window, doors, etc.)	-8	-24	-17	96 m	$\approx$ 45°	RB3

the surface irregularities. This requires that the phase shift of the wave reflected from the top and the bottom of the irregularity not exceed $\lambda/4$. For a normal reflection the value of H cannot be greater than 4, 1.3, and 0.65 mm for 9.6, 28.8, and 57.6 GHz, respectively, in order to fit the smooth surface criterion. Only the metal and concrete (ribbed) surfaces come close to meeting the Rayleigh criterion at the highest frequency and this applies only for patches that seldom exceed one square meter. Beyond an area of one square meter none of the surfaces can be considered smooth for any of the test frequencies used.

The effect of surface roughness is really not apparent from the individual reflection measurements, but a trend as a function of frequency does appear from the averages shown in Table 3.1. These values are adjusted to path length (free space equation) according to a 106 meter calibration path free of multipath signals. This procedure permits the effective reflection coefficient to be calculated from the ratio of the received power that would have occurred if the reflector were perfect taken from the calibration path, versus the power measured from the reflecting surface in question. Precautions observed were that the surface area exceeded the narrower receiver beamwidths and that the total path length exceeded the boundary for far field. For this comparison method, dependence on reflector size and on antenna aperture cancel out of the calculation. Consequently if, for example, a 3 dB power loss was measured in Table 3.1, the effective coefficient of reflection of the surface is -0.5.

Table 3.1 shows a large variation in effective reflection coefficients for identical surfaces when a different path length or spatial position was used in the measurement. The reason for these large variations can best be seen in Figures 3.2 through 3.4. Signal amplitude versus transmitter position data were recorded as indicated in configuration b. (horizontal scan) in Figure 2.4. Figure 3.2 shows variations in signal amplitude as a function of transmitter position offset (relative to the receiver) using as reflecting surface the solid brick wall indicated under Test No. 3-0-44 and 3-1-0 of Table 3.1. As seen, the effective reflection coefficient is a highly variable function of position presumably due to large scale roughness or unevenness of the surface. Figure 3.3 shows the variations for a ribbed metal wall with 2.5 x 2.5 cm vertical ridges separated by 50 cm (2 feet). This surface is the same as listed for Test No. 3-0-14 and 3-0-22 of Table 3.1.

Two scans were made for Figure 3.4 as shown by a heavy and a light trace. The reflecting surface was a pre-cast concrete wall with protruding ribs (Test No. 2-0-22 and 2-1-42 in Table 3.1). These vertical ribs are 13 cm wide and protrude 30 cm from the wall at 100 cm intervals. Each of the two scans appear to show a

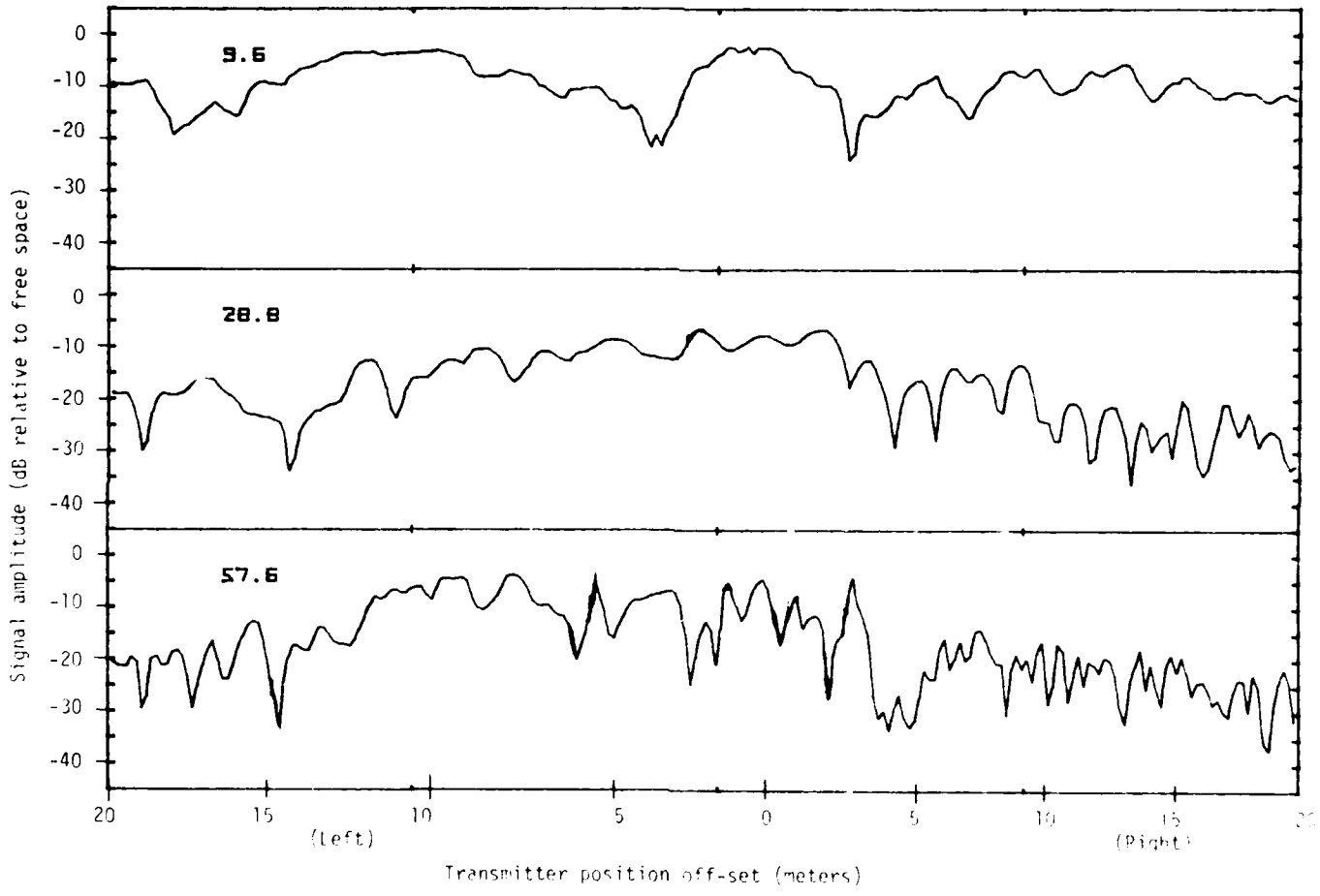

Fig. 3.2 Signal amplitude as a function of transmitter position offset (horizontal scan) using a solid brick wall as reflecting surface at a distance of 95 meters.

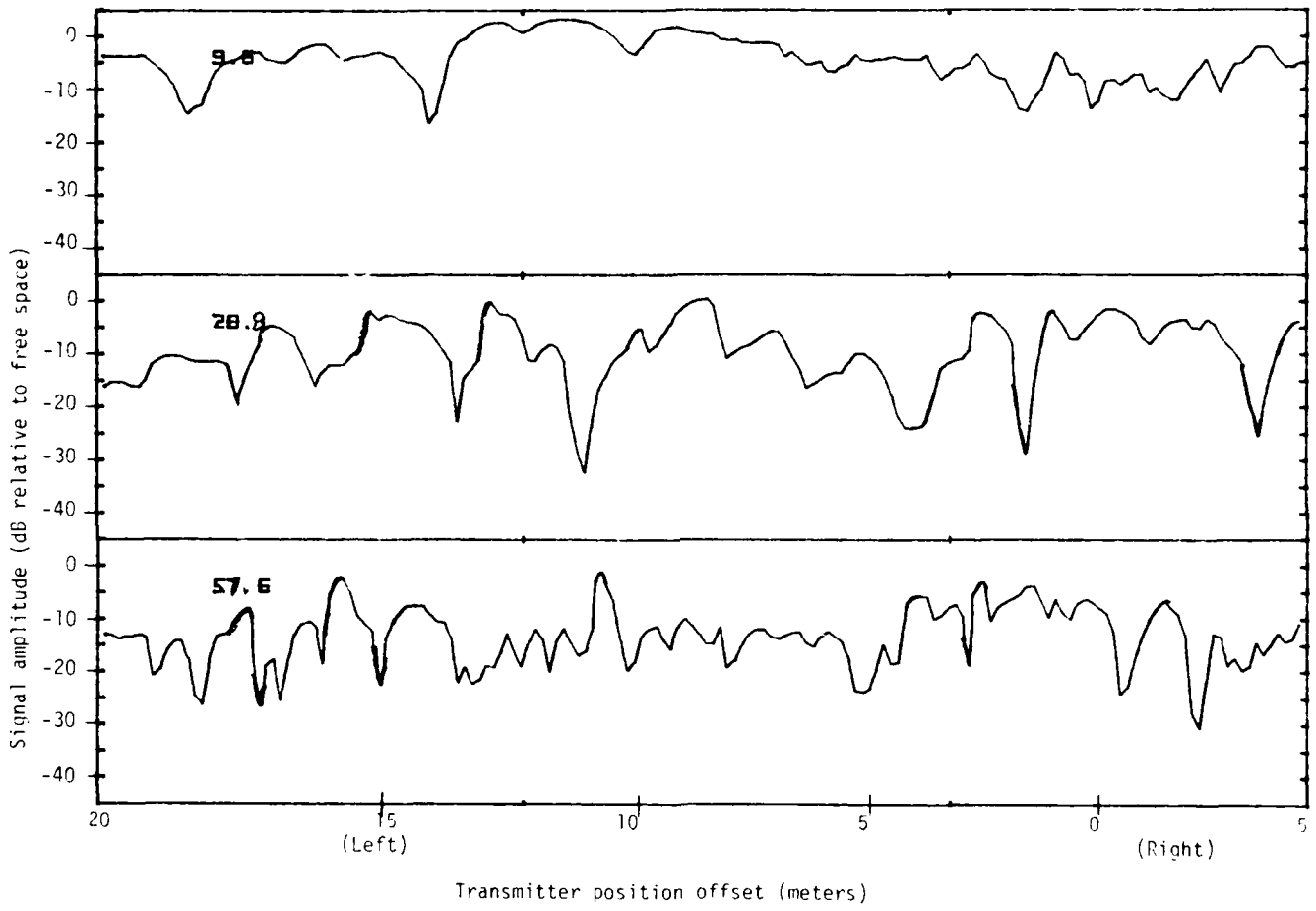

Fig. 3.3 Signal amplitude as a function of transmitter position offset (horizontal scan) using a metal wall as reflecting surface at a distance of 109 meters.

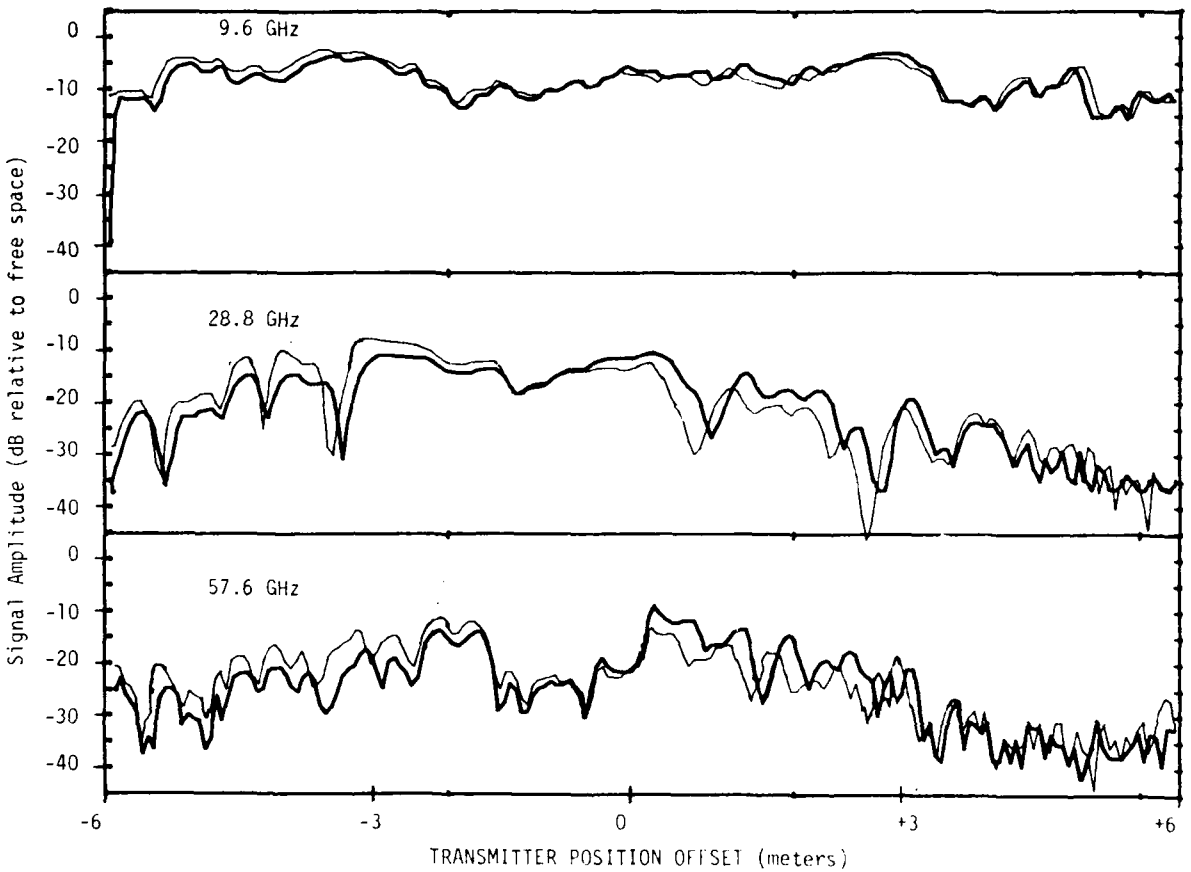

Fig. 3.4 Signal amplitude as a function of transmitter position offset (horizontal scan) using a ribbed concrete wall as reflecting surface at a distance of 64 meters.

periodicity and a mirror-image character, perhaps a result of the regularity of the protrusions. The reflected signals begin to rolloff for the upper two frequencies at about the +3 meter position because of the receiving antenna beamwidth limitation.

B. Reflection From a Reference Surface

The data recorded in Figures 3.2 through 3.4 were surprising both in the presence of 20 dB amplitude variations within the antenna beam and because of the lack of aspect sensitivity of the reflecting surfaces. To determine how these results compare to a smooth reflector, a 3 foot (92 cm) square aluminum flat plate was stationed 58 meters from the co-located transmitter and receiver. The small size of this reflector permitted precision orientation relative to these terminals.

The signal amplitude plots shown in Figure 3.5 are a calibration scan over a "free space" 106 meter path and a calibration scan using the 3 foot square reference reflector over a 116 meter folded path with the reflector positioned perpendicular to the path. A slight ground multipath fade might be present in the 9.6 GHz reflector plot because the less than 1 meter reflector height gave insufficient clearance for the 4.8 degree antenna beamwidth. At the higher two frequencies no appreciable ground multipath could occur due to a 1.2 degree beamwidth for each and in fact no measureable loss resulted on the reflected signal path indicating a reflection coefficient of -1. Also the antenna patterns repeated very closely on the reflected and folded path signal plots except for a slight pointing offset.

Using the same horizontal scan configuration (b of Figure 2.4) as in Figures 3.2 through 3.4, reference reflector plots are shown in Figure 3.6. Three separate horizontal scans with the transmitter were taken. The heavy trace is the signal plot versus transmitter position offset with the flat reflector oriented at zero degrees in azimuth angle. The medium and light traces that peak to the right of center were recorded with the reflector oriented at 1° and 2° counterclockwise, respectively. Signals reflected from a smooth flat plate as seen in Figure 3.6 produce a very well behaved pattern with a high degree of aspect sensitivity as would be expected. The zero degree orientation test was performed in an identical manner as in Figures 3.2 through 3.4 and when compared to those results, suggests that at zero incident angles, building surfaces have irregularities that produce considerable signal variation with slight spatial position change at wavelengths between 0.5 and 3 cm. Even a large, apparently flat brick wall (Figure 3.2) showed these variations.

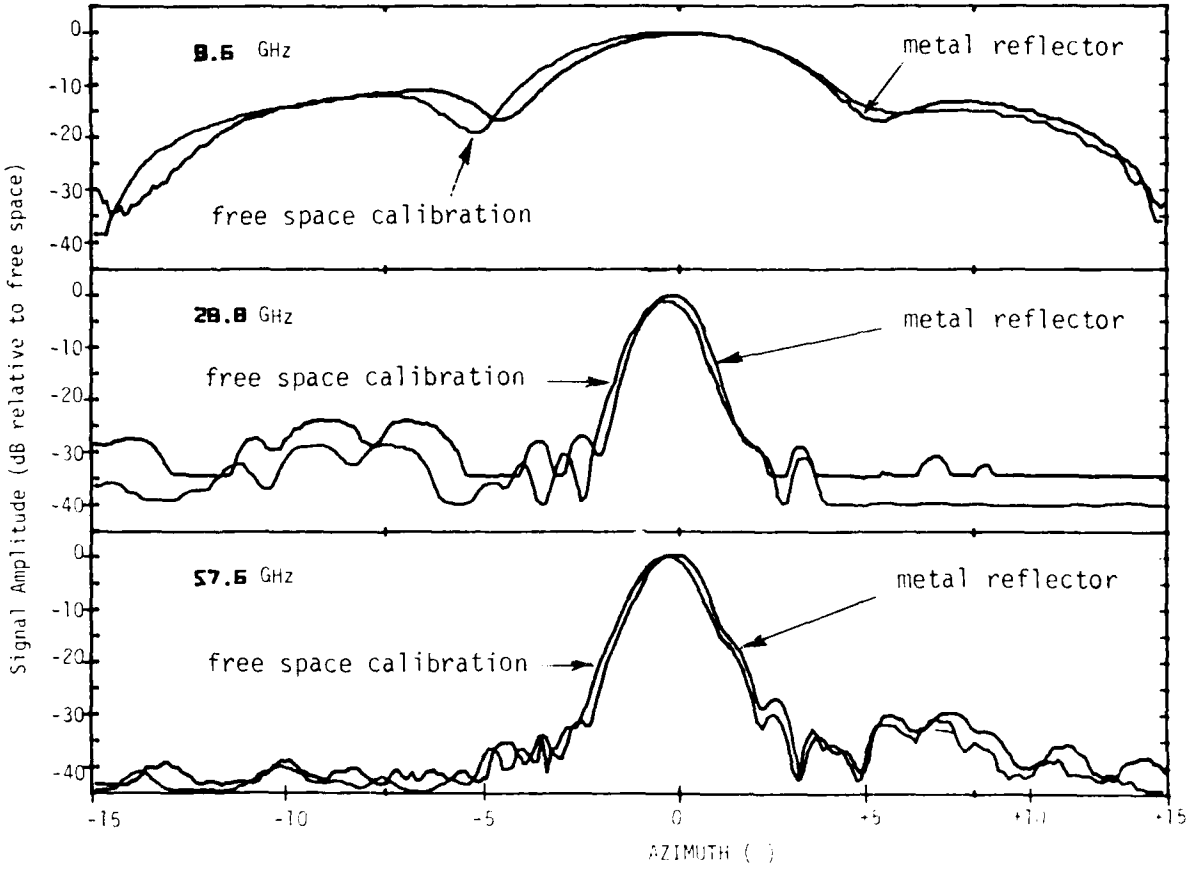

Fig. 3.5 Signal amplitude as a function of azimuthal pointing of the receiving antenna. As indicated the traces are from the 106 meter free space calibration and a 3 foot x 3 foot metal reflector on the 116 meter (round trip) path.

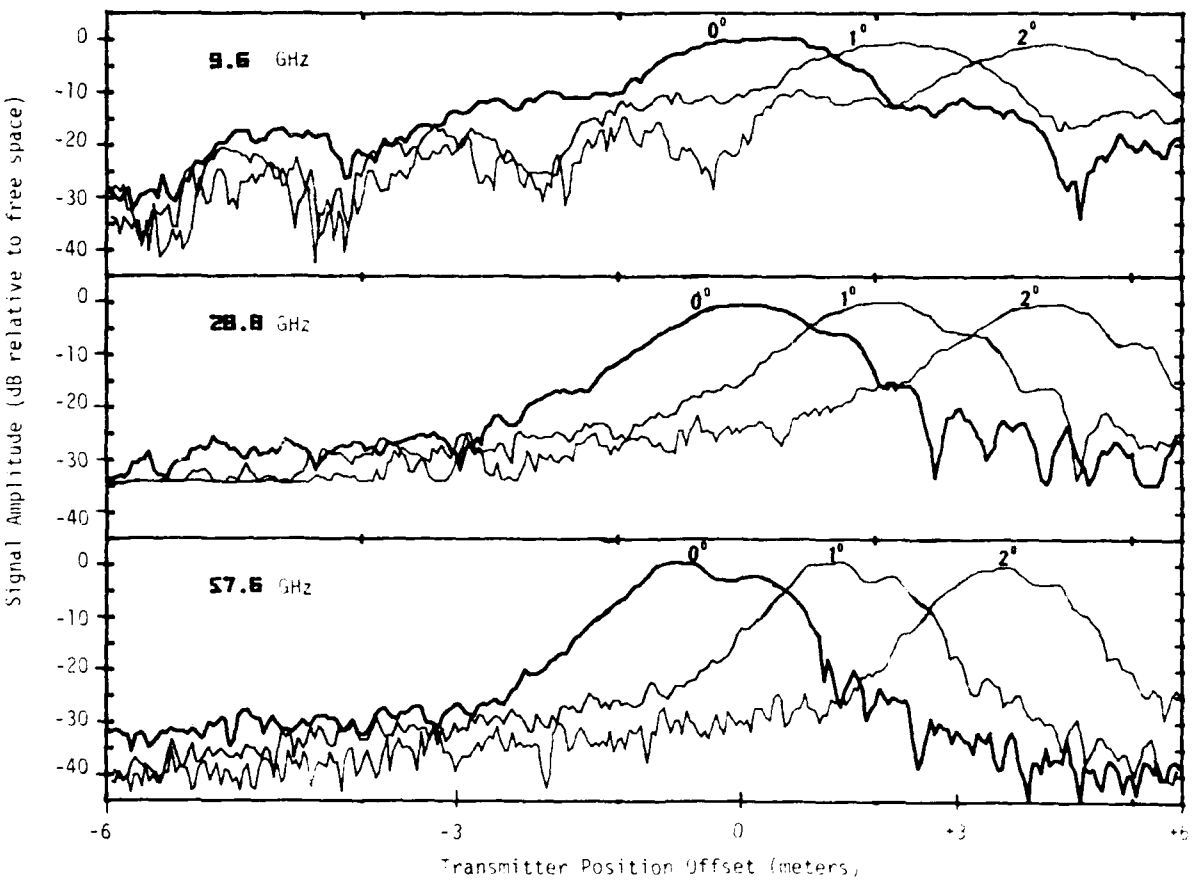

Fig. 3.6 The signal amplitude received from a 3 foot x 3 foot reflector at 116 meters (round-trip). The heavy line trace results from a scan with the transmitter and receiver co-located at the center position and with the reflector perpendicular to the transmitter-receiver to reflector line. The medium line trace is the result of having the reflector oriented 1° from perpendicular and the light line with the reflector at 2° from perpendicular.

C. Signal Amplitude (line-of-sight)

A series of tests were conducted to measure the relative amplitude of the received signal as a function of transmitter-receiver separation. These tests were conducted in an urban area (downtown Denver) and in a rural area (over both asphalt and graveled roads). In Denver, along 17th Street, the tests included three runs over a 0.9 km path. Street intersections occur uniformly at approximately 100 meter intervals. The building off-sets and structural surfaces vary as typically found in metropolitan areas. Three additional sets of data show signal amplitudes as a function of transmitter-receiver separation with receiver antenna pointing a variable. Off-set angles of 0°, 2°, and 4° were used in these tests. A receiver antenna pointing angle of 0° means the antenna is pointed along the transmitter-receiver line and the 2° and 4° pointing means the receiver antenna was pointing respectively 2° and 4° from the transmitter-receiver line. A third set of data was recorded with the transmitters and receivers separated at 485 meters. Azimuthal scans of the receiving antenna (± 15°) were made with the transmitting antennas pointing at 0°, 10°, 20°, and 30° for successive scans. Again the 0° pointing is along the transmitter-to-receiver line and the 10°, 20°, and 30° settings are with the transmitter antenna pointing off-line by 10°, 20°, and 30°.

The tests conducted in the rural areas, were along a 1.6 km path over the asphalt surface and over 1.6 km and 2.0 km paths over a graveled surface. These tests were conducted to obtain data for comparison to the urban results. Strong multipath fading is present in these runs.

1. Urban Area (zero angle pointing)

The tests along 17th Street in Denver were all conducted after 2200 hours to avoid heavy traffic. However, even in the early morning hours between mid-night and 4 o'clock, some traffic was present such as, street cleaners, garbage trucks, newspaper delivery vans, etc., and, it is nearly impossible to conduct a run without at least some minor interference from traffic. Signal variations due to traffic have a characteristically short duration on all channels or if the vehicle is moving along the direct path, a drop in level of 10 to 15 dB occurs.

The drawing in Figure 3.7 shows street intersections along 17th Street for that portion used in the urban tests. Also on the drawing is a height profile of the street. The broken line above the profile indicates the line between the transmitter and receiver which were 2.15 and 1.8 meters above ground, respectively. Line-of-sight was maintained for the entire run.

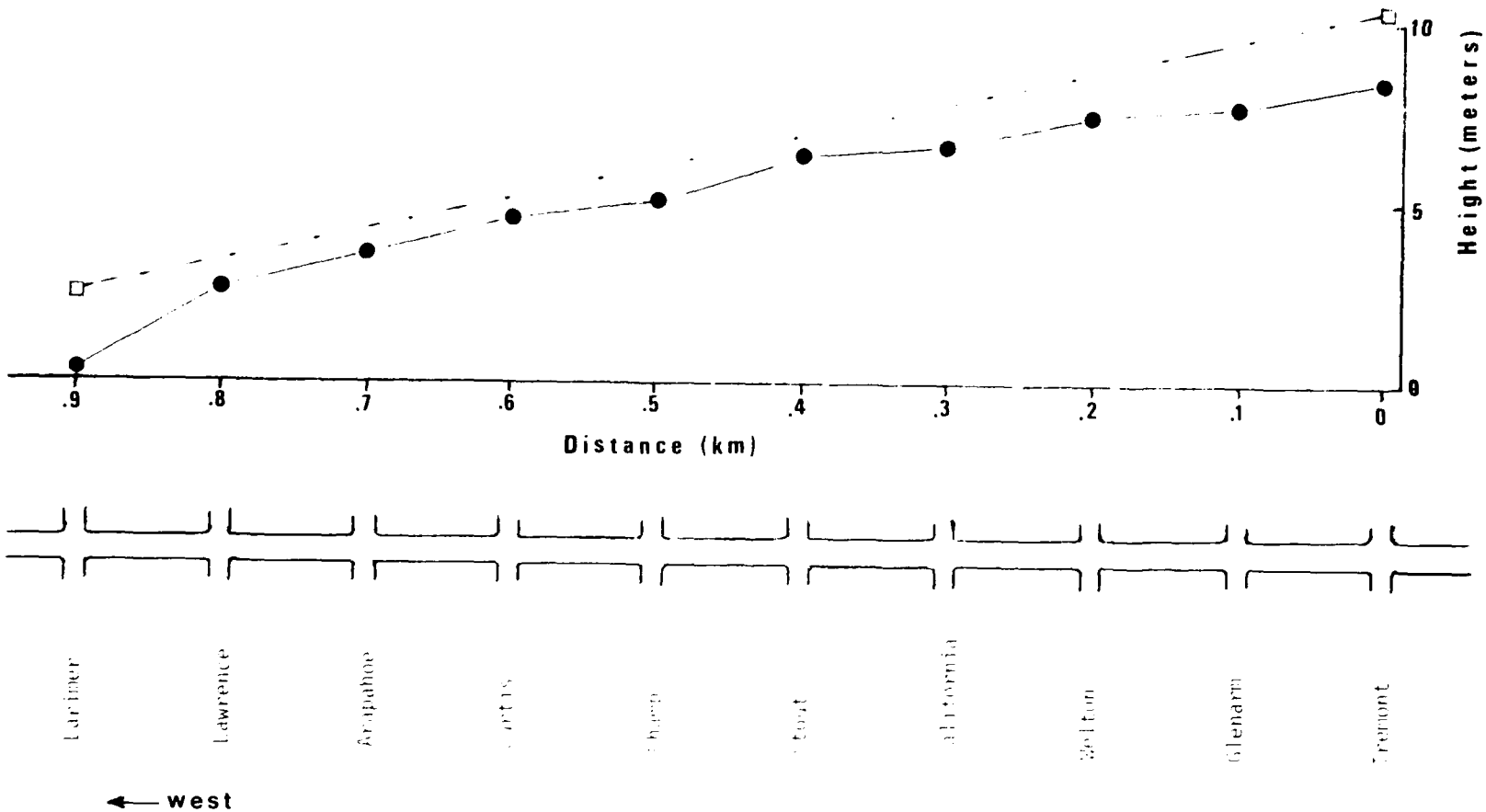

Fig. 3.7 A drawing showing the street intersections and relative height above ground of the portion of the 17th Street in Denver used to measure signal amplitude as a function of distance.

The picture of 17th Street shown in Figure 3.8 was taken at the Broadway intersection looking west. The receiver site for the urban tests was on the right-hand side of the street between Broadway and Tremont (the first intersecting street to the west).

The signal amplitude tracings for frequencies of 9.6, 28.8, and 57.6 GHz in Figures 3.9, 3.10, and 3.11 resulted from three runs along 17th Street starting at Larimer and ending at the receiver location near Tremont. The received signal amplitude 0 dB reference was obtained from a calibration measurement taken with the transmitter located between Welton and Glenarm, 170 meters from the receiver. The tracings exhibit a normal rolloff (-20 log R) as a function of the transmitter-receiver separation (R). The 57.6 GHz amplitude tracings show an additional rolloff due to the molecular oxygen absorption (approximately 10 dB per km at Denver elevation). Observed on all traces are the many shorter-term variations which are most likely multipath fades, some approaching 20 dB. These variations occur all along the path in a near random manner. Vehicles crossing intersections along the path or traveling along 17th Street in the same direction as the transmitter caused simultaneous fades in all channels as indicated by arrows in Figure 3.9. Further comments are made on these data, when compared to an open area over asphalt and graveled roads.

2. Urban Area (Receiver off-angle pointing)

A set of three runs were made along the 0.9 km path from Larimer to Tremont to assess the impact on the received signal amplitude of off-angle receiver antenna pointing. The test configuration for these runs is shown in Figure 3.12a. The street layout in Figure 3.12a shows the transmitter location at the start of the run and the stationary receiver location. For the first run, the receiving antennas are at 0° pointing (along the transmitter-receiver line). For the second and third runs, the receiving antennas are pointed off-angle 2° and 4°, respectively. The resulting signal amplitudes from these three runs are shown in Figures 3.13, 3.14, and 3.15, respectively, in the order of increasing frequency (9.6, 28.8, and 57.6 GHz).

The traces in these three figures are offset to more clearly display the characteristics of each run. All traces are plotted to the same amplitude scale and a 10 dB signal level is indicated in each figure. The top trace in each figure, zero angle pointing (RX = 0°), collectively are a replot of the data in Figure 3.11. The other two traces in each figure were made with the receiving antenna pointing off-angle as indicated (2° and 4°).

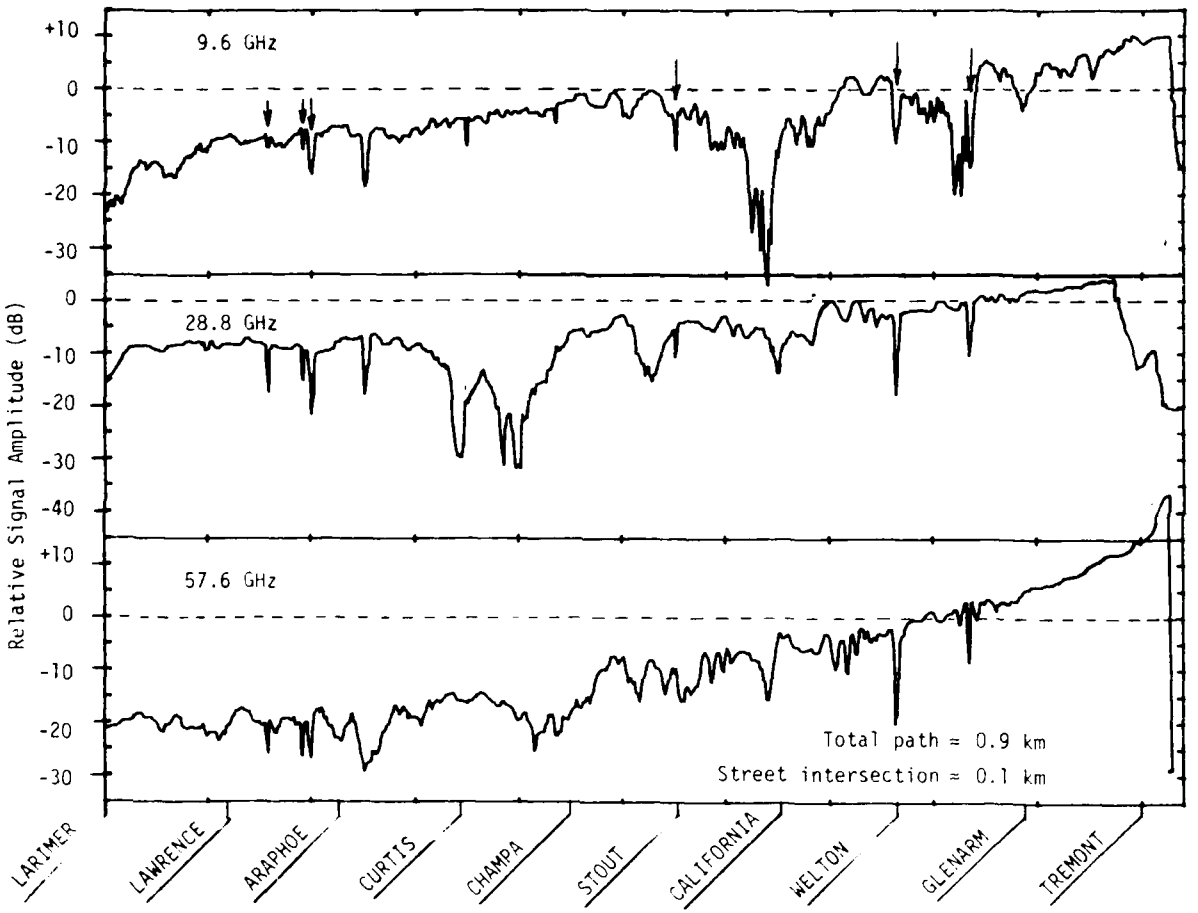

Fig. 3.9 Signal amplitude as a function of range measured along 17th Street in downtown Denver, CO. The transmitter is moved at a nearly constant velocity toward the receiver. The vertical arrows above the 9.6 GHz trace denote vehicles in the transmitter-receiver path. Horizontal antenna polarization.

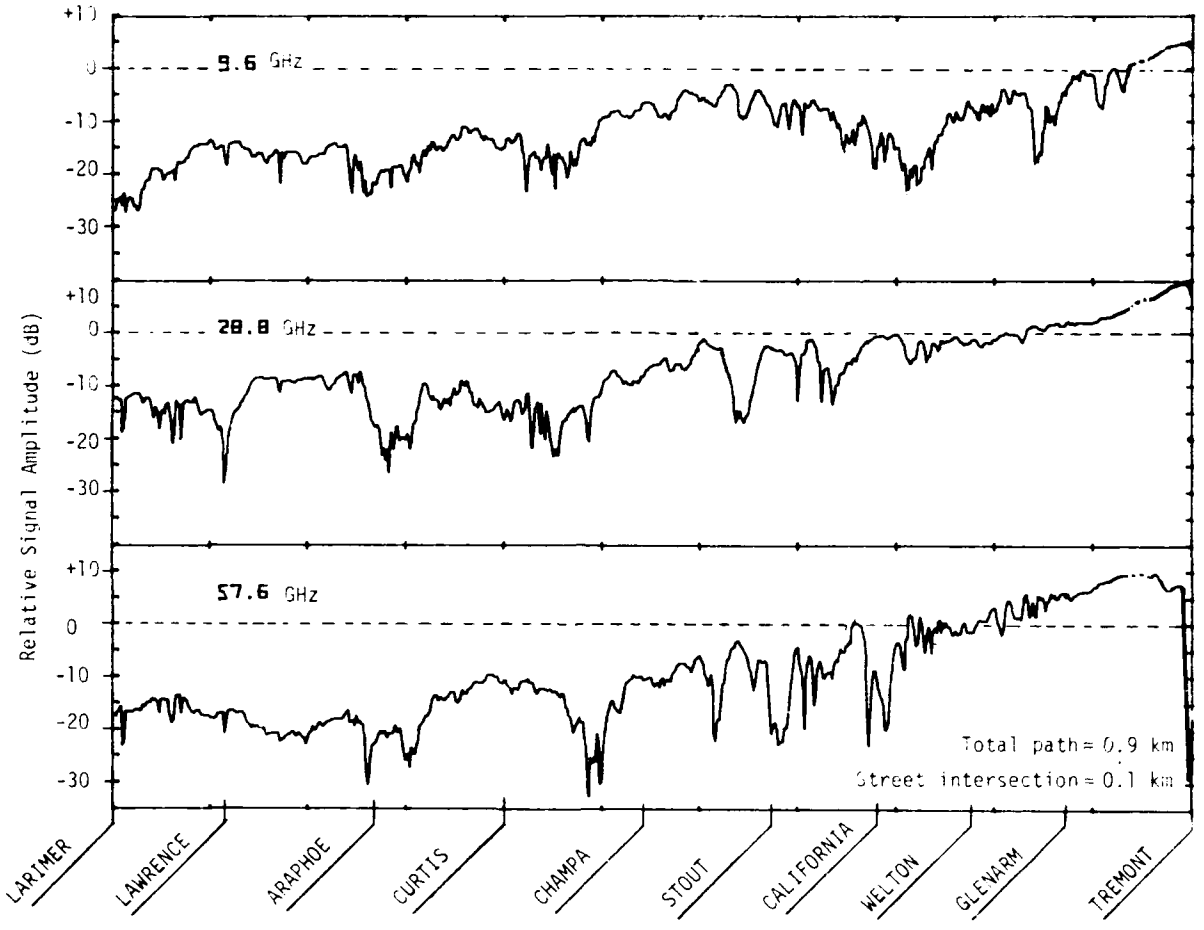

Fig. 3.10 Signal amplitude as a function of range measured along 17th Street in downtown Denver, CO. The transmitter is moved at a nearly constant velocity toward the receiver (run no. 1). Vertical antenna polarization.

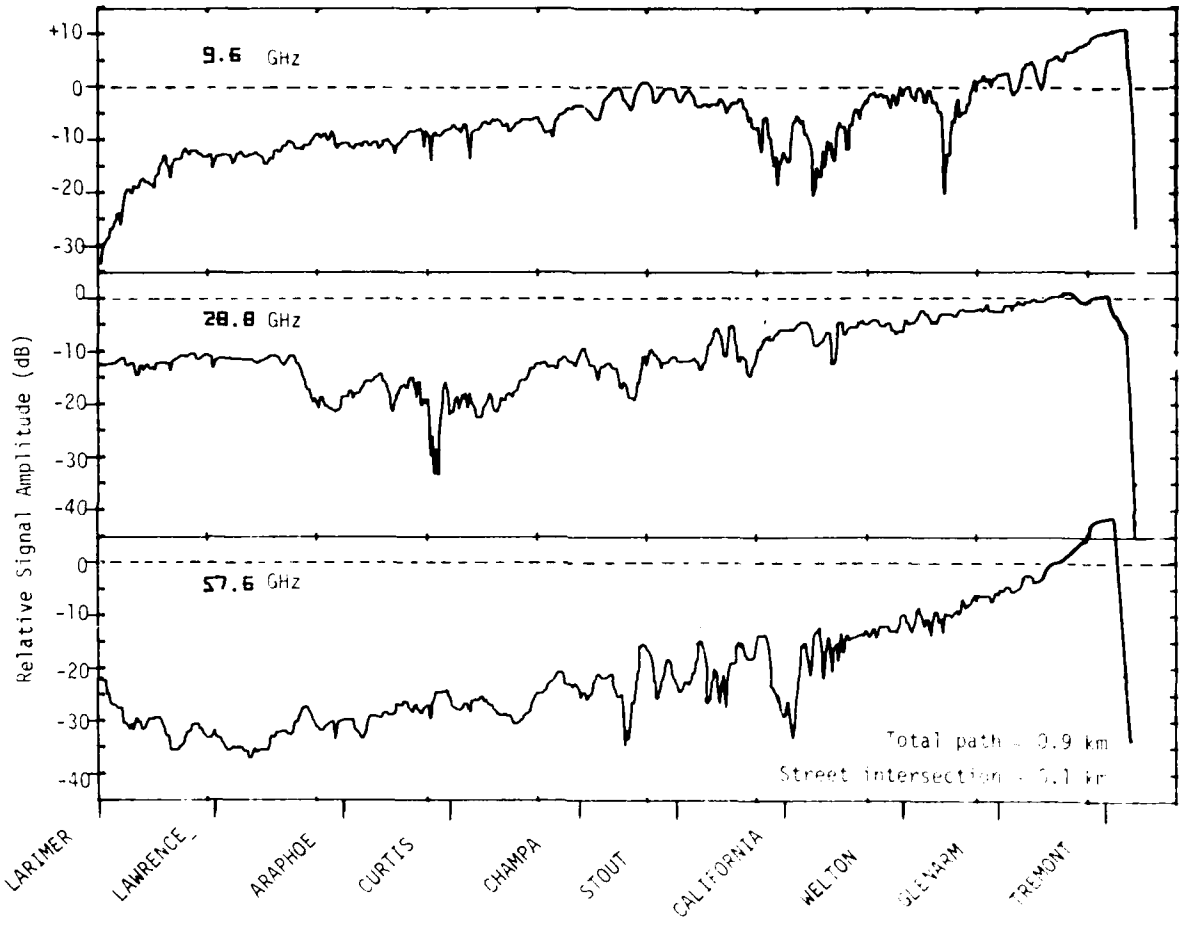

Fig. 3.11 Signal amplitude as a function of range measured along 17th Street in downtown Denver, CO. The transmitter is moved at a nearly constant velocity toward the receiver (run no. 2). Vertical antenna polarization.

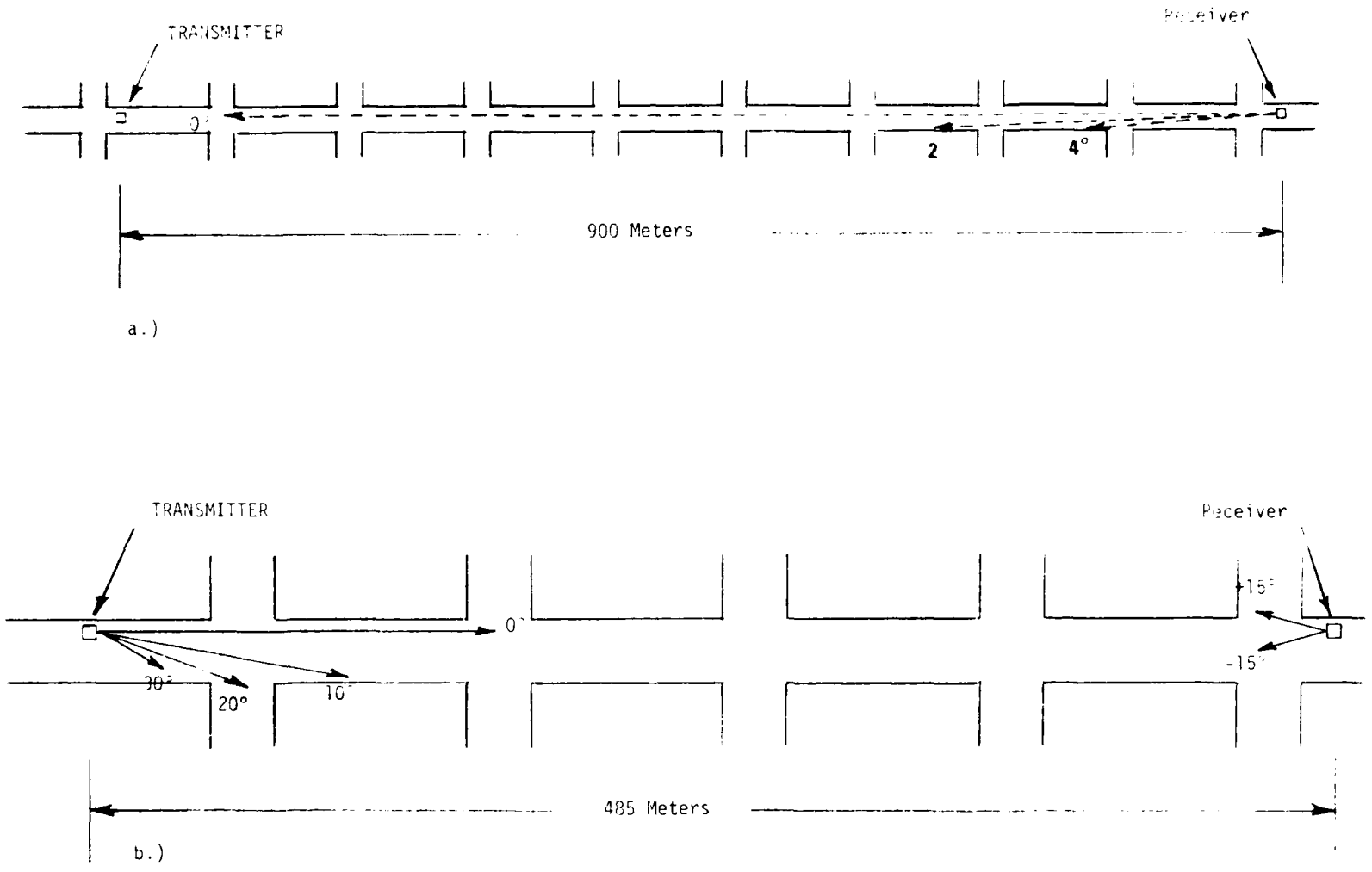

Fig. 3.12 Test configurations for the urban area off-angle runs.
a) Receiver antenna off-angle pointing.
b) Transmitter antenna off-angle pointing.

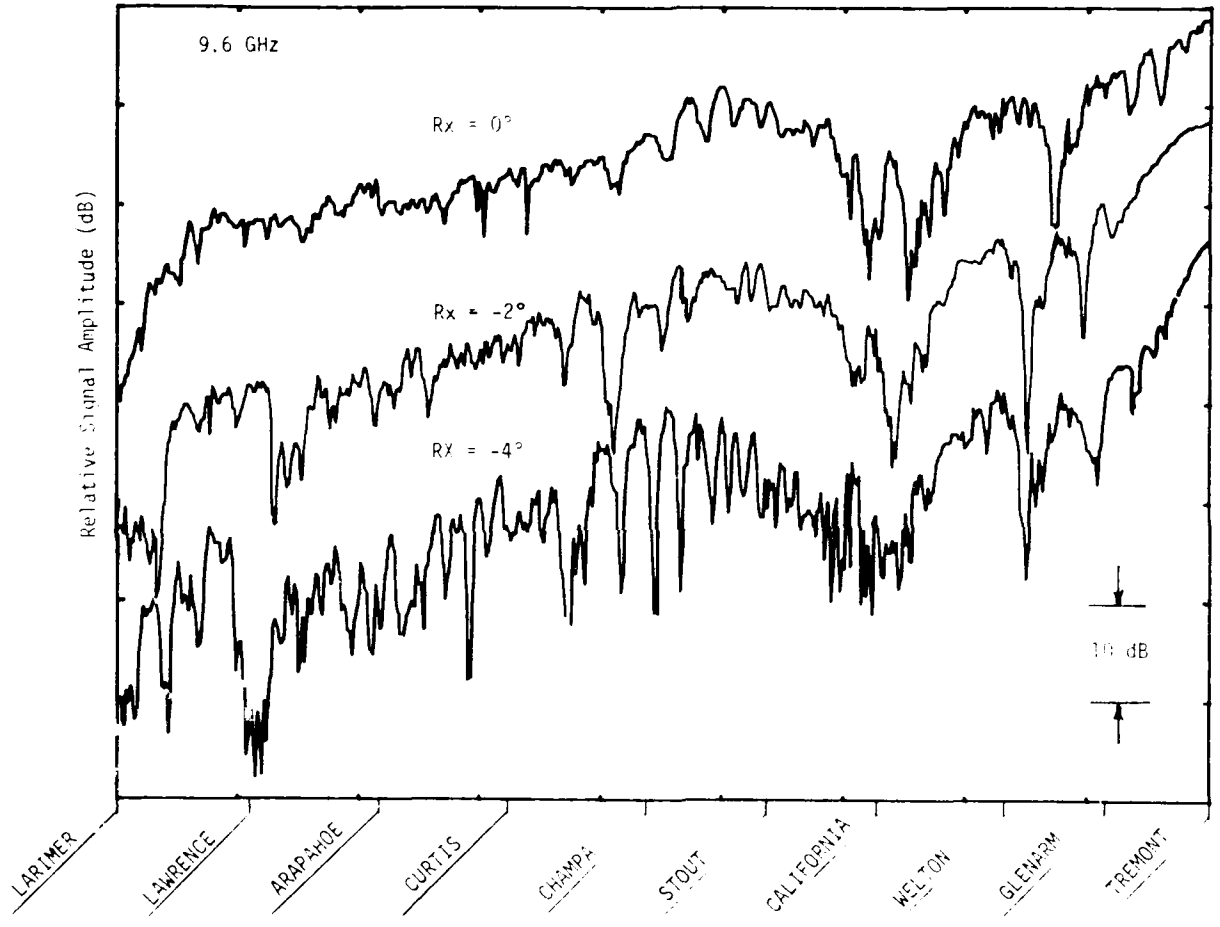

Fig. 3.13 Signal amplitude at 9.6 GHz as a function of range measured along 17th Street in downtown Denver, CO. The transmitter is moved at a nearly constant velocity toward the receiver. Vertical antenna polarization. The receiving antenna is aligned as indicated for each run.

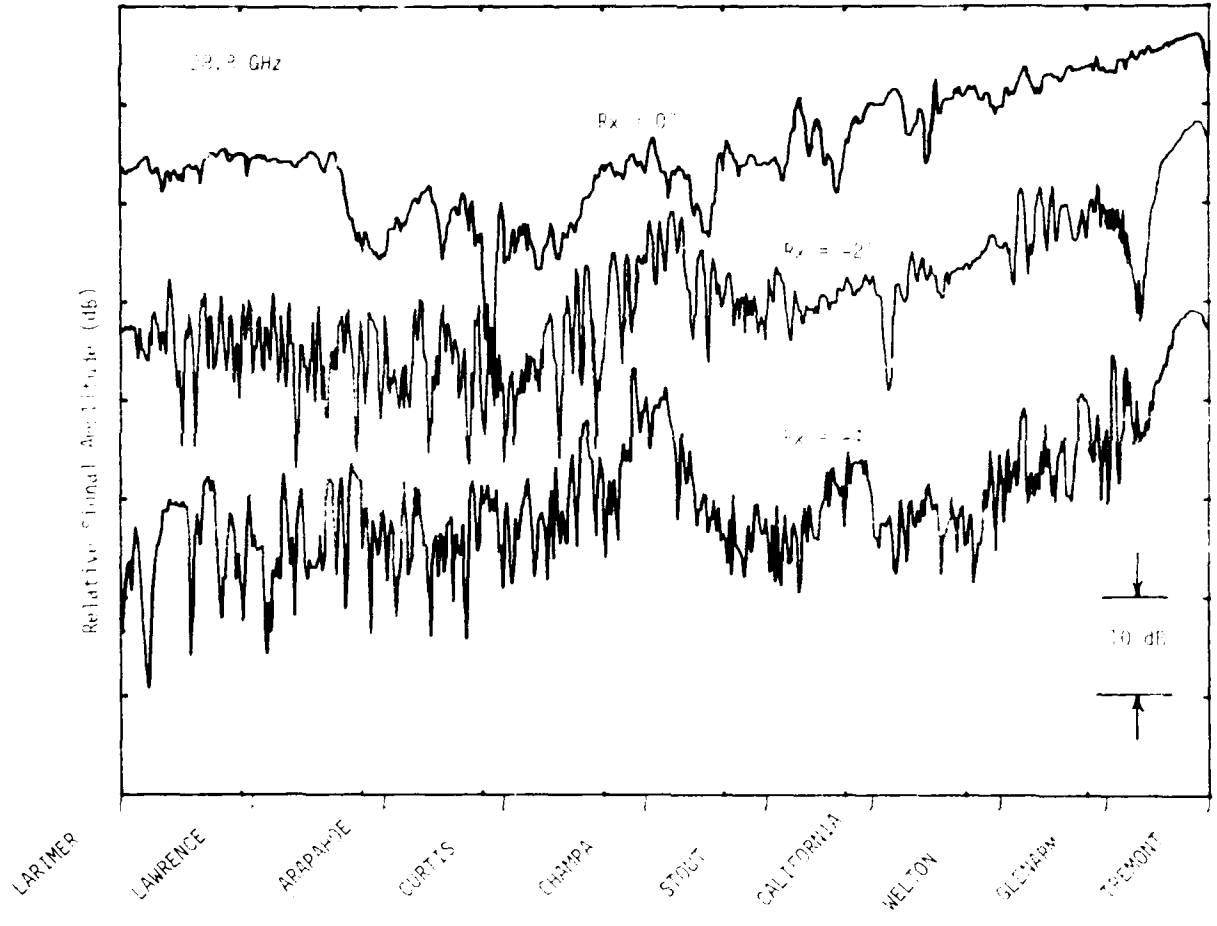

Fig. 3.14 Signal amplitude at 28.8 GHz as a function of range measured along 17th Street in downtown Denver, CO. The transmitter is moved at a nearly constant velocity toward the receiver. Vertical antenna polarization. The receiving antenna is [illegible] each run.

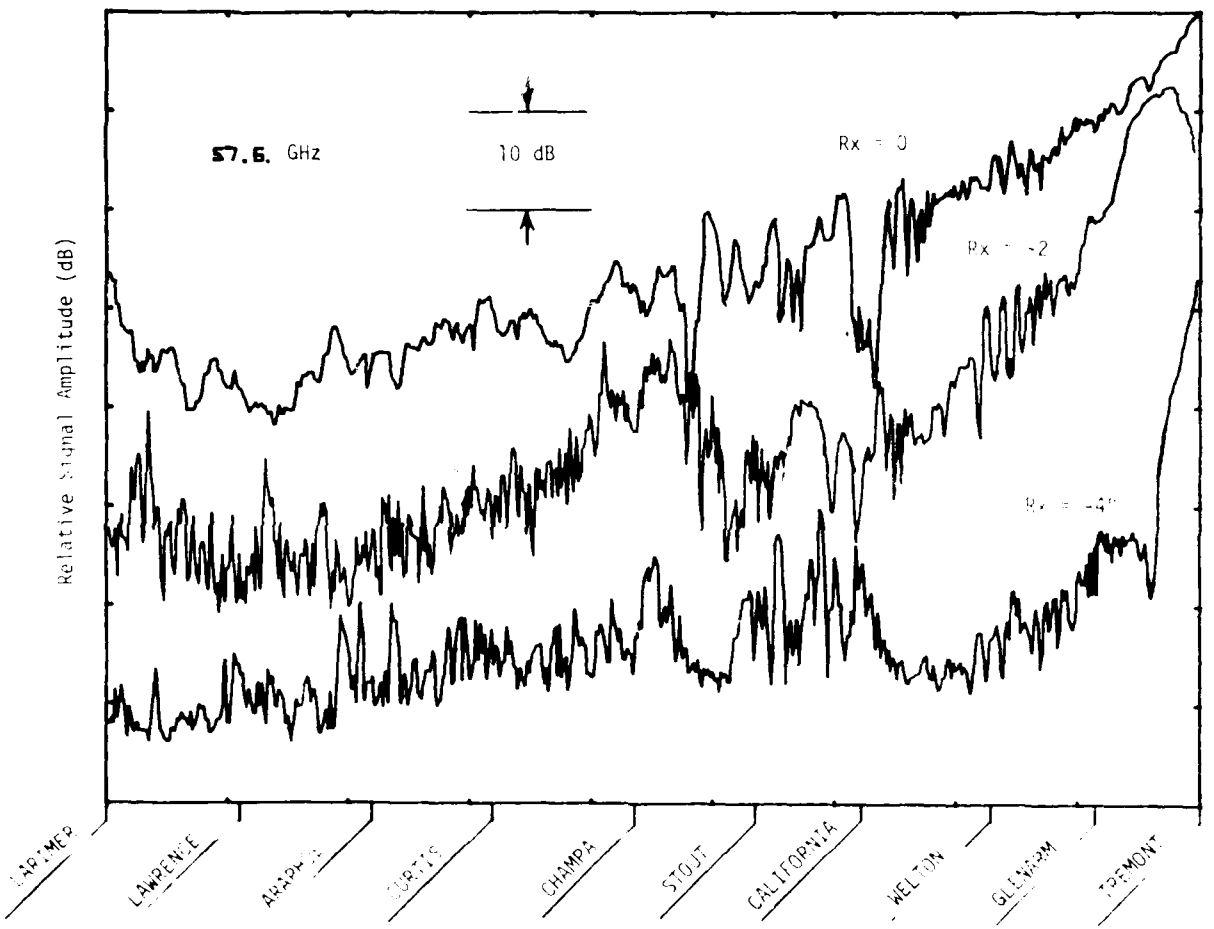

Fig. 3.15 Signal amplitude at 57.6 GHz as a function of range measured along 17th Street in downtown Denver, CO. The transmitter is moved at a nearly constant velocity toward the receiver. Vertical antenna polarization. The receiving antenna is aligned as indicated for each run.

This series of measurements shows an increase in the frequency of amplitude variations in the RX = -2° and RX = -4° compared to the direct pointing (RX = 0°) traces. These amplitude variations are a result of more numerous reflections from the building along the street at off-angle pointing. A succession of deep multipath fades (as a function of distance) occurred at 9.6 GHz between Curtis and Stout Streets for the RX = -4° pointing. Over such paths, more numerous reflections reduce the probability of deep destructive interference type fades. This data pertains primarily to systems using wide beam or omnidirectional antenna configurations where exact terminal locations are not known or multiple terminal coverage is required. Even when deep fades do not occur for these conditions, channel distortion may be present particularly for wide bandwidth channels where frequency selective fading can occur within the bandpass due to long multipath delays. The spacing in frequency (F) of the fade nulls is $F = \frac{1}{t_2 - t_1}$ where $t_2 - t_1$ is the difference in path delay time between the direct signal and the multipath signal.

3. Urban Area (transmitter off-angle pointing)

Another test set conducted at the 17th Street location in Denver, consisted of a series of receiver antenna azimuthal scans with the transmitter antenna pointing at 0° (on-line) and 10°, 20°, and 30° (off-line). The transmitter-receiver configuration for these tests is shown in Figure 3.12b. Data from the off-angle pointing measurements are displayed in Figures 3.16 through 3.21 for both vertical and horizontal antenna polarization at each operating frequency. Figure 3.22 is included to provide a comparison of the "free space" antenna pattern and the 17th Street azimuth scans with the transmitter pointing directly at the receiver (TX = 0°) for all three frequencies and both linear polarizations. In Figure 3.22 it is apparent that very little information on off-angle reflected signals can be obtained with the 9.6 GHz scans, because the widebeam (~ 5°) receiving antenna cannot separate the multipath signals from the direct line-of-sight (LOS) path signal at zero receiver pointing. However, scans for the higher two frequencies with 1.2 degree beamwidth receiving antennas show multipath signals nicely separated. For the two higher frequencies, it can be seen from Figure 3.22 that off-angle multipath components are distinguishable from the transmitted signal arriving on side lobes of the receiving antenna until the multipath signal is about 30 dB below the direct LOS level. This applies for angles greater than + 2 degrees from zero pointing on the main receiving beam. At most other angles the side lobes are approximately 40 dB

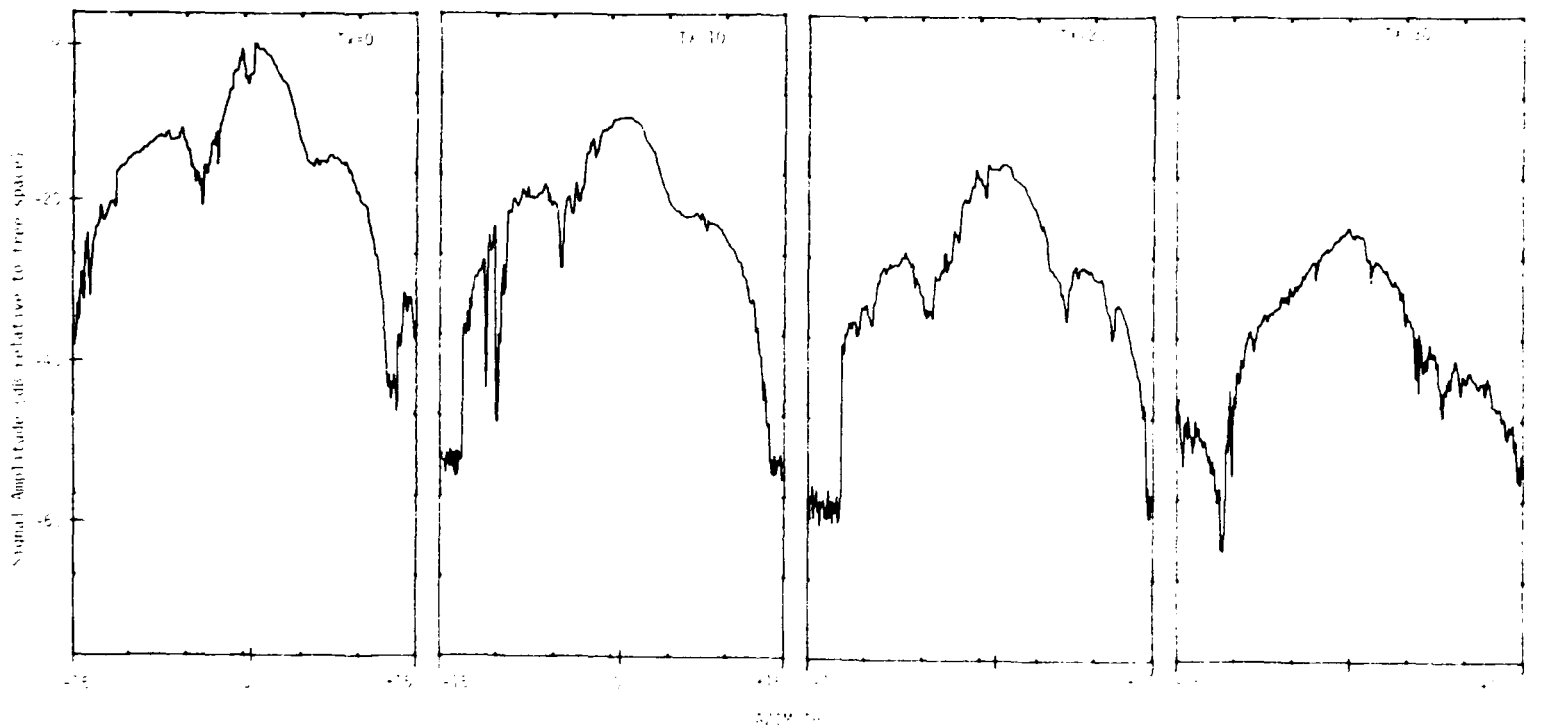

Fig. 3.16 A comparison of measured signal levels for 0°, 10°, 20°, and 30° off-angle transmitter antenna pointing. Vertical-vertical antenna polarization at 9.6 GHz.

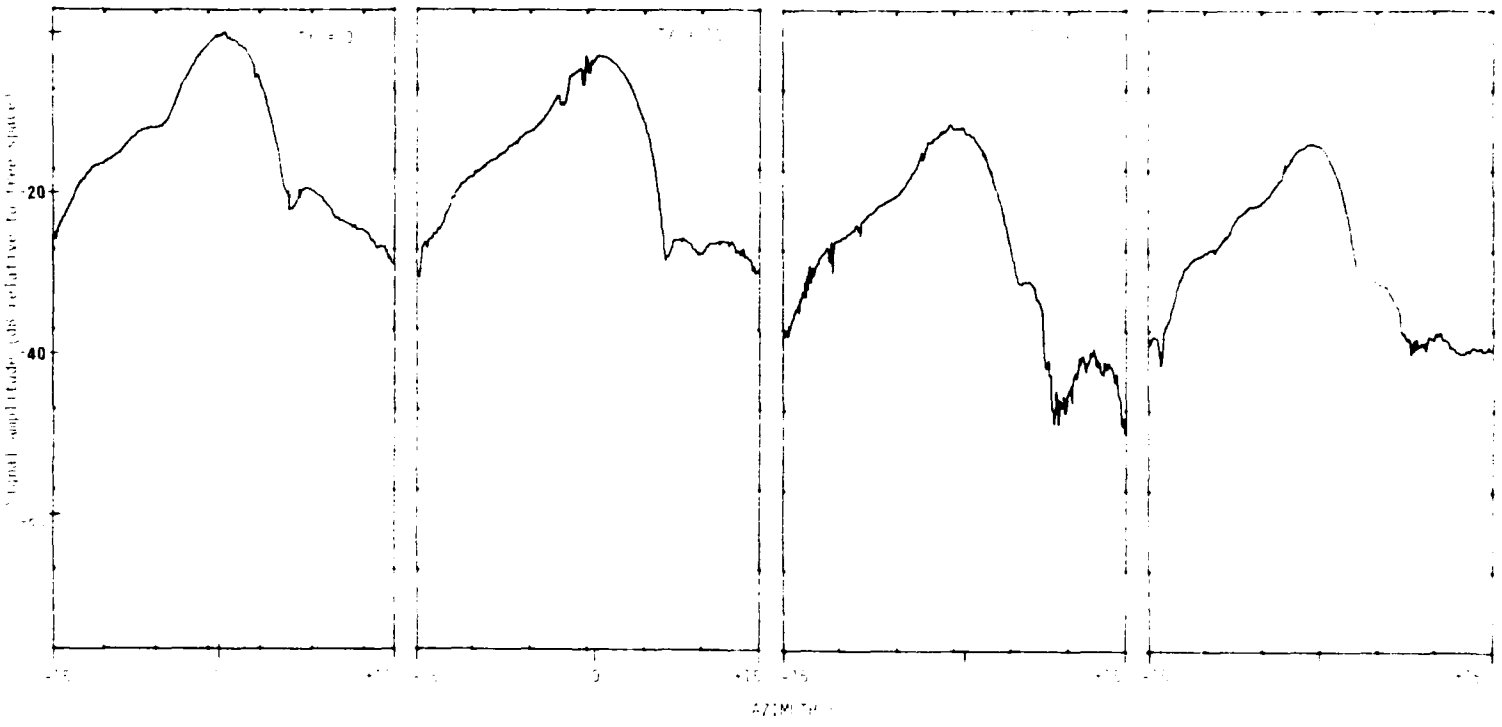

Fig. 3.17 A comparison of measured signal levels for 0°, 10°, 20°, and 30° off-angle transmitter antenna pointing. Horizontal-horizontal antenna polarization at 9.6 GHz.

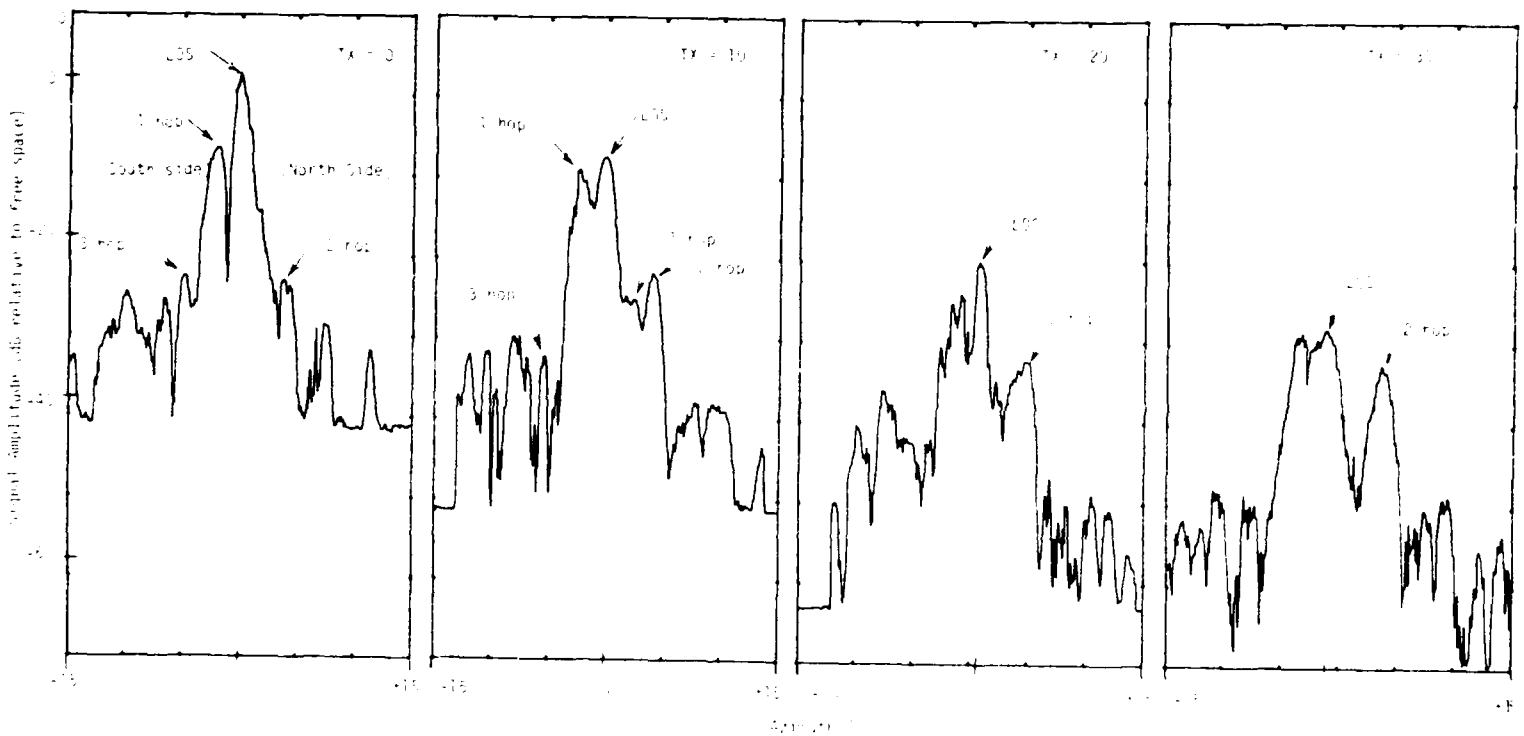

Fig. 3.18 A comparison of measured signal levels for 0°, 10°, 20°, and 30° off-angle transmitter antenna pointing. Vertical-vertical antenna polarization at 28.8 GHz.

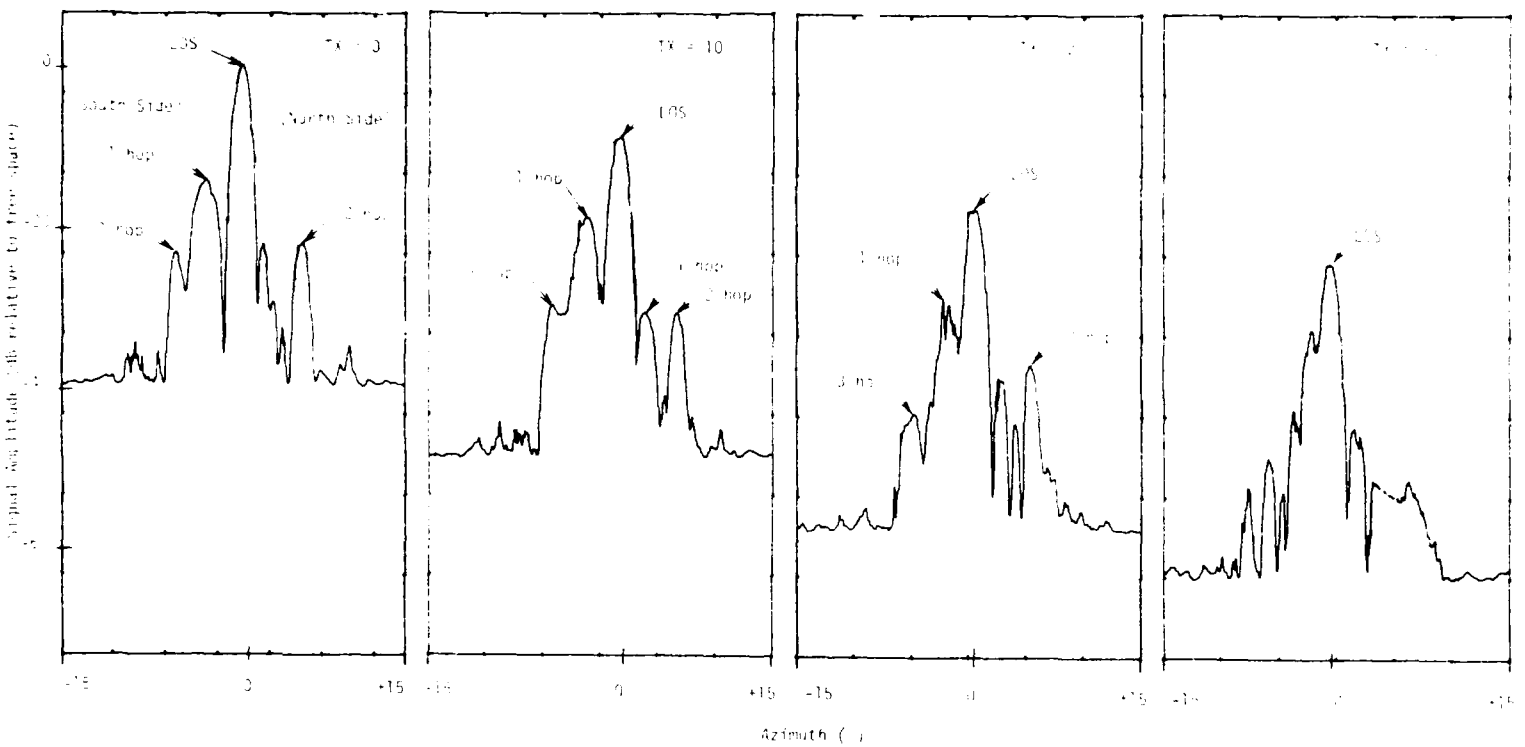

Fig. 3.19 A comparison of measured signal levels for o°, 10°, 20°, and 30° off-angle transmitter antenna pointing. Horizontal-horizontal antenna polarization at 28.8 GHz.

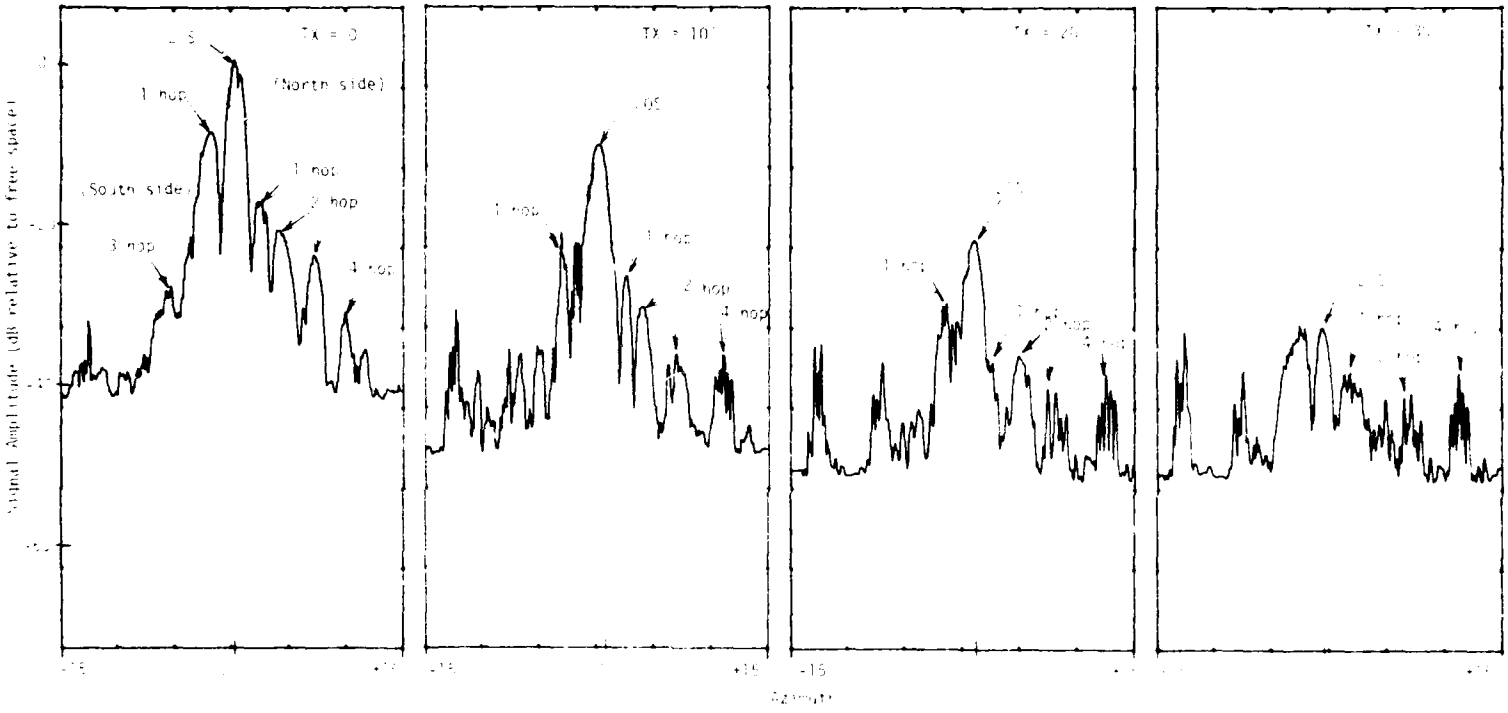

Fig. 3.20 A comparison of measured signal levels for 0°, 10°, 20°, and 30° off-angle transmitter antenna pointing. Vertical-vertical antenna polarization at 57.6 GHz.

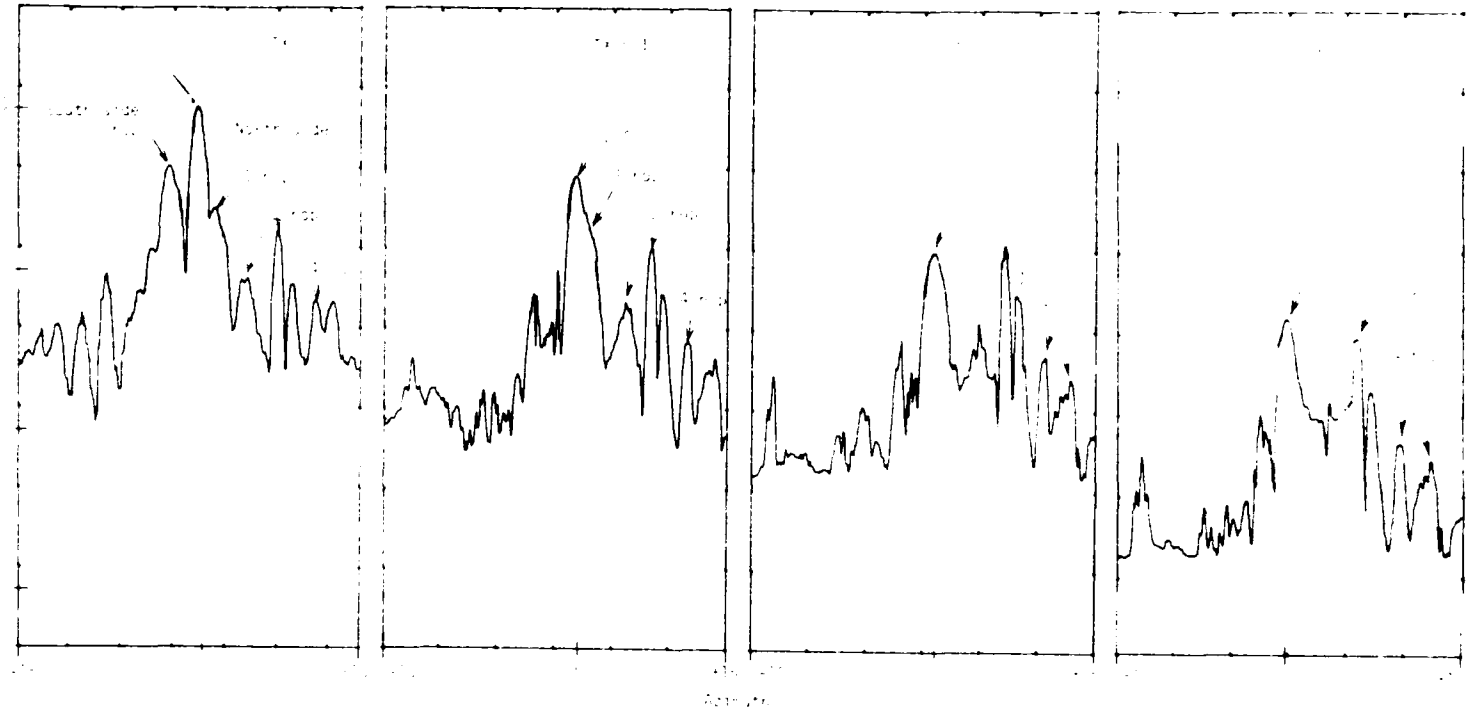

Fig. 3.21 A comparison of measured signal levels for 0°, 10°, 20°, and 30° off-angle transmitter antenna pointing. Horizontal-horizontal antenna polarization at 57.6 GHz.

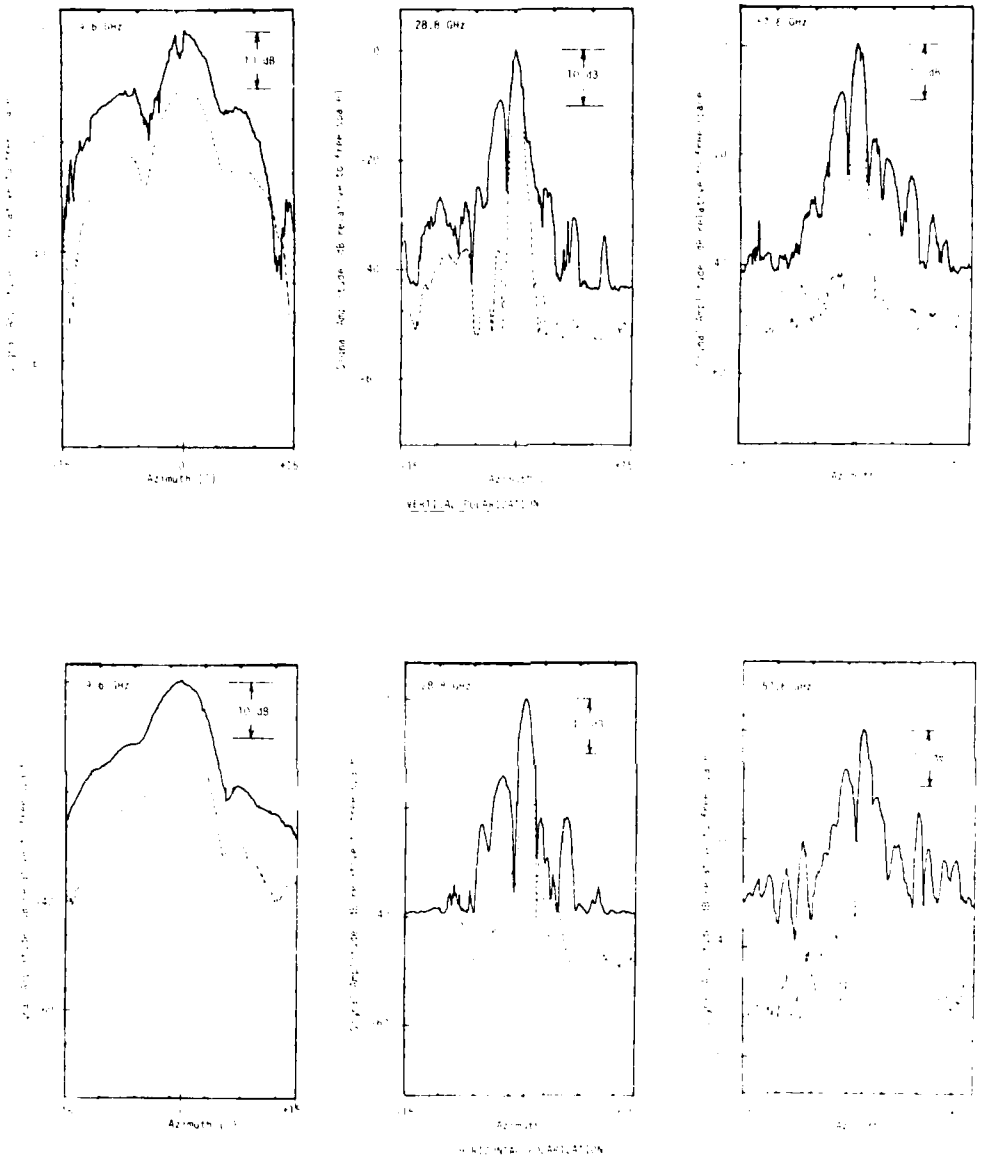

Fig. 3.22 A comparison of measured signal levels for 0° transmitter antenna pointing to open field calibration levels. The calibration trace (broken line) is off-set 10 dB at 0° azimuth.

down which permits the detection of multipath signals within the useful range of interest. If, for example, the multipath reflection were 6 dB greater than the signal received on the direct path from the side of the receiving antenna, the maximum variation of the peak signal due to constructive and destructive interference would be + 3.5 and -6 dB. This variation would show as an irregular fringing of the peak signal envelope as the receiving antenna is scanned (Figures 3.18 through 3.21). Similar fringing will also occur around the peak multipath signal envelope if several multipath reflections are in the scanned beam simultaneously.

3.1 Mechanics of surface reflections

If it is assumed that the off-angle peak signals are from flat surfaces of buildings, the effective two-way reflector gain is expressed by $20 \log \frac{4\pi A_r \cos \theta}{\lambda^2}$ where A is the area of the surface, r is the reflection coefficient, θ is the angle between the incident and reflected ray, and λ is the rf wavelength. The geometry of 17th Street and the sharpness of the off-angle signal peaks in the higher frequency scans (28.8 and 57.6 GHz) both suggest a flat surface reflection is a reasonable assumption. As explained earlier in the text, the A/λ^2 terms are removed from the gain expression when comparing signal levels at the three frequencies because all recorded signal levels are made relative to a 106 meter calibration path. The reflection coefficient (ρ) has a frequency dependency involving the roughness of the reflecting surface relative to λ. Some discussions are found indicating that ρ decreases as the frequency increases at millimeter wavelengths due to conductivity and permittivity properties but quantitative values were not found in a nonexhaustive literature search. For shallow angle of incidence the surface roughness can be greater without appreciable effect on ρ. Using an angle of 5 degrees, for example, a surface is considered to be smooth by the Rayleigh criterion ($H = \lambda/8 \cos \theta$), if H values of 3.5, 1.5, and 0.8 cm are not exceeded for frequencies of 9.6, 28.8, and 57.6 GHz respectively.

Another factor is the effect on r as θ tends toward 180 degrees (shallow incidence angle) as is the case for a long path down a city street. Figure 3.23 shows a plot of r and grazing angle of an incident wave on sea water and medium dry ground, after Hall[3]. Curves for 1 and 3 GHz are shown but little information has been found for higher frequencies. From the curves, one might expect the Brewster angle, the angle where r is a minimum, to occur between 5 and 15 degrees on the 17th Street path. The reader is reminded that the curves of Figure 3.23 are over horizontal reflecting surfaces where the Brewster angle applies to the vertical polarized wave; but for a city street where vertical surfaces are the reflector,

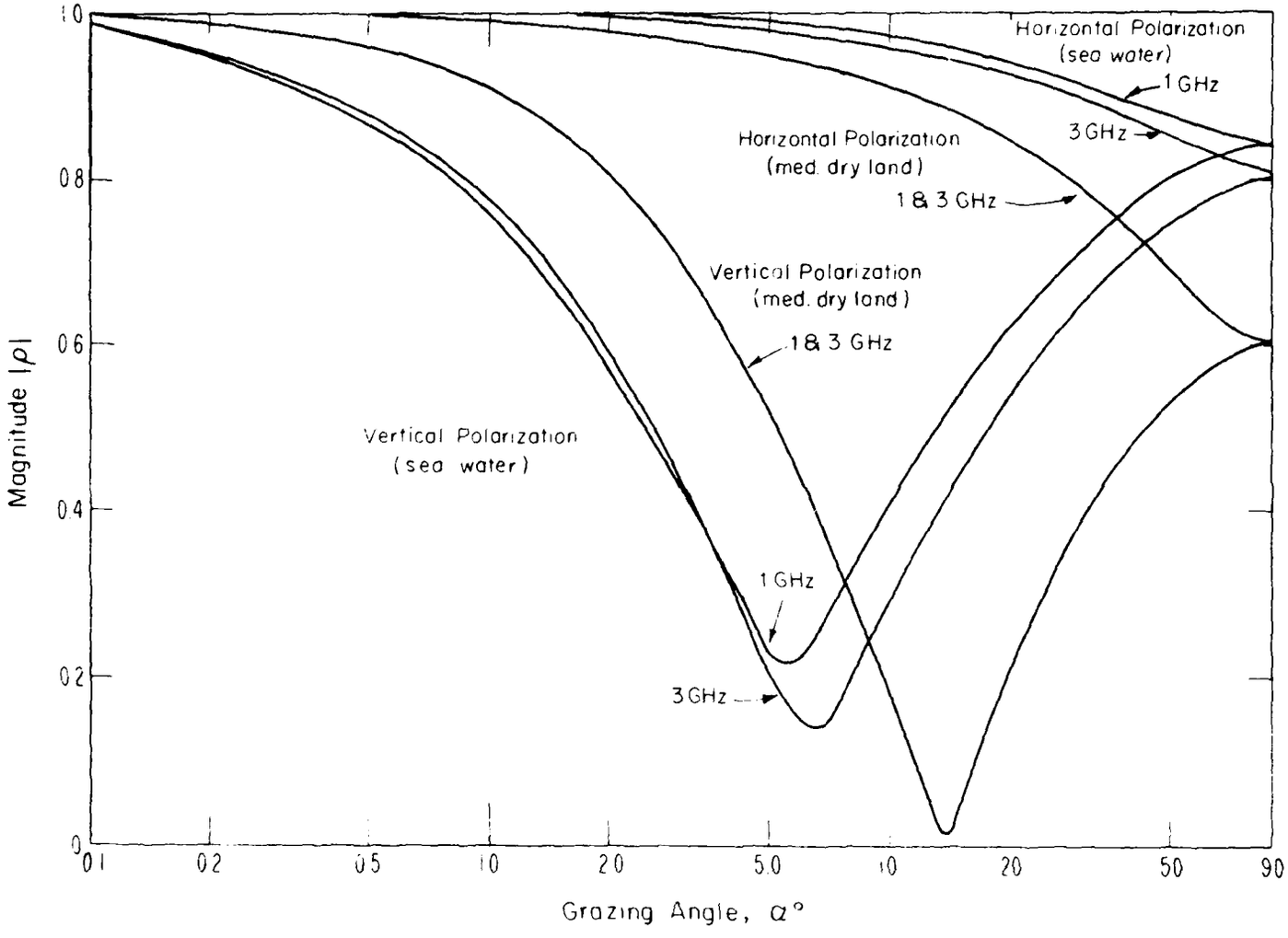

Fig. 3.23 Magnitude (ρ) of the reflection coefficient of a plane surface as functions of grazing angle α for vertical and horizontal polarization at 1 and 3 GHz.

the Brewster angle applies to horizontally polarized wave. The value of . is dependent on the permittivity and conductivity of the reflecting surface and these parameters change quite rapidly at frequencies above 10 GHz for most materials[4]. The primary effect is a marked increase in conductivity resulting in an increase in . . The trend is for reflection characteristics from a plane surface to follow closer to that of sea water as the frequency reaches into the millimeter wave band.

If the reflection surface is large, i.e., exceeds in dimension the axis of the first Fresnel ellipse, a possible additional frequency dependent factor is that the phase shift along the wave front at the receiver can combine to produce a signal reduction. At 30 GHz (λ = 1 cm) a reflection at the midpoint of 485 meter path from a surface at streetside results in a first Fresnel horizontal axis diameter of near 40 meters and near 1.7 meters for a vertical axis diameter. For 60 GHz (λ = 0.5 cm) the horizontal and vertical axes are about 30 and 1.3 meters, respectively. A visual inspection of the path at street level found no surfaces with dimensions of this extent, thus meeting the Rayleigh criterion, but very large surfaces with higher roughness factors are present. Predicting the manner in which surfaces of this complexity in roughness will add in reflected signal amplitude is very difficult. Also apparent by visual observations is the fact that fronts of buildings and frequently adjacent buildings have offset differences of up to 2 meters. This geometry can produce added reflecting surfaces satisfying Snell's law resulting in multiple signals within the receiving antenna beamwidth. A phase interference between signals can result and is believed to cause the ragged shape in the amplitude response near the amplitude peaks in several of the scans.

The 1.2° receiving beam projects an ellipical pattern on the vertical building surface at midpath with axis of about 120 by 5.2 meters at the 1/2 power points which provides an indication of the size of the illuminated area.

3.2 Reflection paths

With this introduction to some of the processes that determine the characteristics of reflected signals along a city street, the path was examined in detail to attempt to determine the source of the signals in Figures 3.18 through 3.21. When the ray paths of the dominant reflections are traced on a scaled drawing of the 485 meter path, the reflecting surfaces are readily located with good agreement in path geometry. This path shown in Figure 3.24 was selected for convenience of terminal location and it was clearly impossible to predict potential reflection points in advance by siting down the path. Photographs of the street in Figure 3.25 show the variety of obstructions lining the streets and along building fronts.

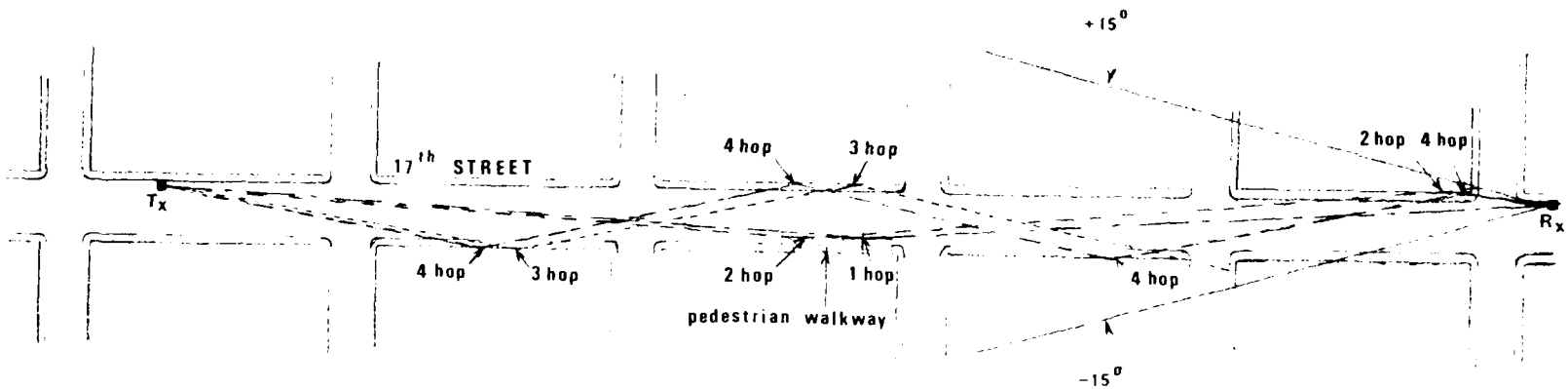

Fig. 3.24 A trace of 1, 2, 3, and 4 hop paths on 17th Street in Denver, CO.

a)

b)

c)

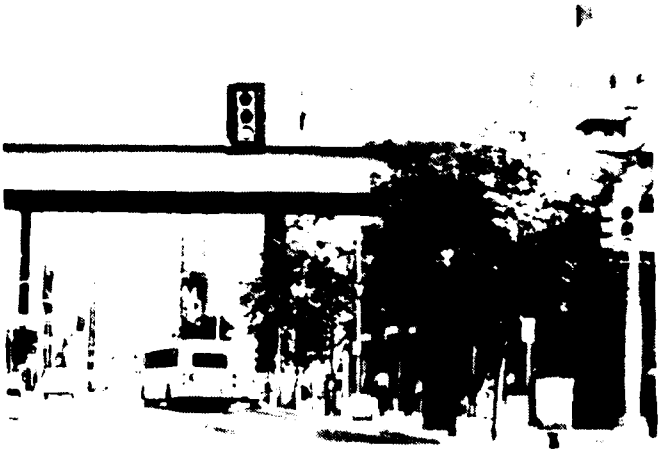

Fig. 3.25 Photographs of street fronts along 17th Street in Denver, CO.

To minimize or eliminate traffic in the path, measurements were made during the 11 PM to 5 AM hours and the timing of data recording was adjusted to reduce the number of vehicles in the path. By using the angle data from the receiver antenna scans and Snell's law the location of the reflection points was calculated. Both the distance down the path and the reflecting structure along the street were determined. In each case, using angles where amplitude peaks occurred, a flat-parallel surface was verified. Six reflection points were located and in each case the extent of the surface was less than 1-1/2 meters in either the horizontal or the vertical dimension without a major break (defined by $H = \frac{\lambda}{8 \cos \theta}$) in flatness or off-set distance. An elevation difference between terminals made it difficult to visually determine the height of the reflection points with precision. Of the six points two of the surfaces were window glass, two were wood, one was brick, and one was concrete aggregate. Several other reflection surfaces were a mixture of brick, glass, wood and concrete aggregate with irregular patterns.

An error of about 45 meters appeared at the scan angle of -2.5° (Figures 3.18-3.21) while tracing the drawing (Figure 3.24) for the 1-hop ray. A physical inspection of 17th Street showed a 3 meter high by 40 meter long wooden-panel pedestrian walkway about 1-1/2 meters on the street side of the curb which placed the ray intersection in perfect agreement. This walkway provides for the 1-hop reflection (south side) and one surface of the 2-hop reflection. The photograph in Figure 3.25a shows this structure which is not covered between 1 and 2 meters of its 3 meter height except for vertical 2" x 4" studding.

The 2-hop mode was reflected from the surfaces shown in Figure 3.25b. Note that this building has a glass surface offset almost 6 meters from the curb and a concrete aggregate surface offset about 5 meters from the curb. The terminal heights and elevation profile resulted in a reflection point that was divided at this offset boundary. This appears to explain the split amplitude peaks that occur at around +4 and +6 degrees which matches the geometry for the surfaces of this offset distance. This same building also supplies the last reflection for the 4-hop mode and similar double peaks are also seen on most scans between 10 and 14 degrees.

It should be noted that the positioning of the antennas is accomplished by manual control of the servo drive. Therefore, some speed changes may take place during a scan, especially if there is nonuniform wind loading, so that a + 1 degree of difference, relative to the zero pointing, is possible between scans. In the data collection an accurate mark is recorded through the computer data logger each 5 degrees of scan which can be used in the analysis when required.

A 3-hop mode should have provided a dominant peak on the scans at minus 6 degrees, but this mode was not pronounced. In tracing the ray, the explanation seemed to be that the last hop occurred at the Glenarm Street intersection partially shielding and/or reflecting the ray away from the receiver. A 1-hop mode from the north side of the street arrives at the receiver between +1.5 to +2 degrees and can best be identified in Figures 3.20 and 3.21 (TX = 0). This north side 1-hop mode, because of the shallow angle on the near side of the street, encounters numerous obstructions in light poles, signs, trees, etc., as seen in the photograph in Figure 3.25c.

As the transmitter is beamed toward the south side of the street at steeper angles (TX = 10°, 20°, and 30°), an increasing number of multiple hops from buildings and reflection from other objects at streetside contribute to the received signal producing an irregular amplitude scan resulting from signal phase interference. As many reflection modes or hops as practical are identified and labelled on Figures 3.18 through 3.21.

A comparison of Figures 3.18 and 3.19 involving the dominant reflections on the 28.8 GHz scans clearly shows that vertical antenna polarization produces the largest reflected signal amplitudes. This could be assumed to be a pseudo-Brewster angle effect; however, for the 57.6 GHz scans of Figures 3.20 and 3.21, no trend in a favored polarization can be established. In fact, the 2-hop modes are much stronger on the 57.6 GHz horizontal polarization. The 2-hop modes occurred at between 4 and 6 degrees, the angle near where one might expect the minimum σ for horizontal polarization at this frequency. It is difficult to speculate the reason for this apparent frequency dependent polarization result, but there is considerable confidence that the effect is not instrumental. Polarization effects, particularly at frequencies above 30 GHz, are obviously unclear and analysis and/or measurements may be possible at a later date.

In comparing the relative amplitude of the dominant reflection modes there is little difference between the 28.8 GHz and the 57.6 GHz scans. But when looking at the general amplitude levels for off-angle transmitter pointing, which presumably result from higher order hops and smaller reflectors or scatterers, the 57.6 GHz scans seems to show stronger levels.

3.3 Conclusions from off-angle measurements

From the off-angle measurements some conclusions can be made about propagation characteristics of this path. These measurements provided a means to separate some of the strongest multipath signals present at a selected 17th Street location over

a 485 meter path. For terminal heights of 2 meters, maximum multipath signals of about 7 dB (R_1/R_2 = 7 dB) below the direct free-space signal were recorded at 28.8 and 57.6 GHz for a midpath 1-hop reflection from buildings. Using the average spacing between building fronts along the street as 24 meters, a maximum multipath delay for these single reflections is 8 nanoseconds. Based on information included in Appendix A, a system with a data rate of up to 10 Mb/s can be used without appreciable intersymbol interference. A multipath delay of 0.1 of the bit duration is chosen as a "no intersymbol interference point" because the average BER due to intersymbol interference at a delay of 0.1 of the bit duration is approximately the same as the average BER due to S/N as a result of multipath for zero relative delay (Figure A.1). Assuming the antenna beamwidth at the half power points is greater than 6 degrees for each terminal and that accurate pointing is maintained, a fade depth of 5 dB and enhancement of 3 dB would be expected from building reflections with small changes in terminal position. However, much deeper fades could result from street surface reflections. The street reflections would have a delay of much less than 0.1 nanosecond relative to the direct signal so intersymbol interference would not occur until a bit rate in excess of 1000 Mb/s were used. It should be noted that in order to prevent street reflection fades from disrupting the link a 20 to 30 dB fade margin would be required above a level providing the minimum acceptable BER.

If a 1-hop multipath (R_1/R_2 = 7 dB) mode from building surfaces is present (8 ns delay) for the 485 meter path at a 10 Mb/s data rate (bit duration = 100 ns), an average bit-error-rate (BER) of 10^{-6} and a peak BER of almost 10^{-3} would be predicted for a system having an energy per bit versus noise power ratio (E_b/N_o) of 14 dB (Figure A.1). Without any multipath fade or distortion the link would perform at a BER of about 5×10^{-7}. If a bandwidth to accommodate 100 Mb/s were used, but the antenna gain and/or power gain increased a total of 10 dB to maintain an E_b/N_o of 14 dB, the above system on the 485 meter path would provide a predicted average BER of 5×10^{-4}. The bit duration for the 100 Mb/s rate is 10 ns resulting in a multipath delay of 0.8 of the bit duration where severe intersymbol interference and phase shifts occur producing a peak BER of about 5×10^{-3}.

If the antenna beamwidth exceeded 11 degrees, a 2-hop mode on this path would produce a maximum delay of about 31 ns which would permit data rates up to 3 Mb/s without damaging intersymbol interference.

Obviously, the degree of degradation of a digital link due to multipath signals depends on the strength of the multipath and E_b/N_o for the link. Figure A.2 gives an indication of the effects of these parameters on BER for a particular 30.3 GHz

system used in obtaining the measured data for the plot. This applies only to the case where the multipath delay exceeds the bit duration. The maximum and minimum excursions of the BER are shown in Figure A.3 for the same 30.3 GHz systems with multipath signals 8 dB below the direct signal.

The use of narrow beamwidth antennas on a link will reduce multipath component levels if pointed accurately. However, misalignment of narrow beam antennas could greatly aggravate multipath problems or on the other hand a careful pointing procedure could be used to discriminate against multipath. Very wide beamwidth or omnidirectional antennas for either or both terminals obviously increases multipath potential.

4. Rural Area with Path Over Asphalt and Graveled Roads

Since an rf link in an urban environment consists of boundaries of asphalt streets and sidewalks in the horizontal plane and building walls primarily in the vertical plane, it would be helpful to isolate the contribution of one of these surfaces in a propagation study. This was accomplished by setting the terminals over flat sections of roadway with no appreciable vertical obstructions. These paths were clear of vertical obstructions except for a mesh wire fence (1 meter high) with posts spaced about 15 meters apart along the side of the asphalt road and a power line about 10 meters high with 75 meters pole spacing. The road was 9 meters wide with 30 meters between fence and power lines. The graveled road was about 5 meters wide on an unobstructed terrain with 8 to 12 cm high dry grass bordering the roadway.

In Figures 3.26 through 3.33, the received signal amplitude as a function of transmitter-receiver separation was recorded as the transmitter is moved along the road toward the stationary receiving van. The received signal amplitude 0 dB reference was obtained from a calibration measurement taken with the transmitters located on path 100 meters from the receiver. These measurements were made in the same manner as the measurements shown in Figures 3.9, 3.10, and 3.11 along 17th Street in Denver. The path length is longer (1.6 km compared to 0.9 km) and the receiving antennas were set at various heights above ground for successive runs (3.25, 2.5, 1.8, and 1.0 meters) compared to 1.8 meters for the Denver runs. All the range measurements in this report were made with the transmitter antennas at a height of 2.15 meters.

The most prominent feature in all these data is the ground multipath effect. These very distinctive multipath fades occur in the range from 0.2 to 0.6 km. Occurrences of fade nulls are in a 1 - 3 - 6 ratio as a function of distance along

the path, the same as the ratios of the operating frequencies. The data in Figures 3.26 and 3.27 were made with the receiver height at 3.25 meters with antenna polarizations of vertical-vertical and horizontal-horizontal, respectively. Both sets of data show uniform multipath fading in the 0.2 to 0.6 km range, with no significant differences due to antenna polarization. The grazing angle of the ground reflection with the roadway is shown in the upper right hand side of Figure 3.26 where the receiver antenna height is 3.25 meters. An angle of about 2 degrees is the maximum for a path of 100 meters of separation, the nearest spacing for dependable antenna pointing between terminals. At angles 2 degrees and less the reflection coefficient is near unity for both horizontal and vertical antenna polarization. The Brewster angle, where the reflection coefficient is minimum, would not be expected to occur until a grazing angle of at least 8 degrees is reached. All other receiver heights produce smaller grazing angles, therefore, very little polarization effect would be expected in this data. Changes in the location of the fade nulls between the two polarization plots is probably the result of a few centimeters of difference in the location of the center position of the receiving antennas with a polarization change. The data in Figures 3.28, 3.29, and 3.30 were made with vertical-vertical antenna polarization at receiver antenna heights of 2.5, 1.8, and 1.0 meter, respectively. These data are very similar to the results in Figures 3.26 and 3.27. In Figure 3.27, the $1/R^2$ free space loss curve (dashed line) is shown crossing 0 dB at the 100 meter calibration point. With the receiving antennas at a 1 meter height (Figure 3.30) the separation between fades is greater because the transmitter terminal must travel further to affect a one wavelength difference between the direct and reflected rays. It is also apparent that the fade depths at the 1 meter receiver height are less than for the greater receiver heights. Normally it would be expected that a lower grazing angle would produce deeper fades because the reflection coefficient tends to be higher, surface roughness produces less distortion to the reflector wave front (Rayleigh criterion), and the ground reflection falls nearer the main lobe of the antennas. These factors add to make the reflected signal more nearly equal to the direct signal, a condition conducive to producing deep fades via destructive interference. However, it is speculated in this mm-wave case that the reflecting surface area illuminated at the small grazing angle exceeds the first Fresnel in the axis along the roadway. This possibly coupled with a slight undulation along the length of the roadway could result in phase front distortion reducing the likelihood for phase cancellation across the receiving aperture with the direct signal.

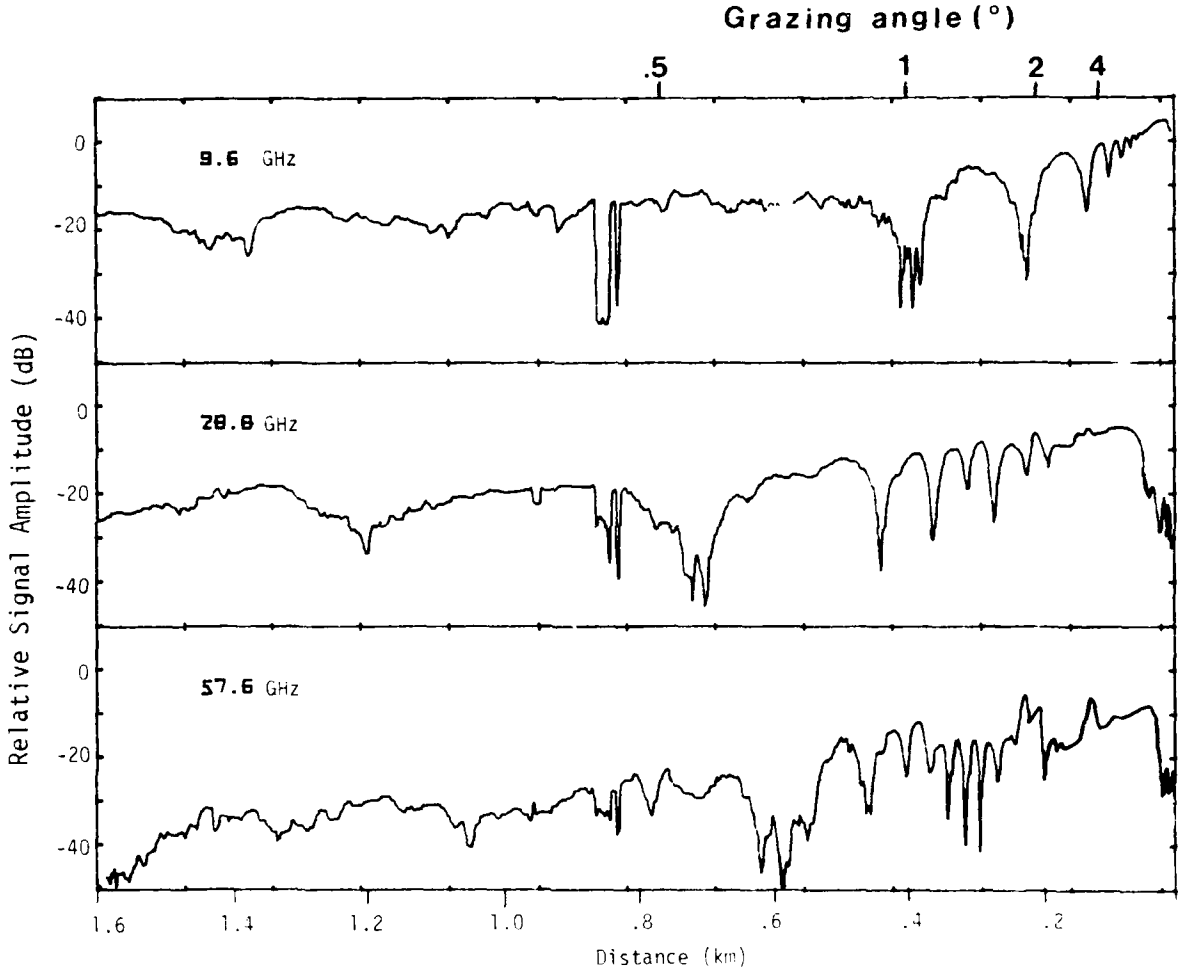

Fig. 3.26 Signal amplitude as a function of range measured along an asphalt road in a rural area. The transmitter is moved at a nearly constant velocity toward the receiver. Vertical antenna polarization. Transmitter height = 2.15 m. Receiver height = 3.25 m.

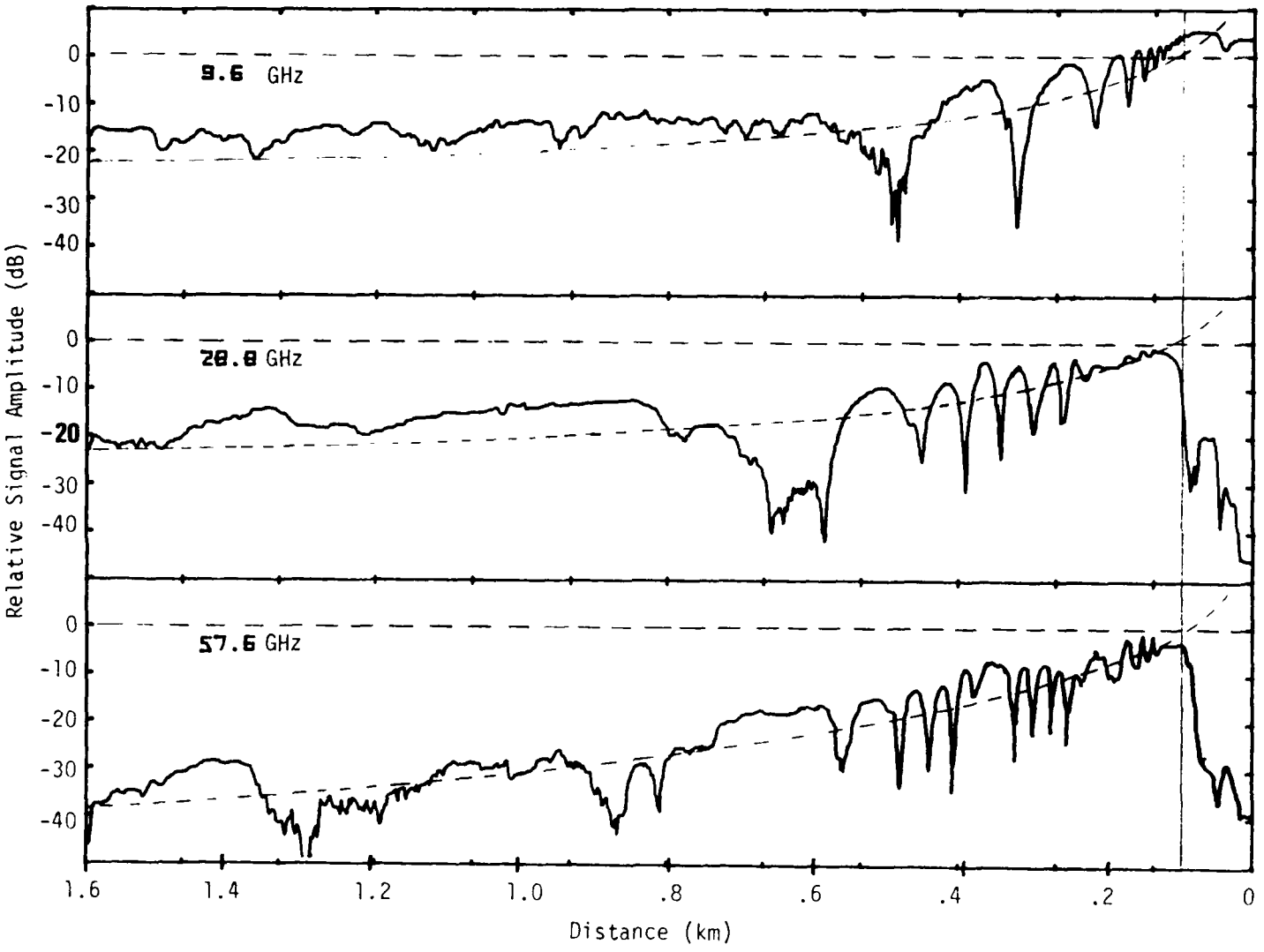

Fig. 3.27 Signal amplitude as a function of range measured along an asphalt road in a rural area. The transmitter is moved at a nearly constant velocity toward the receiver. Horizontal antenna polarization. Transmitter height = 2.15 m. Receiver height = 3.25 m.

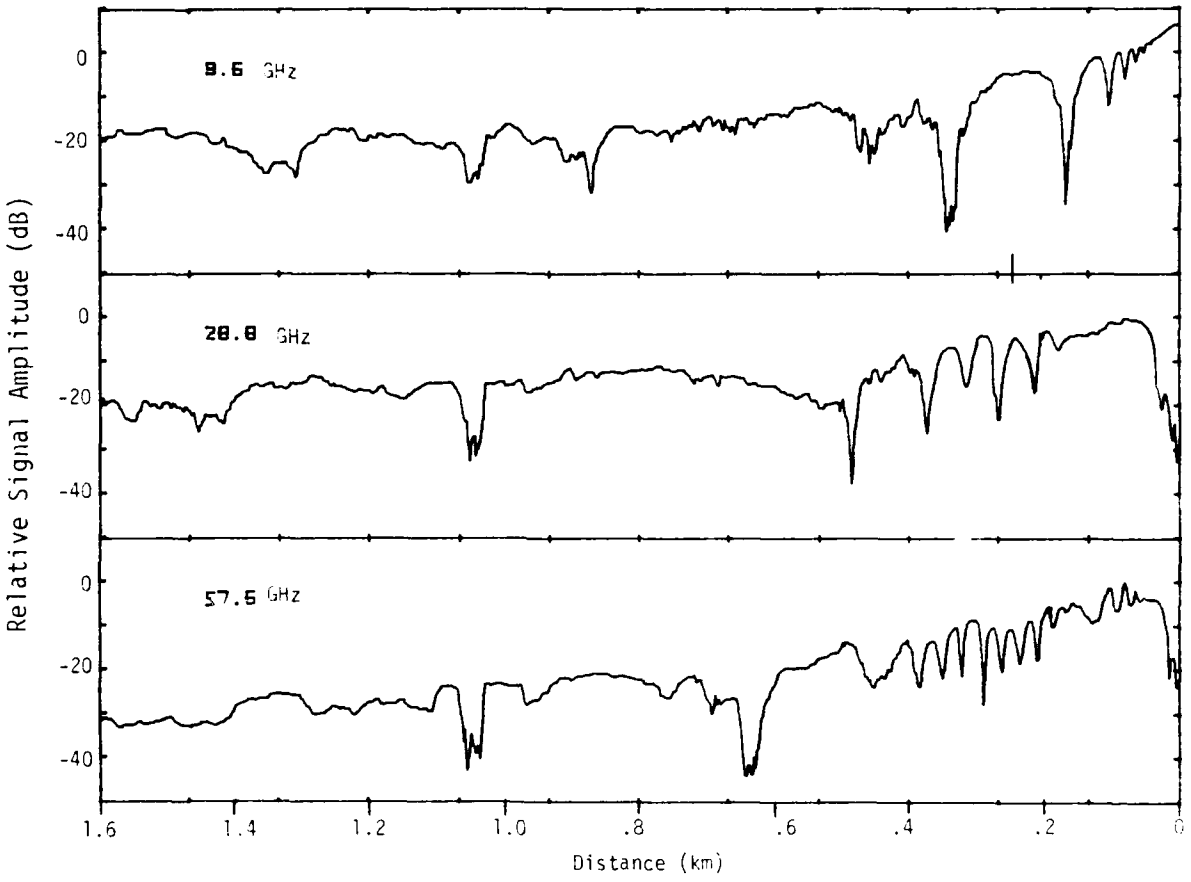

Fig. 3.28 Signal amplitude as a function of range measured along an asphalt road in a rural area. The transmitter is moved at a nearly constant velocity toward the receiver. Vertical antenna polarization. Transmitter height = 2.15 m. Receiver height = 2.5 m.

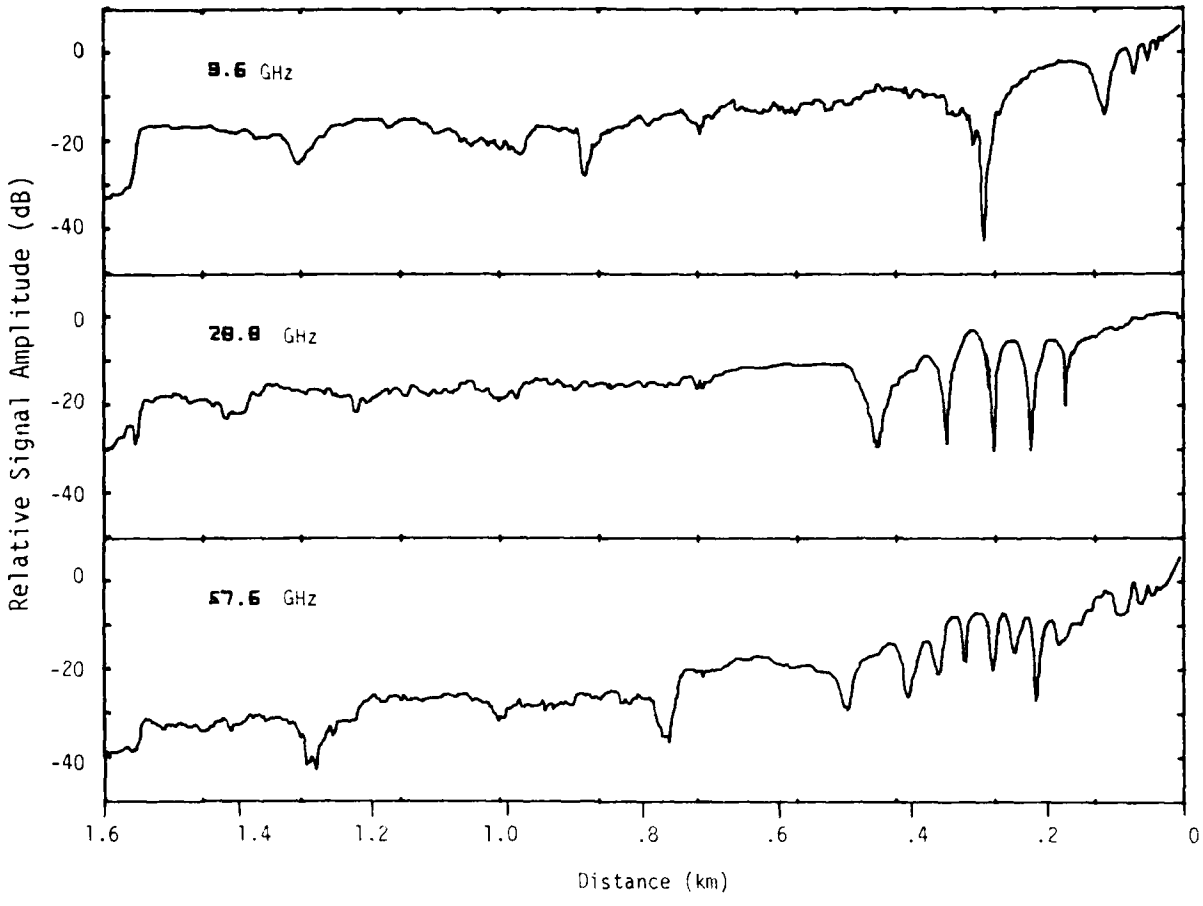

Fig. 3.29 Signal amplitude as a function of range measured along an asphalt road in a rural area. The transmitter is moved at a nearly constant velocity toward the receiver. Vertical antenna polarization. Transmitter height = 2.15 m. Receiver height = 1.8 m.

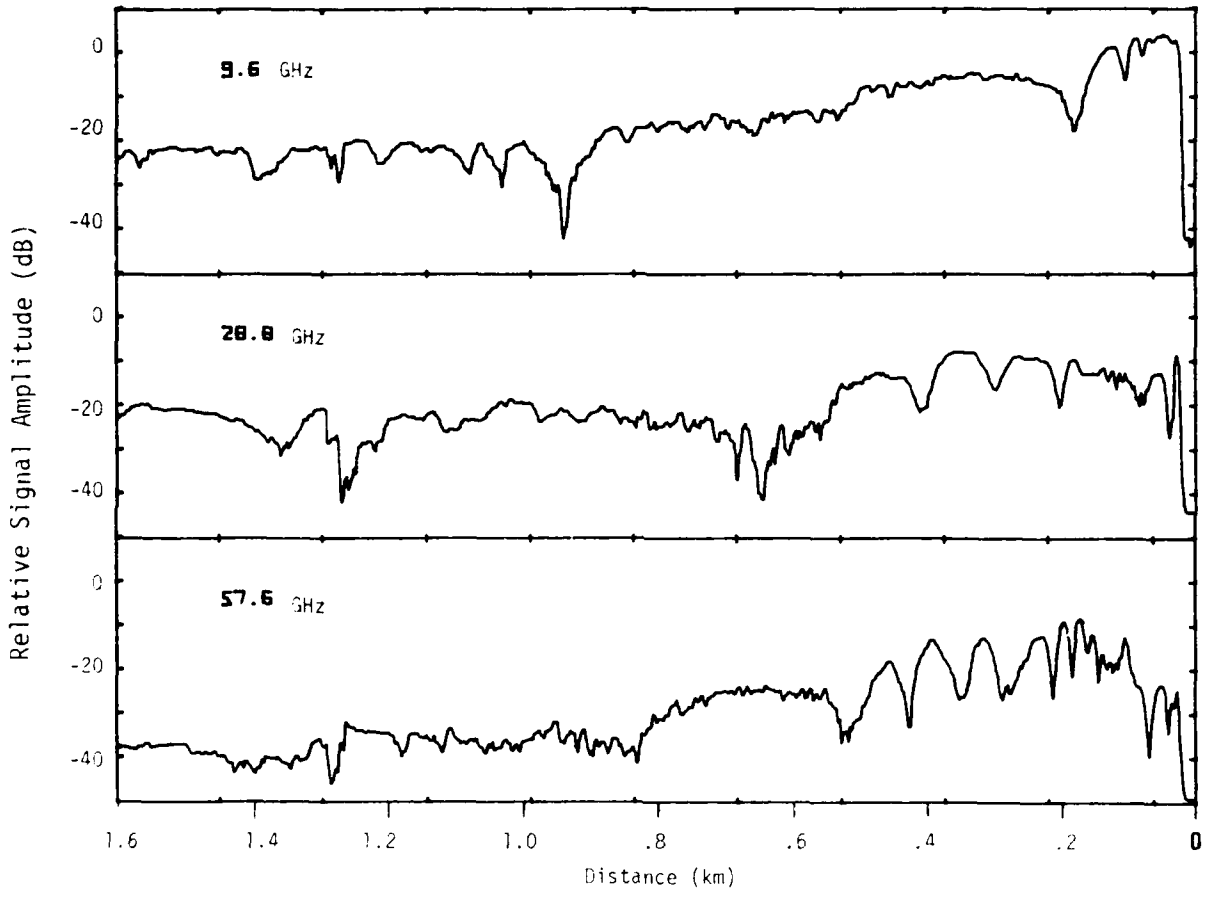

Fig. 3.30 Signal amplitude as a function of range measured along an asphalt road in a rural area. The transmitter is moved at a nearly constant velocity toward the receiver. Vertical antenna polarization. Transmitter height = 2.15 m. Receiver height = 1 m.

Figure 3.31 was made by moving the transmitter along a gravel road. Again the ground multipath fades are apparent and quite similar to the data over the asphalt road at a 1 meter height. Because this road was free of traffic a second run was recorded to observe the repeatability of the measurement. The second run is displaced 10 dB to make the comparison easier to view. Even though the gravel road had a very rough surface, up to 3 cm size aggregate, the ground reflection at this low grazing angle appears as strong as from the asphalt road.

The data presented in Figure 3.32 was taken over a gravel road but with a special path profile which shields most of the ground reflection from the receiver. The first 1650 meters, traveling toward the receiver, rises at a rate of 3.8 meter for each 100 meters of run. At about the 1650 meter point the road crowned and became level for the remaining 350 meters. The full path was just line-of-sight but the effect on the ground multipath is noticeable by its absences. A second run was also performed on this path and shown with a 10 dB offset.

Figure 3.33 shows the effect on the multipath when the receiving antennas are raised 1 degree. This procedure may not improve the signal-to-noise ratio of a channel but multipath distortion can be extensively reduced.

The principal value of this open field run is to provide a direct comparison of received signal characteristics between the urban and rural areas, and to provide a validation of measuring system performance.

D. Signal Amplitude (non-line-of-sight)

In addition to the line-of-sight measurements made along 17th Street in Denver, as reported in the previous section, some data were recorded for non-line-of-sight paths in the same area. Rigorous control was not maintained regarding distance between terminals and transmitter antenna pointing angles. The street maps in Figure 3.34 show the receiver location at the corner of 17th Street and California Street, and several transmitter locations with approximate antenna pointings at each. At each location, received signal amplitude levels and transmitter-pointing angles were recorded. These data are summarized in Table 3.3 and show that signal levels with detectable signal-to-noise ratios were observed for several non-line-of-sight paths. At the 9.6 and 28.8 GHz frequencies, some of these paths would require multiple reflections to travel from the transmitter to receiver. The 57.6 GHz paths showed positive signal-to-noise ratios only on the less complex paths.

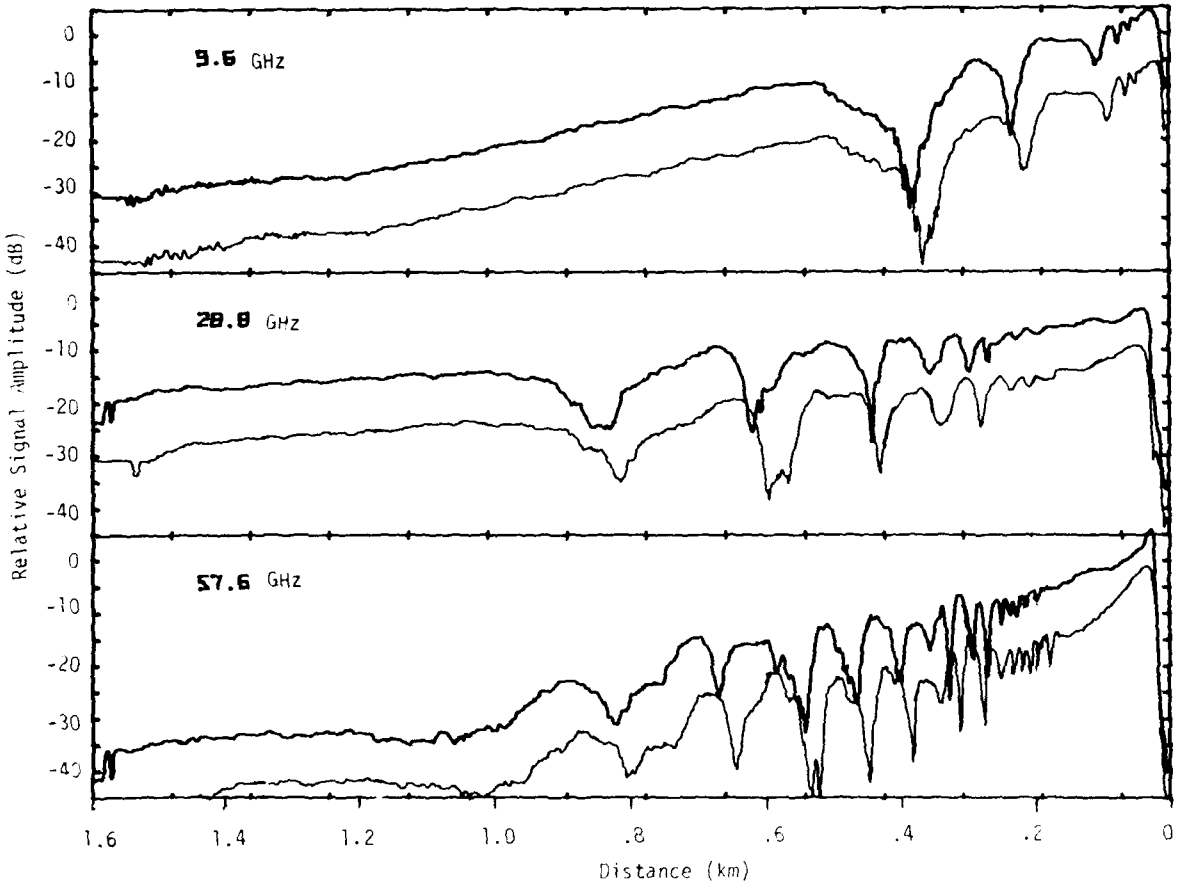

Fig. 3.31 Two separate traces of signal amplitude as a function of range along a gravel road in a rural area. The transmitter is moved at a nearly constant velocity toward the receiver. Vertical antenna polarization. The transmitter height = 2.15 m. Receiver height = 1 m. The traces are off-set by 10 dB.

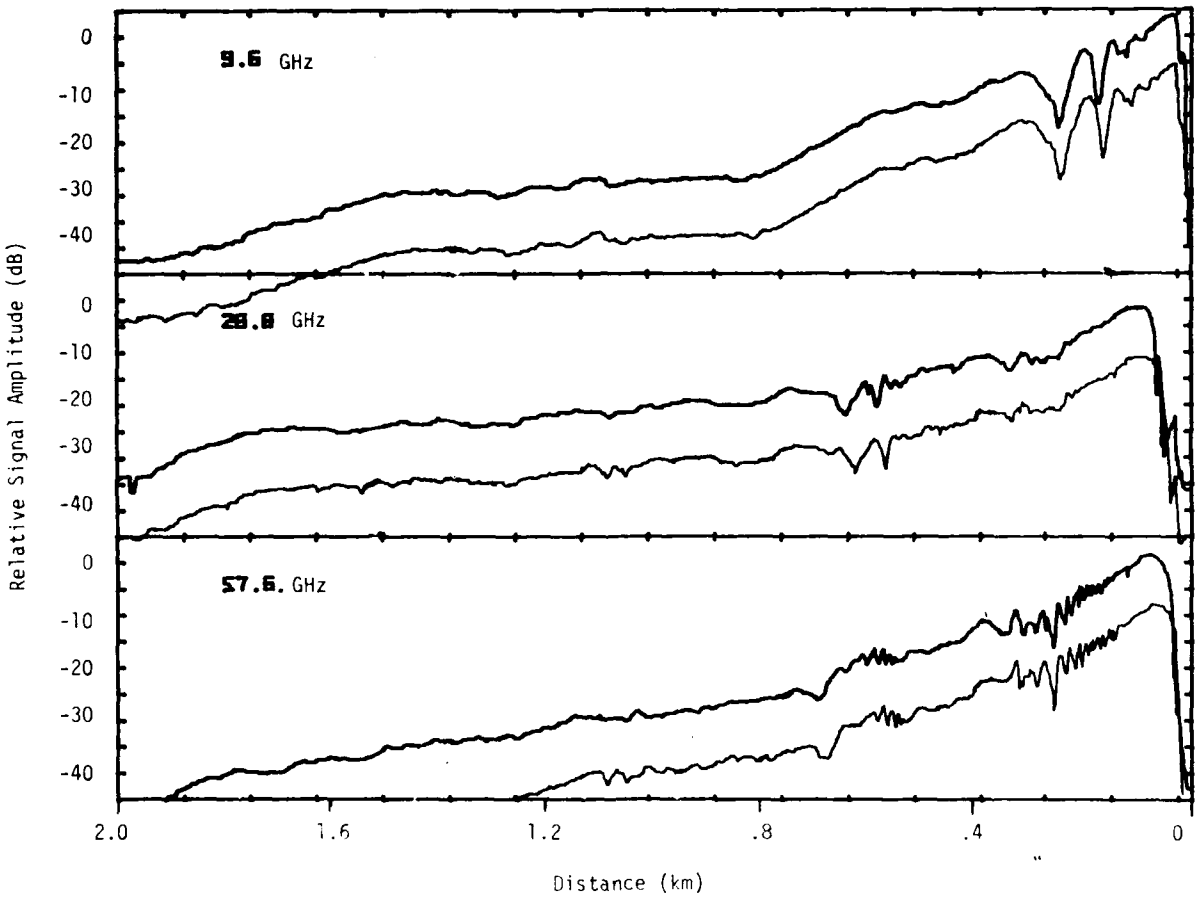

Fig. 3.32 Two separate traces of signal amplitude as a function of range along a gravel road in a rural area. The transmitter is moved at a nearly constant velocity toward the receiver. Vertical antenna polarization. The transmitter height = 2.15 m. Receiver height = 1 m. The traces are off-set by 10 dB.

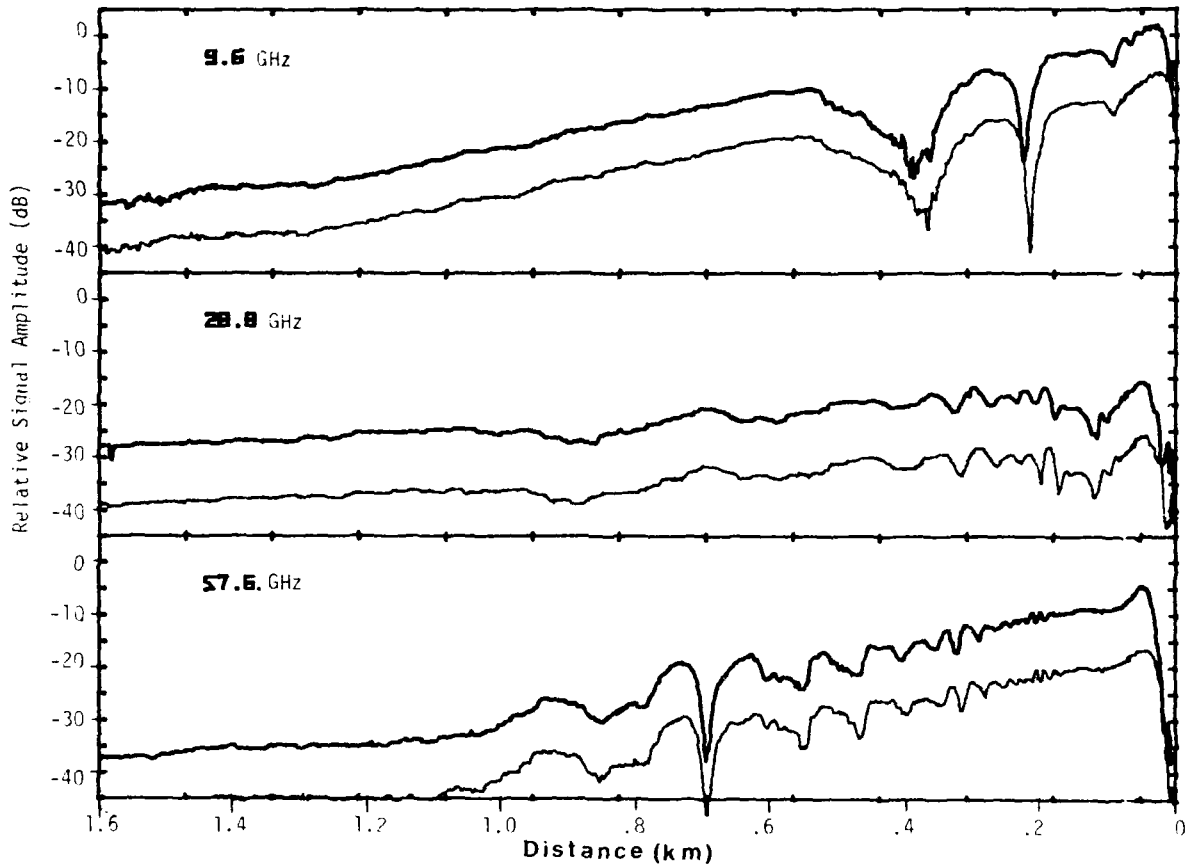

Fig. 3.33 Two separate traces of signal amplitude as a function of range measured along a gravel road in a rural area. The transmitter is moved at a nearly constant velocity toward the receiver. Vertical antenna polarization. Transmitter height = 2.5 m. Receiver height = 1 m. The receiver antennas are pointed up (elevation) by 1° from Figure 3.27. The traces are off-set by 10 dB.

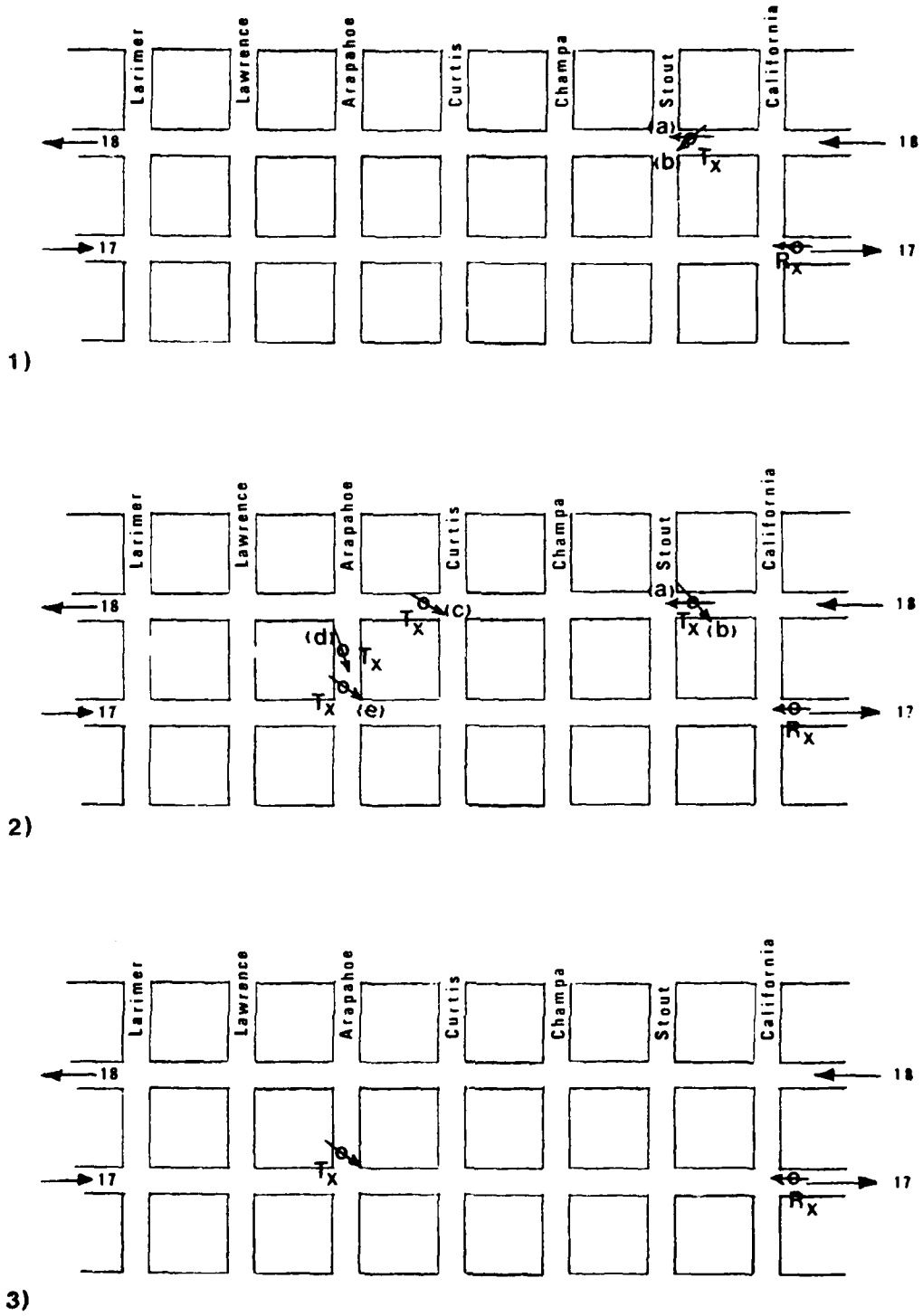

Fig. 3.34 Test locations using the 9.6, 28.8, and 57.6 GHz millimeter wave test system in downtown Denver for non-line-of-sight measurements.

TABLE 3.3

MEASUREMENT RESULTS FOR NON LINE-OF-SIGHT TESTS
IN DOWNTOWN DENVER

Locations		Distance Between Terminals	Pointing Angle		Received Signal (dB relative to free space)			Location Figure
Receiver	Transmitter	(m)	Rx	Tx	9.6 GHz	28.8 GHz	57.6 GHz	3.34
Corner of California and 17th	18th and Stout	125	270°	270°	-65 25 dB(S/N)	-82 5 dB(S/N)	-57 0 dB(S/N)	1(a)
"	"	125	270°	240°	-59 31 dB(S/N)	-76 11 dB(S/N)	-57 0 dB(S/N)	1(b)
"	"	125	270°	275°	-61 29 dB(S/N)	-85 2 dB(S/N)	-57 0 dB(S/N)	2(a)
"	"	125	270°	135°	-54 36 dB(S/N)	-71 14 dB(S/N)	-57 0 dB(S/N)	2(b)
"	18th and Curtis	370	270°	135°	-44 36 dB(S/N)	-56 20 dB(S/N)	-49 0 dB(S/N)	2(c)
"	Arapahoe 150' back from 17th	430	270°	170°	-35 43 dB(S/N)	-47 30 dB(S/N)	-42 3 dB(S/N)	2(d)
"	Arapahoe 20' back from 17th	425	269°	125°	-23 55 dB(S/N)	-41 35 dB(S/N)	-32 13 dB(S/N)	2(e)
"	"	425	264°	125°	-15 67 dB(S/N)	-19 59 dB(S/N)	-11 35 dB(S/N)	3

At several locations, the receiving antennas were scanned in search of signal changes. A specific example is noted in the last two entries of Table 3.3 (2e and 3). Comparing the received signal amplitude levels for two orientations of the receiving antenna shows increases in amplitude of 8 dB, 22 dB, and 21 dB for 9.6, 28.8, and 57.6 GHz, respectively, when the receiving antennas were rotated 5° from a 269° pointing to a 264° pointing in the azimuthal plane. Other results not tabulated, but noted in Figure 3.34 as follows.

1.) Location 1b. Receiver antenna azimuthal scanning at this location produced signal reductions of 30 dB at 9.6 GHz and 10 dB at 28.8 GHz and an enhancement of 10 dB at 57.6 GHz.

2.) Location 2b. Receiver antenna azimuthal scanning produced enhancements of 8 dB at 28.8 GHz and 10 dB at 57.6 GHz. These peak values occurred with the antenna azimuthal angle at 273°.

3.) Location 2c. Receiver antenna azimuthal scanning produced a 5 dB enhancement at 9.6 GHz and a 10 dB enhancement at 28.8 GHz for an antenna azimuthal angle of 267° and increased the 57.6 GHz amplitude to 15 dB above the noise level at an antenna azimuthal angle of 263°.

These tests indicate that millimeter wave signals can propagate along complex non-line-of-sight paths using multiple reflections from building surfaces. Antenna pointing caused changes in the peak reflected or scattered signal. At the lower two frequencies a signal above receiver threshold was nearly always present regardless of antenna pointing for either terminal.

E. Edge Diffraction

A potential propagation mode, when buildings obscure the LOS path, is diffraction from edges or corners. The transmission loss over a diffraction path depends on the shape and electrical characteristics of the diffracting edge. A vertical corner of a building may approach a "knife edge" shape which provides the minimum transmission loss, if it is perfectly conducting, compared to any edge that is less sharp.

To evaluate signal levels resulting from diffraction, a set of measurements was made for comparison with theoretical values taken from developed models. These measurements compliment the work done by N. Rokkos and R. Johnson to determine system parameters required to maintain a communications link using edge diffraction or to determine the interference level which may be generated by edge diffraction[5].

A corner of a building formed from poured and finished concrete was used to make "knife-edge" diffraction loss measurements at the three operating frequencies. The path lengths and geometries are shown in Figure 3.35. Three sets of data are presented in Figures 3.36, 3.37, and 3.38. These data were measured using, respectively, locations T_1 and R_1, a 62 meter path; T_1 and R_2, a 106 meter path; and T_2 and R_2, a 146.5 meter path. The solid line traces in these figures show the measured signal amplitudes for each frequency as indicated for horizontal-horizontal and vertical-vertical polarizations and the broken line traces show predicted diffraction losses due to a "knife-edge."

The predicted values shown in the figures were generated from equations based on the Geometrical Theory of Diffraction[6] which assumes the incident field at the edge to be a plane wave. The gain of the diffracted ray is assumed to fall off as $1/\sqrt{r_d}$, i.e. a cylindrical wave, where r_d is the distance from the edge. When the electric field vector is polarized parallel to the edge (VV polarization for vertical edge) the field intensity is expected to be less in the shadow region than when the electric field vector if polarized perpendicular to the edge. Measured data of Figures 3.36 through 3.38 show this dependence. However, the measured values gave a diffraction loss greater than the predicted values, particularly, as the terminal moves further into the shadow region. This increase in loss compared to predicted values may occur because the corner is not a "knife-edge" as assumed in calculating the predicted values. In fact, the concrete corners are formed such that the last 1-1/2 centimeter has a flat level at 45° to each side. This double edge can be described as very straight and sharp relative to wavelength for the highest frequency. The predicted values assume the edge to be a perfect conductor, which concrete is not, and there is some penetration into the material, as well, at the measurement frequencies.

A different path length was used for Figure 3.36 compared to Figure 3.37 by positioning the receiver terminal 35.5 meters from the edge in the first case, and 79.5 meters from the edge in the second case, keeping the transmitter terminal 26.5 meter from the edge for both cases. As seen by comparing these figures, there is little difference in diffraction loss as expected. The data in Figure 3.38 was taken with the transmitter distance from the edge increased to 67 meters and shows no appreciable difference in diffraction loss for equal angles from the grazing line. Note that when the terminal was in the clear, beyond grazing, each terminal's antenna continued to point at the edge thus showing the diffraction loss in this direction as well. However, in the case of the wider beam antenna at 9.6 GHz the antennas remained coupled for this portion of the scan but the

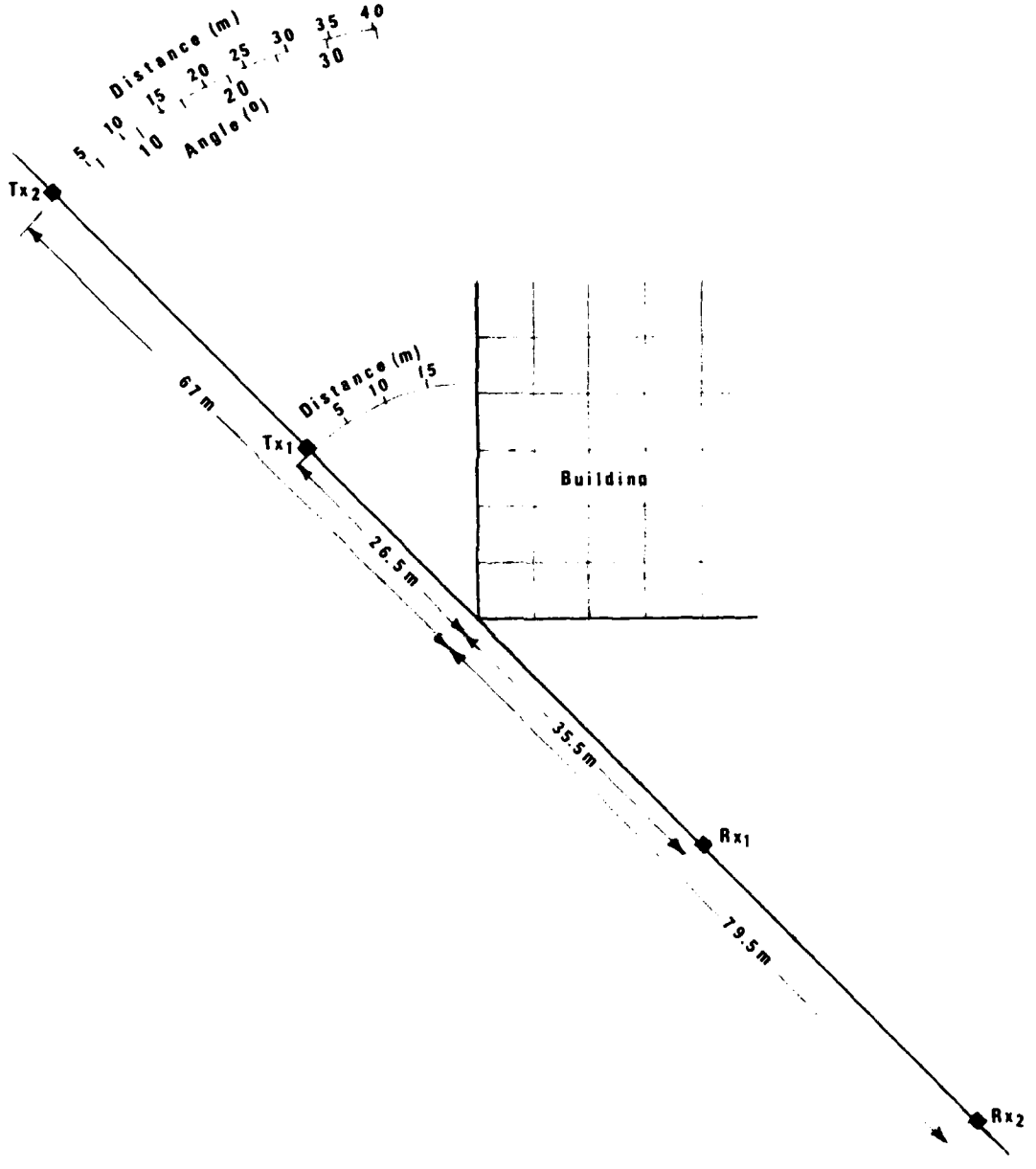

Fig. 3.35 A drawing showing the transmitter and receiver locations for the data in Figures 3.36, 3.37, and 3.38.

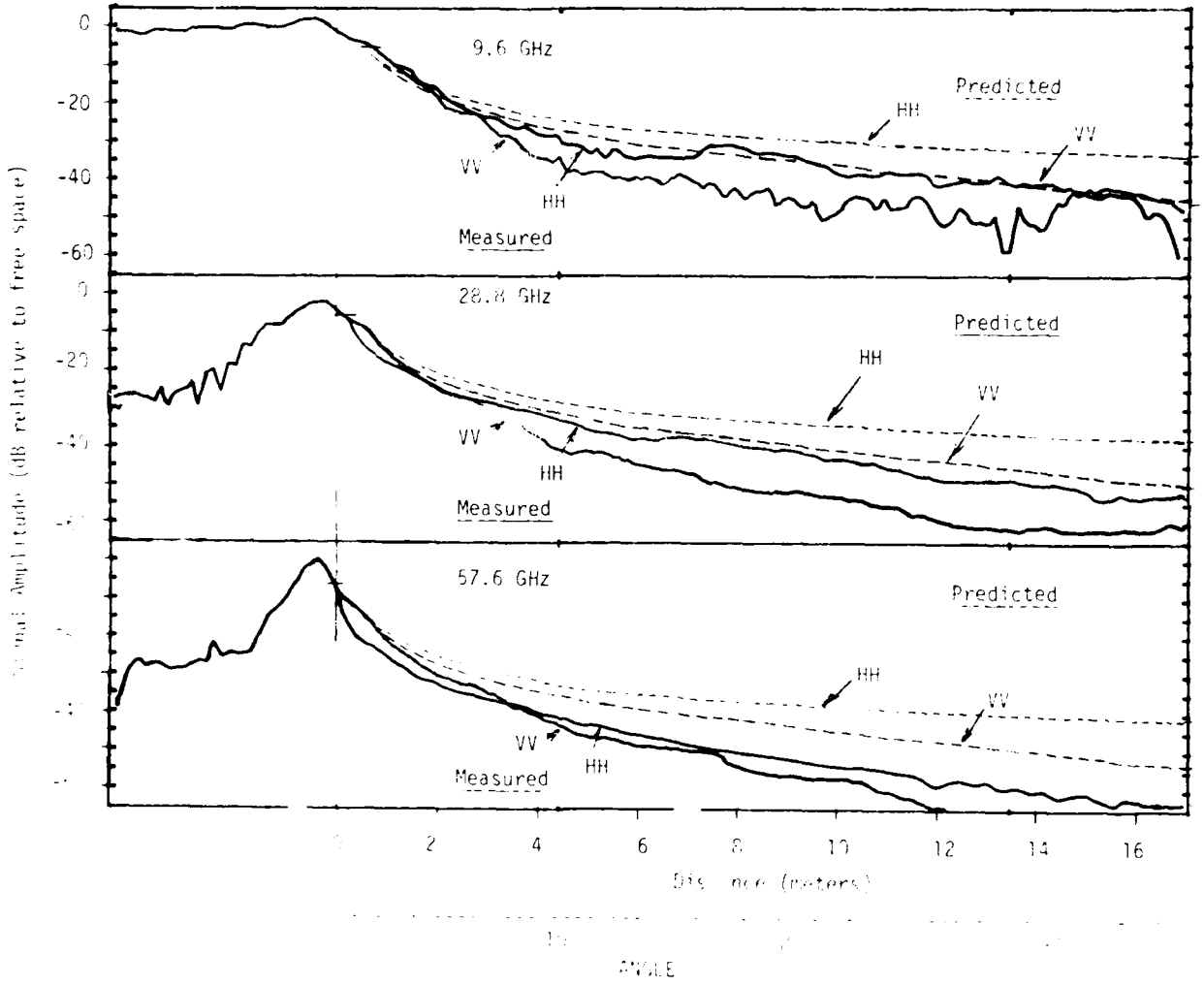

Fig. 3.36 Signal amplitude measurements from an edge diffraction for 9.6, 28.8, and 57.6 GHz. Edge to receiver = 35.5 m and the edge to transmitter = 25.5 m.

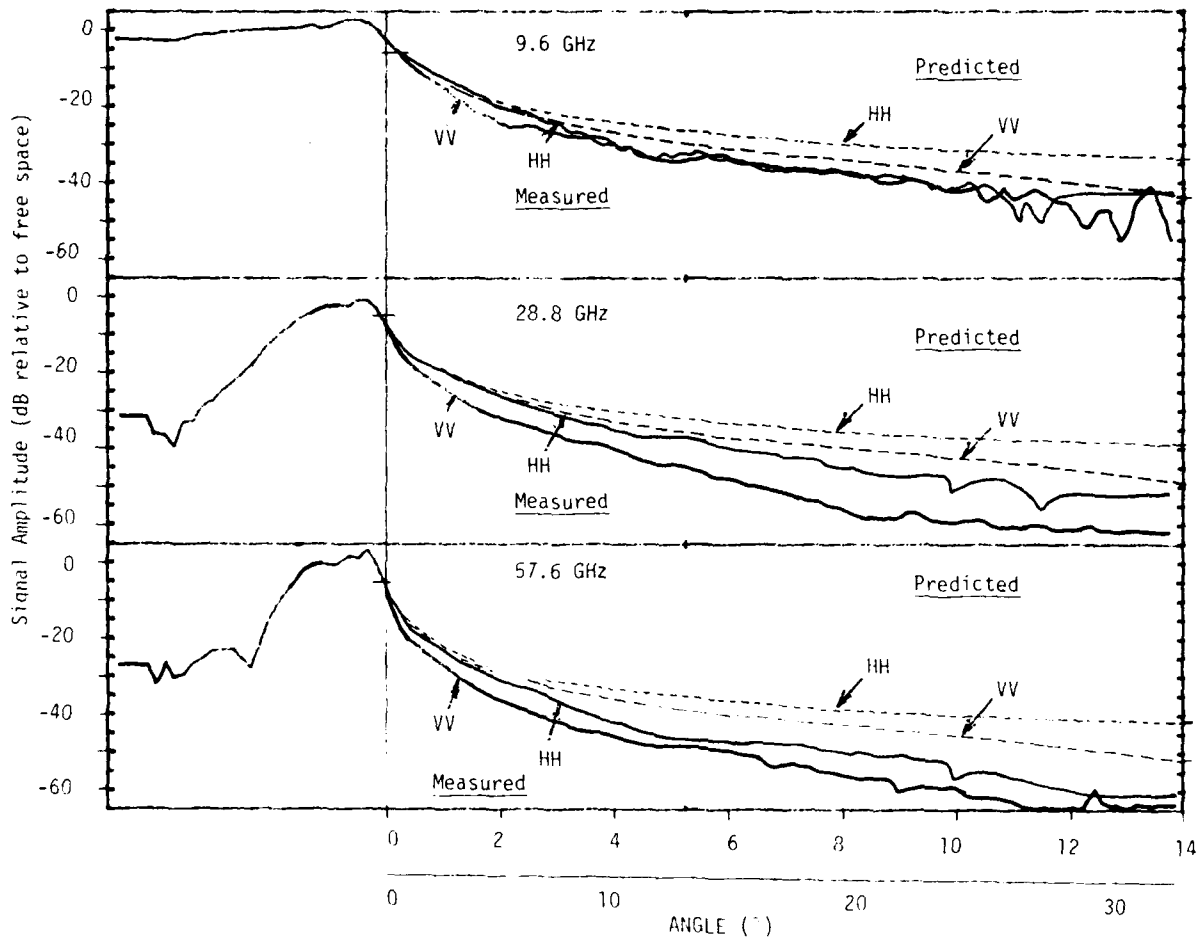

Fig. 3.37 Signal amplitude measurements from an edge diffraction for 9.6, 28.8, and 57.6 GHz. Edge to receiver = 79.5 m and the edge to transmitter = 25.5 m.

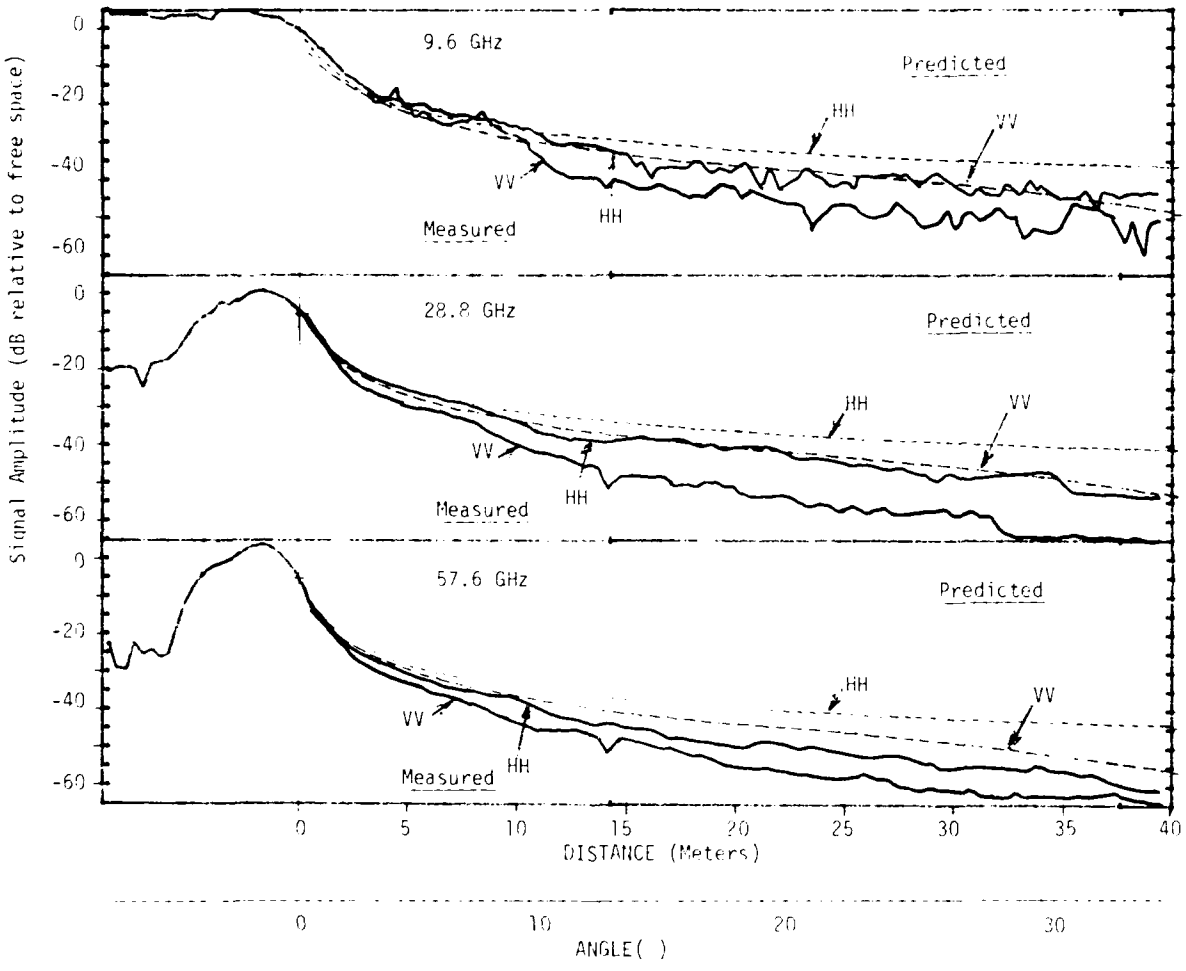

Fig. 3.38 Signal amplitude measurements from an edge diffraction for 9.6, 28.8, and 57.6 GHz. Edge to receiver = 79.5 m and the edge to transmitter = 67 m.

phase interference pattern between the direct ray and the diffracted ray is apparent by the wave-like trace in signal amplitude.

Measurements (electric vector parallel to edge) were made on a building with a double corner as illustrated in Figure 3.39. Figure 3.40 shows the recorded results where an enhancement caused by the second edge appears in the data between 2 and 3 meters into the shadow region of the first edge. Diffraction loss as a function of angle was very similar to the results of Figures 3.36, 3.37, and 3.38. This data suggests that the shape of the edge does not appreciably alter the diffraction loss for the range of edge shapes and frequencies used in the measurements made in this section.

A study of edge diffractions based on the theories of Fresnel, Sommerfeld, and Keller is presented in Appendix B.

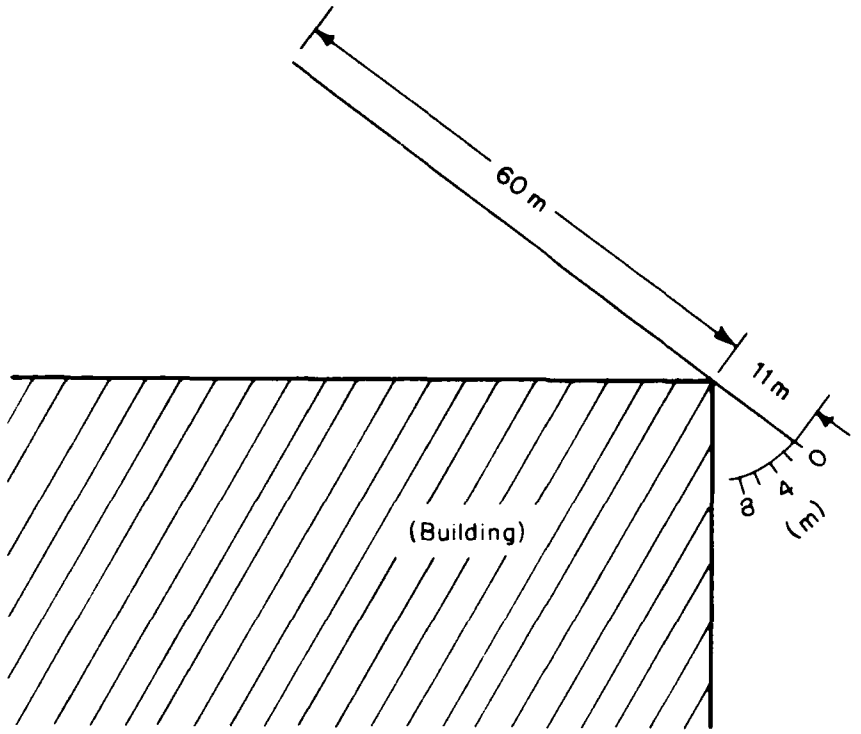

(a) Path geometry.

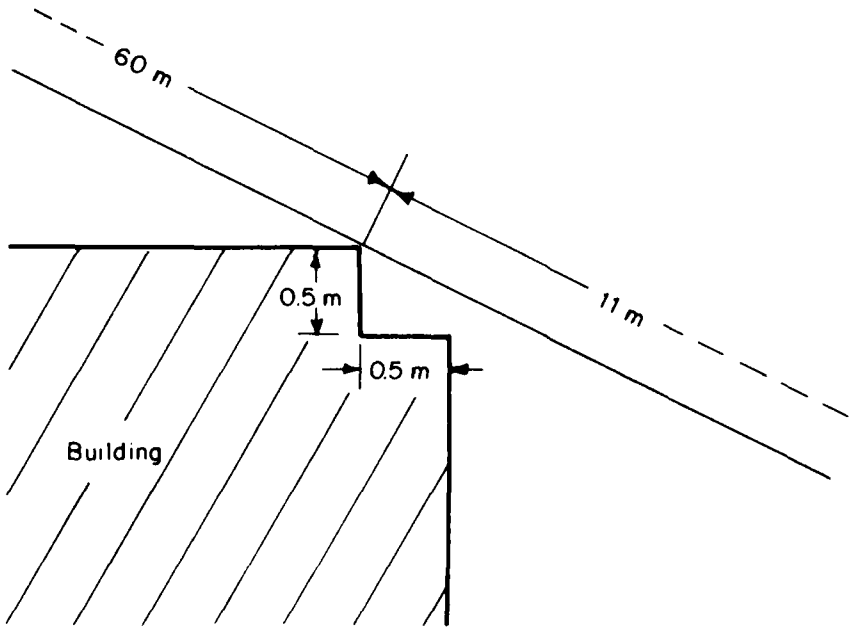

(b) Expanded view of the "knife edge".

Fig. 3.39 The measurement configurations for results in Figure 3.40.

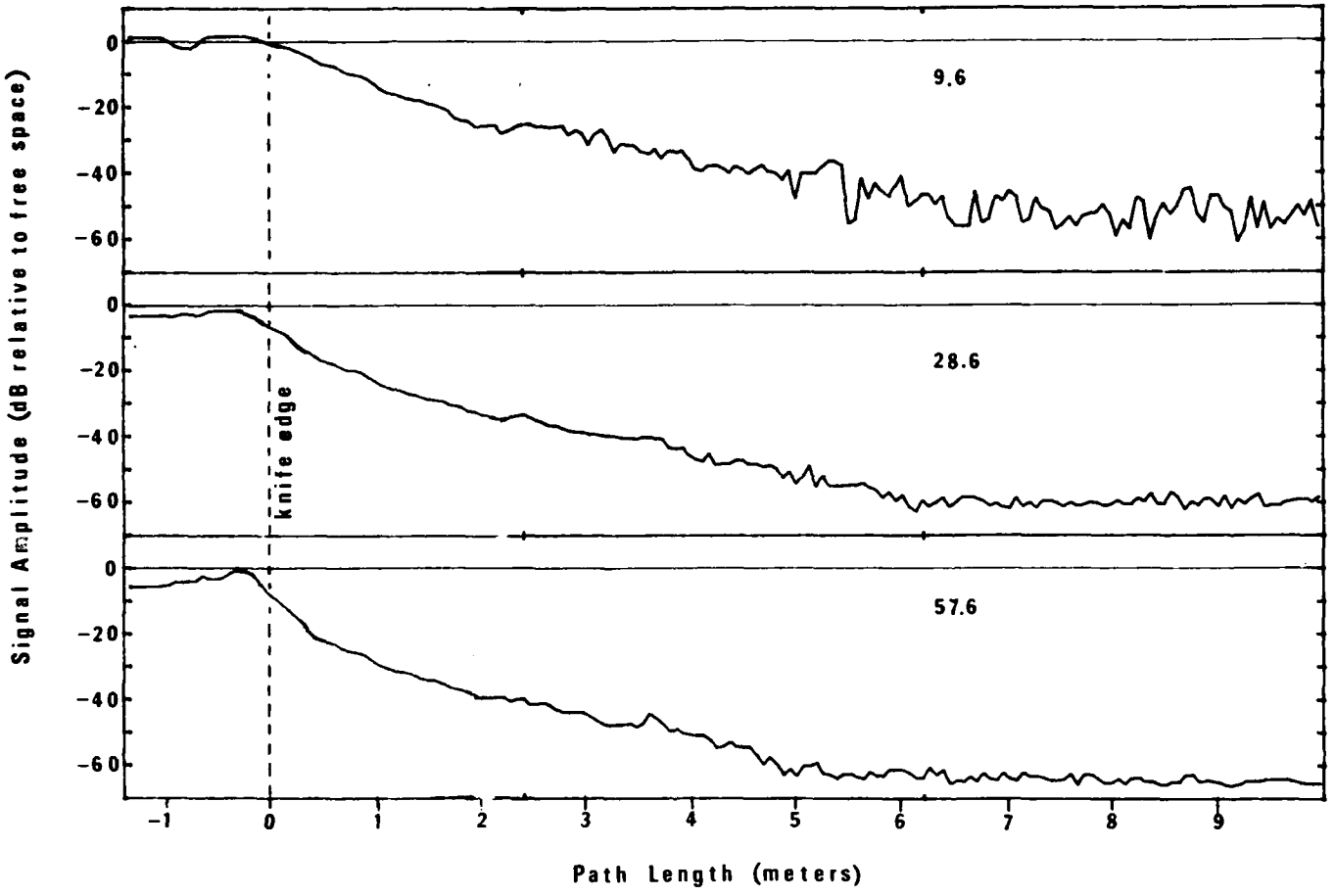

Fig. 3.40 Measured results from a building with a double knife-edge corner. Vertical-vertical antenna polarization.

IV. FIELD MEASUREMENTS USING THE 60 GHz HAND-HELD COMMUNICATORS

A pair of 60 GHz hand-held communicators received a brief operational check-out during the same tests conducted to evaluate the LOS and non-LOS performance of the 9.6, 28.8, and 57.6 GHz transmitter-receiver links.

These transceiver units are intended for line-of-sight operation over a range of 1-2 km in clear air conditions. General system specifications include:

Transmitted Power	25 mw
Antenna Size	10 cm (lens)
" Beamwidth	3°
" Gain	34 dB
Channel Bandwidth	5 MHz
Receiver Noise Figure	14 dB

Maps of the test area along 17th Street in Denver are shown in Figure 4.1. The receiver location for all tests was at the intersection of California Street and 17th Street. The first map in Figure 4.1 shows the receiver and transmitter locations for path lengths of 170 meters, 400 meters, and 600 meters. For each path careful pointing was required to establish lock and the once-established link was often prone to drop-out, due to vehicles in the path. The table below shows the results of these tests indicating transmitter location, path length, signal level, and voice quality.

Transmitter Location	Path Length	Signal Level	Voice Quality
1a)	170 m	-35 dBm	Very good
1b)	400 m	-55 dBm	" "
1c)	600 m	-65 dBm	" "

An evaluation of the effects of transmitter pointing was made at the 400 meter location. With the transmitter stationed at location (2a), which was LOS, azimuthal pointing changes of ± 5° and elevation pointing change of ± 20° did not cause a loss of communications. Similar results were obtained for the link with the transmitter station 10 feet in from the curb at location (2b), Map 2 in Figure 4.1. This was a non-LOS path with a measured signal level of -64 dBm. Voice quality was good at both of these locations.

The scenario in Map 3 of Figure 4.1 shows the transmitter located 25 feet from the curb, which is a non-LOS path. In this case, an optimum signal level of -58 dBm was obtained when both the transmitter and receiver were pointed in the general area labeled (3a). This observed non-LOS signal level was only 3 dB below the direct LOS signal for the same path. Very good voice quality was observed on this link.

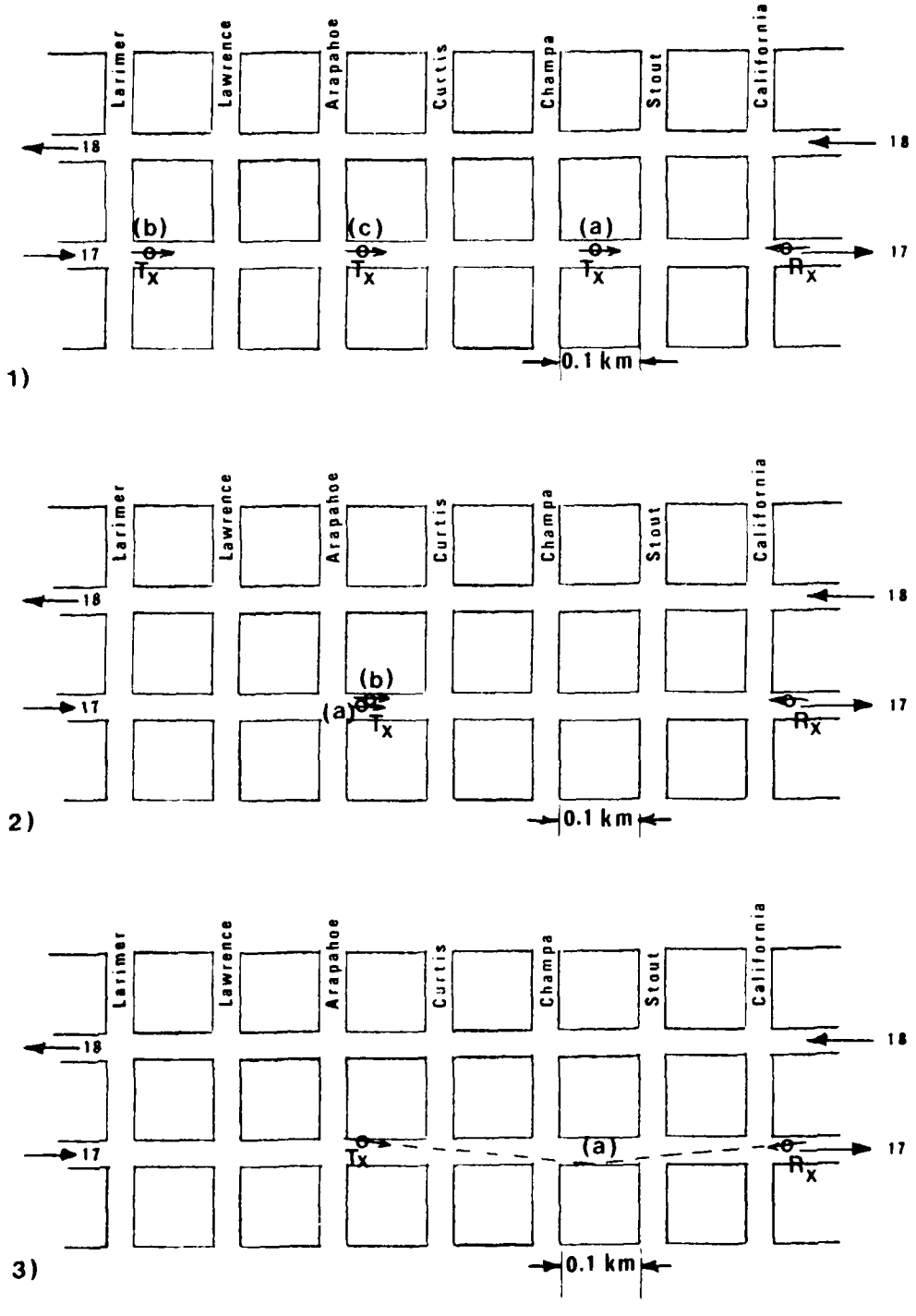

Fig. 4.1 Test locations using the 60 GHz hand-held communicators for line-of-sight and non-line-of-sight measurements.

An observation of link reliability was performed while one communicator was operated from the back of a truck traveling down 17th Street at about 5 MPH from Curtis to Tremont, about 600 meters. Both terminals were in clear view but it was nearly impossible to establish voice contact because of frequent automatic frequency controller drop-out and the lengthy time required to relock. Three attempts were made all without a successful voice contact. The drop-outs were probably a combination of signal fades and antenna pointing error at the moving terminal.

V. CONCLUSIONS

An urban environment presents a wide variety of situations for communication links in the mm wave spectrum. The ideal link for the compact size of the mm wave equipment with small, yet narrow beamwidth antennas is from rooftop to rooftop of the tallest buildings. The only conceivable problem with a line-of-sight (LOS) link of this type would be excessive attenuation from rain in the path or gaseous absorption (in a molecular resonance band) if the path is long. If, however, a link is required at street level, many additional problems can face the user. One of the major concerns is interference paths created by reflected signals in addition to the direct LOS signal. Reflected signals can cause deep fades to occur, especially from street surfaces and even from building walls, vehicles, road signs, etc. For wide bandwidth links (high-rate digital for example), distortion may result from reflected multipath signals that affect the efficient transmission of information. The severity of these problems depends upon such link parameters as the length of the paths, antenna beamwidths, frequency, and path clearance.

The data contained in this report provide information on reflection properties from streets and several of the more common building surface types. A series of measurements made within a 10-block area in downtown Denver, CO, and the analysis of the resulting data provides some insight on propagation characteristics at millimeter wavelengths.

The recent development of a very wide bandwidth impulse probe (500 Mb/s), used in acquiring the data for Appendix A of this report, provides a means to measure time delay spread resulting from multipath or scattered signals with a resolution of less than one nanosecond[7]. Signal distortion associated with multipath or scattering and corresponding bit error rates can also be measured with the wideband probe. It is planned that follow-on work of millimeter wave propagation studies in an urban environment will include the wideband probe at 30 GHz.

VI. REFERENCES

[1] E.J. Violette, R.H. Espeland, A.R. Mitz, F.A. Goodknight, and F. Schwering, "SHF-UHF propagation through vegetation on Colorado East Slope," CECOM-81-CS020-F, U.S. Army Communications-Electronics Command, Fort Monmouth, NJ 07703 (1981).

[2] P. Beckman and A. Spizzichino, "The Scattering of Electromagnetic Waves from Rough Surfaces," (Pergamon Press Ltd., Oxford), p. 10 (1963).

[3] M.P.M. Hall, "Effects of the Troposphere on Radio Communications," IEE Electromagnetic Waves Series 8, the Institution of Electrical Engineers, London and New York (Peter Peregriners Ltd., Stevenge, UK, and New York), p. 90 (1979).

[4] CCIR, "Electrical Characteristics of the Surface of the Earth," Volume 5, Recommendation 527, International Telecommunication Union, 2 Rue Varembe 1211, Geneva 20, Switzerland, (1978).

[5] N. Rokkos and R.A. Johnson, "Diffraction of Millimeter Wave Communications Signals into Shadow Regions," CORADCOM-81-1, U.S. Army Communications Research and Development Command, Fort Monmouth, NJ 07703 (1981).

[6] J.B. Keller, "Geometrical Theory of Diffraction," J. Optical Soc Am; Vol. 52, No. 2, pp. 116-130 (1962).

[7] E.J. Violette, R.H. Espeland, and K.C. Allen, "A Diagnostic Probe to Investigate Propagation at Millimeter Wavelengths," NTIA Report 83-128 (1983).

APPENDIX A

Effects of Multipath on Digital Link Performance

An experiment was conducted by the Institute for Telecommunication Sciences using a millimeter wave "diagnostic probe" to determine effects of multipath signals on an atmospheric link. Data taken on a 250 meter folded path with dual reflectors (one fixed and one movable) using the 30.3 GHz, 500 Mb/s coherent BPSK probe is compiled to give a view of multipath effects[1]. Figure 1A contains a plot of contributions to BER by S/N variations and intersymbol interference as a function of the time delay of a multipath signal relative to the direct signal normalized to bit duration. For this plot, the direct-to-multipath signal ratio (R_1/R_2) is 7 dB taken for an E_b/N_o of 14 dB. With no multipath present and a 14 dB signal-to-noise ratio, the BER is 5×10^{-7}. At zero multipath delay the change in BER is due only to S/N changes with an average BER of about 1.5×10^{-6}. This average BER is greater than the no multipath case because fades of 5.1 dB and enhancements of only 3.2 dB occur for a R_1/R_2 of 7 dB. Since a psuedo-random sequence bit generator is used to produce the data stream, the amplitude variations diminish as the multipath delay extends to 1 bit duration. Hence, the error changes due to S/N diminishes as shown by the narrow hatched marked, "BER due to S/N only." Delay times greater than 1 bit duration theoretically produce no changes in BER due to S/N because no amplitude variations occur as a result of the multipath signal. Actually there is an amplitude variation in the system due to cw components in the signal used for reconstructing the carrier, but this variation is very small.

Errors due to intersymbol interference for this controlled multipath case (Figure A.1) are shown to diverge from zero delay, where a BER of 5×10^{-7} is that for a no multipath state. This indicates that there is no intersymbol interference contribution at zero multipath delay relative to the direct signal. As the multipath delay increases, the maximum and minimum contributions from intersymbol interference are shown by the broad spaced hatch-lines extending to coincide with the total contribution of errors at a delay time equal to 1 bit duration. Part of the errors attributed to intersymbol interference are the result of the composite of the direct signal and multipath signal producing a phase shift in the reconstructed carrier. The reconstructed carrier is manually phase adjusted to provide a zero reference to the phase detector in the demodulator for recovery of the baseband

process occurs with the reconstruction of the bit rate clock and is also modulated at the rf rate by multipath signals, but it is a result of intersymbol interference.

A second technique to reconstruct the carrier by multiplying the PSK or QPSK modulated carrier by four to produce an unmodulated reference was tested. A voltage controlled oscillator at the carrier frequency was phase-locked to the times 4 output to provide the reference carrier. This means of generating the reference carrier produced the same maximum and minimum BER excursions as the injected carrier technique. However, for QPSK modulation four possible phase-lock states exist, but only one is correct. Excessive time was required to obtain carrier lock-up and data word synchronization, which proved not suitable for flexible link operation.

The BER due to a multipath signal is dependent on the channel S/N and the strength of the multipath signal. For a direct-to-multipath signal ratio of 8 dB, Figure A.2 shows measured and extrapolated values of BER as a function of S/N compared to a curve showing system performance without a multipath signal. All values plotted are for a case where the multipath signal delay is one bit duration or greater. The measured points using the passive reflectors to simulate multipath are indicated by the small circles on the figure. These points include minimum, average, and maximum BER as a result of the multipath signal being continuously varied in delay time over several rf cycles.

Bit error rate versus S/N curves are extrapolated from measured data for three different ratios of direct to multipath signal level in Figure A.3. An estimated scale of R_1/R_2 starting at 7 dB and extending to ∞, which is the no multipath state, is included for the case where the multipath delay time is 1 bit duration or greater.

Multipath signals in a high data rate channel have a serious effect on data transfer rates due to increased errors. This treatment of multipath involving a single discrete signal may not always be representative of an actual path. Several components of multipath may occur or numerous scatters may exist such as reflections from irregular terrain. However, the measurements made for this analysis will provide an order of magnitude of channel degradation for the conditions that may be encountered on atmospheric paths.

REFERENCE

[1] E.J. Violette, R.H. Espeland, and K.C. Allen, "A Diagnostic Probe to Investigate Propagation at Millimeter Wavelengths," NTIA Report 83-128, (1983).

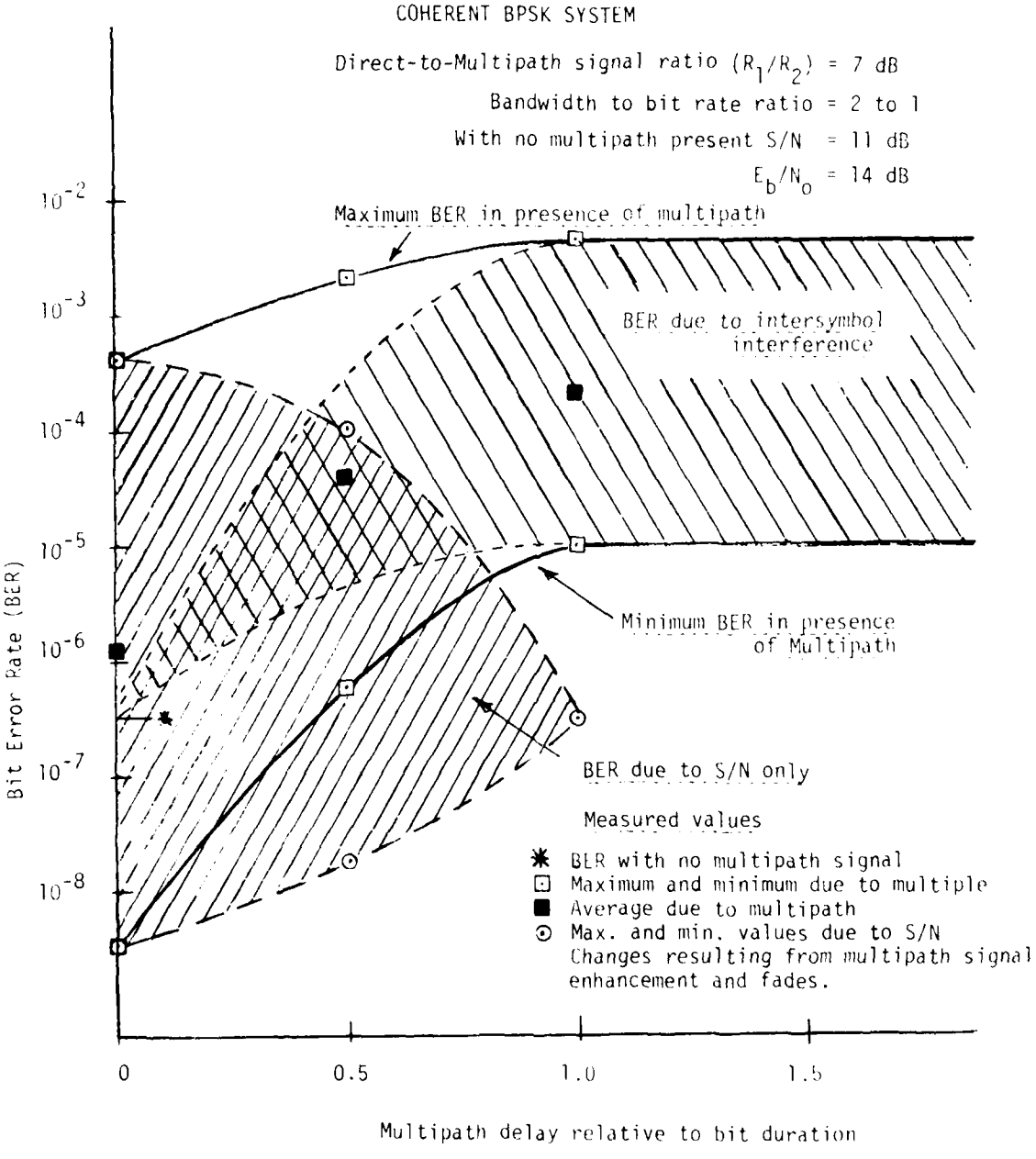

Figure A.1 BER in the presence of multipath signals due to S/N and to intersymbol interference for a S/N of 11 dB and a direct-to-multipath signal ratio of 7 dB.

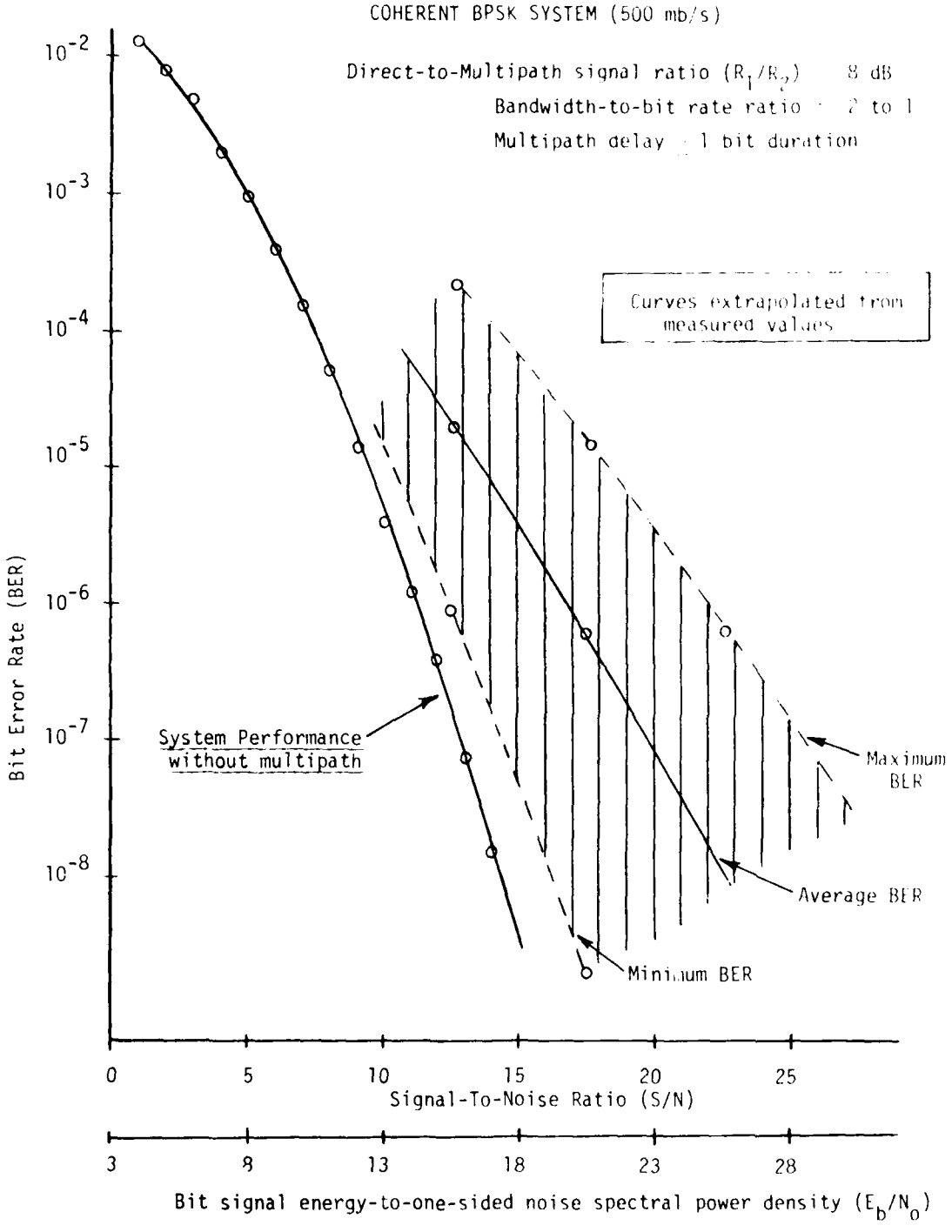

Figure A.2 BER as a function of S/N for a direct-to-multipath signal ratio of 8 dB for multipath delays greater than 1 bit duration.

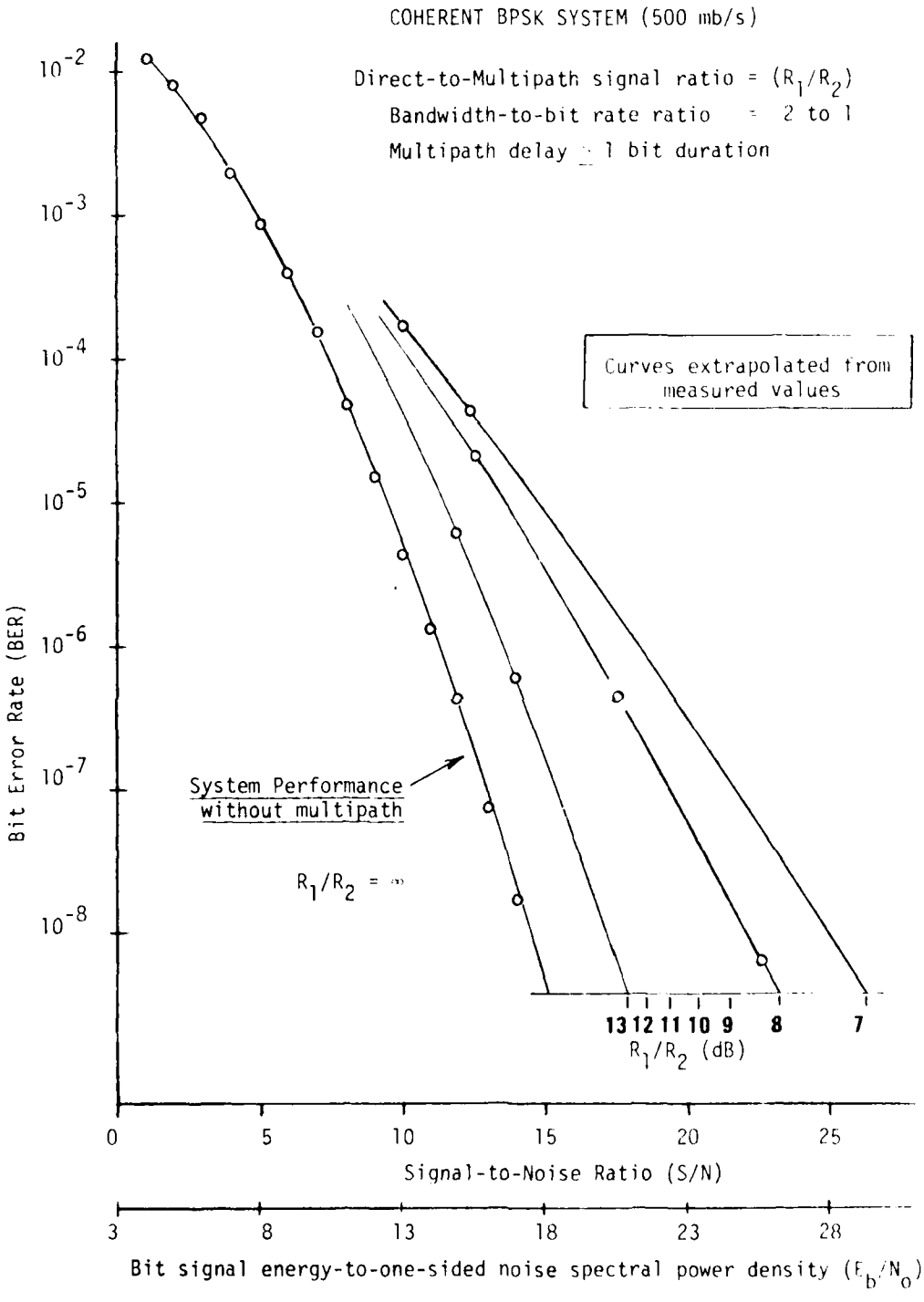

Figure A.3 BER as a function of S/N for direct-to-multipath signal ratios (R_1/R_2) from 7 to 13 dB for multipath delay greater than 1 bit duration.

APPENDIX B

Report on Edge Diffraction Effects for Urban Propagation Studies

When studying the propagation of microwaves and millimeter waves in an urban environment, the diffraction effects of the corners of buildings are naturally of interest. This type of diffraction is called edge diffraction and several scientific models have been developed for it. The theories of Fresnel, Sommerfeld, and Keller will be discussed.

Fresnel's theory of diffraction [1], [2] is a scalar model that assumes a continuous train of waves from a source at a finite distance away impinges on an infinitely thin half plane screen that stops and absorbs the waves. The waves that do not intersect the screen are assumed to travel on unaffected. Here Huygen's principle and the principle of interference are applied to produce the Fresnel diffraction pattern at a finite distance on the other side of the screen from the source. The drawing in Figure B.1 shows the source, screen, and observation plane for this model. In Figure B.2 the normalized received amplitude is shown relative to position on the observation plane.

The distance from the source to the screen is a and the distance from the screen to the observation plane is b. The distance in the observation plane from the geometrical shadow boundary to the observation point is ℓ. If ℓ is normalized for the wavelength and the distances a and b by

$$\nu = \ell \left(\frac{b\lambda(a+b)}{2a} \right)^{-1/2} \tag{1}$$

then the ratio of the magnitude of the field u at the observation point to the magnitude of the field u_o which would have occurred without the diffracting screen is given by

$$\left| \frac{u}{u_o} \right| = \frac{1}{\sqrt{2}} \left| F(\nu) + \frac{1+i}{2} \right| \tag{2}$$

where

$$F(\nu) = \int_0^{\nu} \exp\left(\frac{i\pi x^2}{2} \right) dx \ . \tag{3}$$

Fresnel's theory has the limitation that it does not apply at large angles of diffraction and at observed points close to the diffracting edge. However, experimental observation has proven its usefulness for a variety of diffraction problems. In particular, observation of diffraction from many types of materials show close agreement with Fresnel's theory so that the idealized use of a perfectly absorbing screen does not limit the theory. Observations have shown that the sharpness of the edge is not important at wavelengths of 10 cm and less [3],[4]. Edges with radius of curvature which are very large relative to the rf wavelength, have essentially the same diffraction pattern as a knife edge. However, blunter edges tend to reflect some energy that effects the field in the non-shadow region near the edge. Polarization effects not considered by the theory are small for small angles of diffraction. In general, at large angles of diffraction, the material, form of the edge, and polarization become more important.

Sommerfeld [5] gave a more complete treatment of diffraction from an edge based on electromagnetic theory. He assumed that the material was perfectly reflective but generalized from an infinitely thin screen to a wedge coming to a perfect edge. He also considered the cases where the electric field vector is parallel and perpendicular to the diffracting edge. For small angles of diffraction his results agree with the less rigorous treatment of Fresnel. For larger angles the effects of polarization become evident. When the electric vector is perpendicular to the diffracting edge, the theory predicts that the amount of electromagnetic energy diffracted into the shadow region should be several times greater than the amount for the electric vector parallel to the edge. Experiment has confirmed that more electromagnetic energy is diffracted into the shadow when the electric vector is perpendicular, but the factor of increase is much smaller than indicated by the theory In general, the amount of electromagnetic energy diffracted into the shadow falls off more rapidly with increasing angle than the theory predicts.

Sommerfeld's results also confirm that the field diffracted into the shadow has the form of a cylindrical wave eminating from the diffracting edge. To an observer in the shadow the edge appears illuminated, i.e., the source of electromagnetic energy. Kalaschnikow [6] described experiments that demonstrated this effect. A photographic plate (with sewing needles extending from it) was mounted perpendicular to the diffracting edge. When developed, the plate showed that each needle had cast a shadow so as to indicate that the light had come from the diffracting edge, i.e., radiating outward from the edge.

The appearance of the edge as the source in the shadow region was used by Keller [7] in his development of the geometrical theory of diffraction (an extension of geometrical optics to account for diffraction). In Keller's theory the field is described in terms of rays. As an example, for an edge diffraction field, a ray from the source combines with a ray from the edge, as shown in Figure B.3. The field diffracted from the edge is given as

$$u_e = D\, u_i\, r^{-1/2}\, e^{ikr} \tag{4}$$

where u_i is the field incident on the edge and r is the distance from the edge, $k = 2\pi/\lambda$. The diffraction coefficient is found by comparison with Sommerfeld's result for large kr. For the diffracting screen

$$D = -\frac{e^{i\pi/4}}{2(2\pi k)^{1/2}\sin\beta}\left[\sec\frac{1}{2}(\theta-\alpha) \pm \csc\frac{1}{2}(\theta+\alpha)\right] \tag{5}$$

where β is the angle between the incident ray and the edge (normally $\pi/2$). The angles between the incident and diffracted rays from the normal to the screen are α and θ, respectively, as shown in Figure B.4.

If the screen is replaced by a wedge of angle $(2-n)\pi$. the comparison of (4) with Sommerfeld's exact solution for $\beta \neq \pi/2$ gives

$$D = \frac{e^{i\pi/4}\sin\frac{\pi}{n}}{n(2\pi)^{1/2}\sin\beta}\left[\left(\cos\frac{\pi}{n} - \cos\frac{\theta-\alpha}{n}\right)^{-1} \mp \left(\cos\frac{\pi}{n} - \cos\frac{\theta+\alpha+\pi}{n}\right)^{-1}\right]. \tag{6}$$

Figure B.5 shows how θ and α are measured. Even though equation (6) was derived for $\beta \neq \pi/2$ it can be used for computing the diffracted field when $\beta = \pi/2$.

The formulas in (5) and (6) are not good near the shadow boundary but they do retain the valuable attribute of Sommerfeld's results of predicting the field for large diffraction angles. The upper and lower signs in (5) and (6) correspond to the electric vector polarized perpendicularly and parallel to the edge, respectively. Pauli [8] developed an asymptotic series which can be used to determine the diffraction coefficient and which is good even near the shadow boundary but his results were not used for the fields computed here.

In general, Keller's formulas for the diffracted field show that the field intensity for a fixed angle into the shadow is proportional to the wavelength and fairly independent of the orientation of the screen or wedge. It is only when the incident or diffracted ray nears a side of the wedge or screen that the field intensity is affected. This effect is greatest when the electric vector is parallel to the edge and results in the field intensity decreasing rapidly as the incident or diffracted ray nears the side of the screen or wedge (i.e. when the transmitter or receiver are very close to the side of the building). For the electric vector perpendicular to the edge, there is a small increase in the field intensity when the incident ray or diffracted ray are near a side of the screen or wedge.

When the electric vector is perpendicular to the edge, a screen and a 90 degree wedge give nearly the same field intensity in the shadow region (slightly higher than that predicted by the Fresnel theory). When the electric vector is parallel to the edge the field intensity is lower in the shadow of the wedge than the screen and the factor increases with angle.

In summary, the following should be noted. The type of material does not affect the diffracted field significantly except within a few wavelengths of the edge. The roundness of the edge is not important except that some reflected energy may affect the field near the edge. The effects of polarization become more important at greater angles into the shadow region, but even there the intensity would be expected to be only a few dB higher for an electric vector perpendicular as opposed to parallel to the edge. For a normal urban environment, the Fresnel theory of diffraction should be adequate since finer diffraction effects are likely to be masked by other effects in the measurement environment such as reflected waves. And finally, some caution should be exercised in considering the effects of the antenna apertures upon the observations.

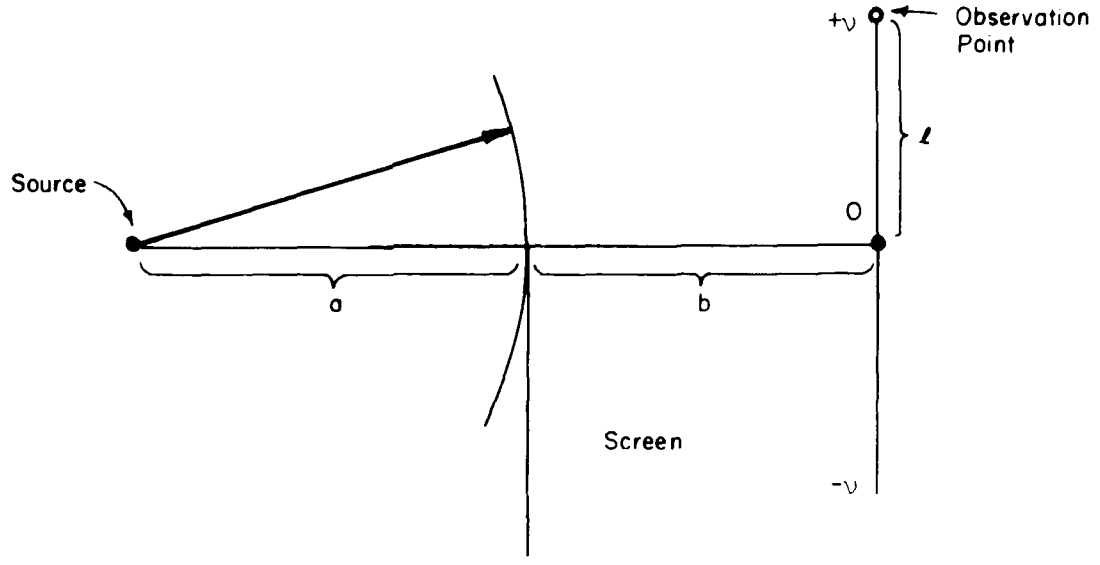

Figure B.1 A sketch of the scalar model geometry.

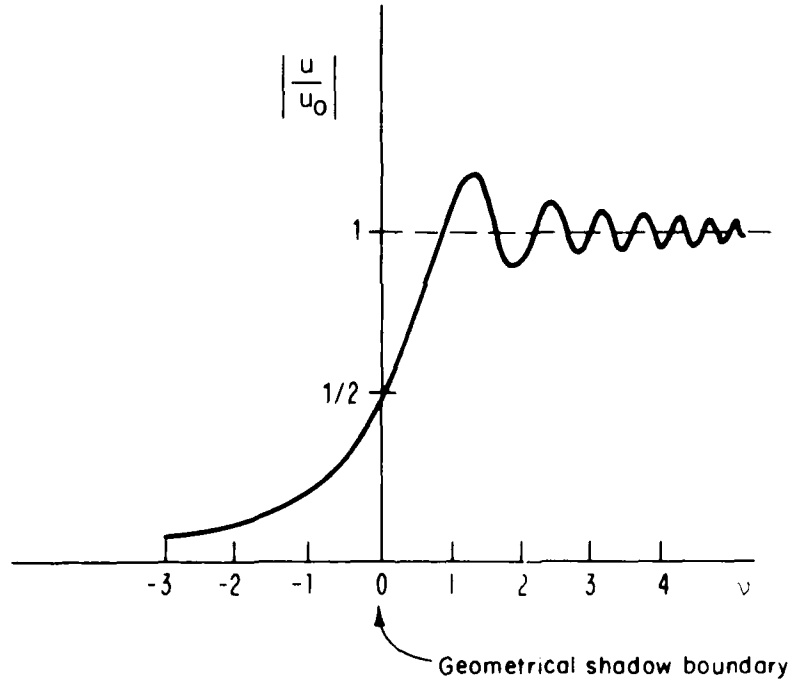

Figure B.2 Normalized amplitude as a function of position along the observation plane.

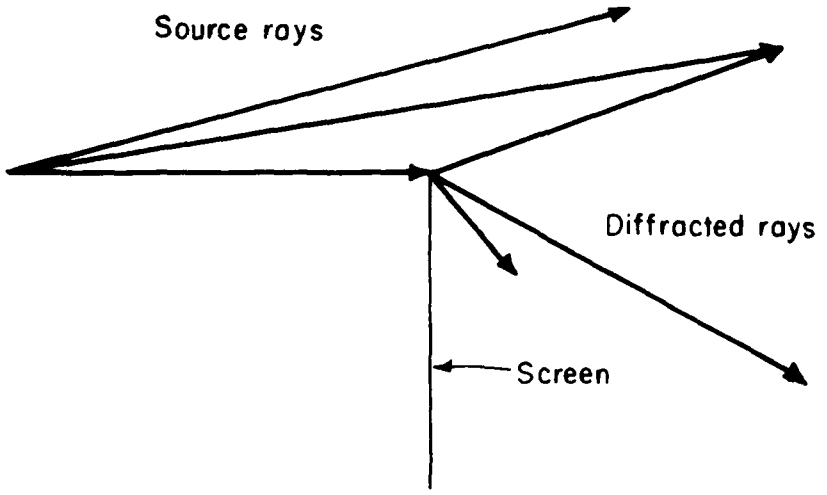

Figure B.3 The ray geometry for Keller's geometrical theory of diffraction.

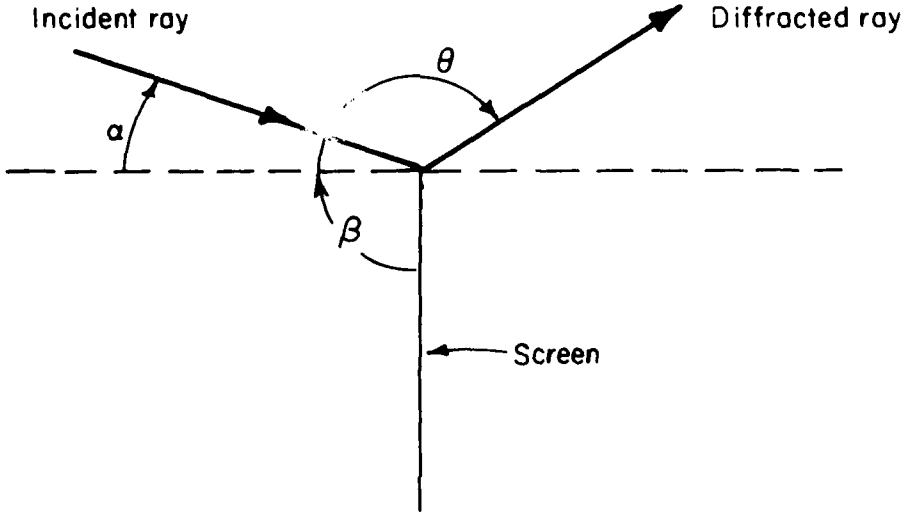

Figure B.4 A drawing showing the angular relationship of the incident and diffracted rays with a screen at the point of diffraction.

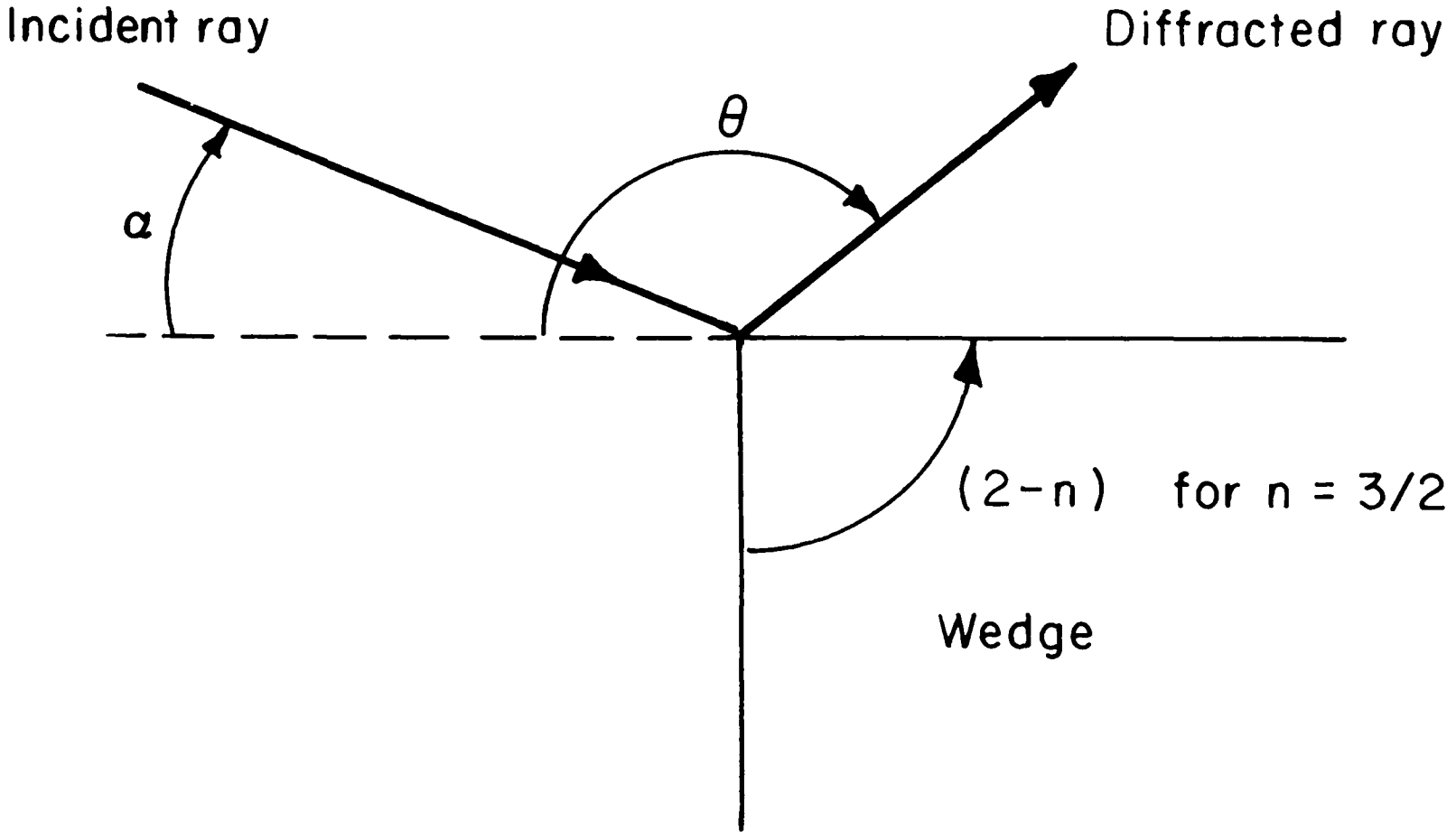

Figure B.5 A drawing showing the angular relationship of the incident and diffracted rays with a wedge at the point of diffraction.

AD-A134 465 URBAN MILLIMETER WAVE PROPAGATION STUDIES(U) ARMY COMMUNICATIONS-ELECTRONICS COMMAND FORT MONMOUTH NJ E J VIOLETTE ET AL. APR 83 CECOM/DRSEL-83-3 2/2

UNCLASSIFIED F/G 20/14 NL

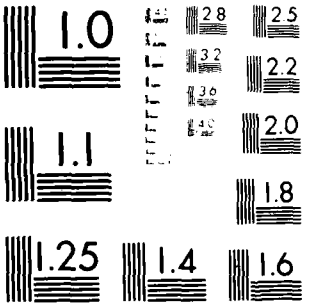

REFERENCES

[1] C. F. Meyer, "The Diffraction of Light, X-Rays, and Material Particles," Edwards Brothers, Inc., Ann Arbor, Michigan, (1949; 2nd ed., 1949).

[2] F. A. Jenkins and H. E. White, "Fundamentals of Optics," McGraw-Hill, New York, (1937; 3rd ed., 1957).

[3] E.J. Haakinson, E.J. Violette, and G.A. Hufford, "Propagation Effects on an Intervisibility Measurements System Operating in the SHF Band," NTIA Report 80-35, (1980), NTIS Access. No. PB 80-167471.

[4] K.C. Allen, R.H. Ott, E.J. Violette, and R.H. Espeland, "Height-Gain Study for 23 km Links at 9.6, 11.4, and 28.8 GHz," IEEE Trans. Ant. Prop. AP-30, No. 4, (January 1982).

[5] A. Sommerfeld, "Optics," Academic Press, New York, 1954, (translated from Optik. Wiesbaden: Dieterichsen Verlagsbuchhandlung, 1950).

[6] A. Kalaschnikow, Journal of the Russ. Phys. Soc., Vol. 44, p. 133, (1912).

[7] J. B. Keller, "Geometrical Theory of Diffraction," J. Optical Soc. Am., Vol. 52, No. 2, pp. 116-130, (Feb. 1962).

[8] W. Pauli, "On Asymptotic Series for Functions in the Theory of Diffraction of Light," Physical Review, Vol. 54, pp. 924-931, (Dec. 1938).


MED
8